

On the α -element gradients of the Galactic thin disk using Cepheids $\star, \star\star$

K. Genovali¹, B. Lemasle², R. da Silva¹, G. Bono^{1,3}, M. Fabrizio⁴, M. Bergemann^{5,6}, R. Buonanno^{1,4}, I. Ferraro³, P. François^{7,8}, G. Iannicola³, L. Inno^{1,9}, C.D. Laney^{10,11}, R.-P. Kudritzki^{12,13,14}, N. Matsunaga¹⁵, M. Nonino¹⁶, F. Primas⁹, M. Romaniello⁹, M.A. Urbaneja¹⁷, and F. Thévenin¹⁸

¹ Dipartimento di Fisica, Università di Roma Tor Vergata, via della Ricerca Scientifica 1, 00133 Rome, Italy

² Anton Pannekoek Institute for Astronomy, University of Amsterdam, Science Park 904, PO Box 94249, 1090 GE, Amsterdam, The Netherlands

³ INAF – Osservatorio Astronomico di Roma, via Frascati 33, Monte Porzio Catone, Rome, Italy

⁴ INAF – Osservatorio Astronomico di Teramo, via Mentore Maggini s.n.c., 64100 Teramo, Italy

⁵ Max-Planck-Institut für Astronomie, D-69117, Heidelberg, Germany

⁶ Institute of Astronomy, University of Cambridge, Madingley Road, CB3 0HA, Cambridge, UK

⁷ GEPI, Observatoire de Paris, CNRS, Université Paris Diderot, Place Jules Janssen, 92190 Meudon, France

⁸ UPJV, Université de Picardie Jules Verne, 33 rue St. Leu, 80080 Amiens, France

⁹ European Southern Observatory, Karl-Schwarzschild-Str. 2, 85748 Garching bei München, Germany

¹⁰ Department of Physics and Astronomy, N283 ESC, Brigham Young University, Provo, UT 84601, USA

¹¹ South African Astronomical Observatory, PO Box 9, Observatory 7935, South Africa

¹² Institute for Astronomy, University of Hawaii, 2680 Woodlawn Drive, Honolulu, HI 96822, USA

¹³ Max-Planck-Institute for Astrophysics, Karl-Schwarzschild-Str.1, D-85741 Garching, Germany

¹⁴ University Observatory Munich, Scheinerstr. 1, D-81679 Munich, Germany

¹⁵ Department of Astronomy, School of Science, The University of Tokyo, 7-3-1 Hongo, Bunkyo-ku, Tokyo 113-0033, Japan

¹⁶ INAF – Osservatorio Astronomico di Trieste, via G. B. Tiepolo 11, 34143, Trieste, Italy

¹⁷ Institute for Astro- and Particle Physics, University of Innsbruck, Technikerstr. 25/8, A-6020 Innsbruck, Austria

¹⁸ Laboratoire Lagrange, CNRS/UMR 7293, Observatoire de la Côte d'Azur, Bd de l'Observatoire, CS 34229, 06304 Nice, France

Received / accepted

ABSTRACT

We present new homogeneous measurements of Na, Al and three α -elements (Mg, Si, Ca) for 75 Galactic Cepheids. The abundances are based on high spectral resolution ($R \sim 38\,000$) and high signal-to-noise ratio ($S/N \sim 50\text{--}300$) spectra collected with UVES at ESO VLT. The current measurements were complemented with Cepheid abundances either provided by our group (75) or available in the literature, for a total of 439 Galactic Cepheids. Special attention was given in providing a homogeneous abundance scale for these five elements plus iron (Genovali et al. 2013, 2014). In addition, accurate Galactocentric distances (R_G) based on near-infrared photometry are also available for all the Cepheids in the sample (Genovali et al. 2014). They cover a large fraction of the Galactic thin disk ($4.1 \leq R_G \leq 18.4$ kpc). We found that the above five elements display well defined linear radial gradients and modest standard deviations over the entire range of R_G . Moreover, the [element/Fe] abundance ratios are constant across the entire thin disk; only the Ca radial distribution shows marginal evidence of a positive slope. These results indicate that the chemical enrichment history of iron and of the quoted five elements has been quite similar across the four quadrants of the Galactic thin disk. The [element/Fe] ratios are also constant over the entire period range. This empirical evidence indicates that the chemical enrichment of Galactic Cepheids has also been very homogenous during the range in age that they cover ($\sim 10\text{--}300$ Myr). Once again, [Ca/Fe] vs. $\log P$ shows a (negative) gradient, being underabundant among youngest Cepheids. Finally, we also found that Cepheid abundances agree quite well with similar abundances for thin and thick disk dwarf stars and they follow the typical Mg-Al and Na-O correlations.

Key words. stars: abundances – stars: variables: Cepheids – stars: oscillations – Galaxy: disk – open clusters and associations: general

1. Introduction

Massive and intermediate-mass stars play a crucial role in different fields of modern astrophysics. They are the main contributors

* Based on spectra collected with the UVES spectrograph available at the ESO Very Large Telescope (VLT), Cerro Paranal, Chile (ESO Proposals: 081.D-0928(A), PI: S. Pedicelli; 082.D-0901(A), PI: S. Pedicelli; 089.D-0767(C), PI: K. Genovali).

** Tables 1 and 3 are only fully available in electronic form at the CDS via anonymous ftp to cdsarc.u-strasbg.fr (130.79.128.5) or via <http://cdsweb.u-strasbg.fr/cgi-bin/qcat?J/A+A/>

in the UV and in the NIR emission of unresolved stellar systems (Crowther 2007). Moreover, they also play a crucial role in the chemical enrichment of the interstellar medium (Ventura et al. 2002; Decressin et al. 2007; Maeder 2009; Karakas et al. 2012). Blue and red supergiants are also fundamental stellar tracers to constrain the metallicity gradients in external early type galaxies (Urbaneja et al. 2005; Kudritzki et al. 2008; Bresolin 2011; Evans et al. 2011).

The distribution of the elements along the disk of external spiral galaxies generally follows a radial gradient with metallicity increasing towards the center. This can be seen for

instance in M31 (e.g., Sanders et al. 2012; Zurita & Bresolin 2012), M33 (Magrini et al. 2010a), M81 (e.g., Kudritzki et al. 2012; Stanghellini et al. 2014), NGC 300 (e.g., Stasinka et al. 2013), NGC 3621 (e.g., Kudritzki et al. 2014), NGC 5668 (e.g., Marino et al. 2012), or in large samples such as Pilyugin et al. (2014a) and Sanchez et al. (2014). The Milky Way shows an iron gradient comparable to other galaxies, in particular a well investigated negative iron gradient (see, e.g., Luck & Lambert 2011; Genovali et al. 2013, and references therein). In general, shallower [O/H] gradients (Vila-Costas & Edmunds 1992; Edmunds & Roy 1993; Zaritsky et al. 1994; Martin & Roy 1994) have been found in barred galaxies in comparison with the ones in non-barred galaxies (but see also Pilyugin et al. 2014b; Sanchez et al. 2014).

The gradient in the Milky Way has been well investigated using different stellar tracers of different age and nature: H II regions, O/B-type stars, Cepheids, open clusters (OC), and planetary nebulae (PNe). Several authors investigated, together with the iron gradient, also the α -element abundances along the disk (e.g. Yong et al. 2006; Lemasle et al. 2007; Luck et al. 2011; Luck & Lambert 2011; Lemasle et al. 2013) and provided gradients based on Cepheids spanning from -0.039 to -0.095 dex kpc $^{-1}$, depending on the element. In particular, Korotin et al. (2014) using a non-LTE abundance analysis of the oxygen triplet in the near-infrared give an [O/H] gradient of -0.058 dex kpc $^{-1}$.

[O/H] gradients spanning from -0.030 to -0.08 dex kpc $^{-1}$ had been inferred from H II regions (e.g., Quireza et al. 2006; Rudolph et al. 2006; Balser et al. 2011), very similar to that obtained from O-B1 stars, -0.03 and -0.07 dex kpc $^{-1}$ (see, e.g., Smartt & Rolleston 1997; Daflon & Cunha 2004; Rolleston et al. 2000). In particular, Daflon & Cunha (2004) provide abundance gradients based on α elements in OB stars spanning from -0.032 ± 0.012 dex kpc $^{-1}$ for oxygen to -0.052 ± 0.014 dex kpc $^{-1}$ for magnesium.

Planetary nebulae observed up to Galactocentric distances (R_G) = 10 kpc show either shallow [O/H] gradients, from -0.02 to -0.085 dex kpc $^{-1}$ (Maciel & Quireza 1999; Costa et al. 2004; Henry et al. 2004; Perinotto & Morbidelli 2006; Pottasch & Bernard-Salas 2006; Henry et al. 2010), or no evidence of radial gradient (Stanghellini et al. 2006).

Twarog et al. (1997) first suggested that instead of a break in the slope the radial metallicity gradient could experience an abrupt drop of the order of 0.2-0.3 dex around 10 kpc. This feature was also proposed in other studies (e.g., Daflon & Cunha 2004; Andrievsky et al. 2004). The exact location of the possible jump in metallicity has not been properly defined. Lépine et al. (2011) claimed the presence of such a metallicity discontinuity in the gradients of both iron and α elements (an average of O, Si, S, Mg, and Ca) based on Cepheids and associated it with the depression in velocity displayed around 10 kpc in the rotation curve of the Galaxy.

The theoretical scenario that better seems to describe the gradient of iron and α elements in the Milky Way is the so-called inside-out scenario (e.g., Matteucci & François 1989; Chiappini et al. 1997; Prantzos & Boissier 2000; Chiappini et al. 2001; Mollá & Díaz 2005; Fu et al. 2009). According to this model, the Milky Way primarily forms during two episodes of gas infall (the first giving birth to the halo and the bulge, the second producing the disk) with an almost independent evolution between the halo and the thin disk.

Although the inside-out model is not unique, it reproduces the majority of the observed features of the Milky Way. Cescutti et al. (2007) computed new radial gradients for nu-

merous elements and closely reproduced Cepheid-based observations based on the nucleosynthesis prescription provided by François et al. (2004), who adopted the star formation and infall laws based on observed features of the Milky Way. The most important factor in reproducing the [element/Fe] vs. [Fe/H] relations, as well as the solar absolute abundances in the solar neighborhood, is the combination of the yields from supernovae (SNe) type Ia and II whose progenitors are, respectively, low/intermediate mass and massive stars. In this context, it is worth mentioning that α -element abundances play also a crucial role in constraining the plausibility of the physical assumptions (instantaneous mixing, instantaneous recycling) adopted to compute chemical evolution models (Spitoni et al. 2009).

The α -enrichment of Cepheids is also often investigated by means of abundance gradients scaled to iron. Iron is mainly produced in SNe Ia, with contributions from SNe II, whereas α -elements are the principal yields of core-collapse SNe, but with contributions of SNe Ia for Ca and Si. Therefore, the [α -element/Fe] ratio is an interesting diagnostic to constrain the chemical enrichment history. A comprehensive study of open clusters abundance gradients was provided by Yong et al. (2012) collecting results from different groups (Bragaglia et al. 2008; Carraro et al. 2007a,b; Chen et al. 2003; Friel et al. 2002, 2010; Jacobson et al. 2008, 2009, 2011a,b; Magrini et al. 2009, 2010b; Pancino et al. 2010; Sestito et al. 2006, 2007; Yong et al. 2005). They found different trends for the [α /Fe] ratios based on open clusters. Ca abundances attain solar values over the entire range of Galactocentric distances, while Mg and Si display a marginal evidence of a slope (~ 0.01 - 0.02 dex kpc $^{-1}$). On the other hand, the average [α /Fe] ratio attains (see their Fig. 21) enhanced values in the outer disk due to the increase in O and Ti abundances. However Ti abundances, as noted by the anonymous referee, display large variations in different investigations and may be dominated by systematic effects. In general, the large majority of investigations on radial dependence based on OCs found a linear gradient of approximately -0.06 dex kpc $^{-1}$ in the range of 5-10 kpc. Concerning the outer disk, however, several authors found evidence of a flattening of the gradients ([Fe/H] ~ -0.3) for distances larger than 12-14 kpc (Magrini et al. 2009; Pancino et al. 2010; Yong et al. 2012, and references therein).

The abundance gradients of the elements along the disk of the Milky Way provide strong constraints to chemical evolution models as they are connected to the evolution of the Galaxy disk. In this context, the α elements play a key role since they are good tracers of the chemical enrichment history of stellar populations. In particular, an overabundance of α elements is typically associated with a fast chemical enrichment in which iron played a minor role (Tinsley 1979; Matteucci 2003). However, the theoretical and empirical scenario is far from being settled, since the Initial Mass Function (IMF, Calura et al. 2010) and the radial gas flows (Spitoni et al. 2013) can also affect the abundance gradients. In particular, gas flows can have similar effects on the gas density distribution, and in turn they can have an impact on the star formation rate (Colavitti et al. 2008, and references therein). Recent chemical evolution models including both radial gas flows and radial stellar migrations (Kubryk et al. 2014a,b; Minchev et al. 2013, 2014) indicate a steady decrease in the slope as a function of time.

In this paper we investigate the gradient associated to three α elements (Mg, Si, Ca), together with Na and Al, focusing on the inner and outer disk regions. The paper is organized as follows: in Sect. 2 we briefly recall the observations and data analysis; in Sect. 3 we present and discuss the radial gradients, and in Sect. 4 the metallicity distributions. In Sect. 5 we discuss some correla-

tions involving the derived abundances, and finally, in Sect. 6 we give a summary of our findings.

2. Observations, data reduction and analysis

2.1. Spectroscopic data

In this work we used the same high-resolution ($R \sim 38\,000$) and high signal-to-noise (S/N) ratio spectra analyzed by Genovali et al. (2014, hereafter G14). The spectra of 75 Galactic Cepheids were collected with the UVES spectrograph at the ESO VLT (Cerro Paranal, Chile). In particular, we collected 122 spectra using two different instrument settings: *i*) the former one makes use of the UVES DIC2 configuration which allow the blue and red arms to operate in parallel. With this setting, we collected (between October 2008 and April 2009¹) 80 spectra of 74 stars, with wavelength ranges of ~ 3760 – 4985 Å, ~ 5684 – 7520 Å, and ~ 7663 – 9458 Å; *ii*) the latter one uses the UVES red arm configuration and the cross disperser CD 3. By adopting this setting we collected (between May and September 2012²) 42 spectra of a control sample of 11 Cepheids, with wavelength ranges of ~ 4786 – 5750 Å and ~ 5833 – 6806 Å.

The 11 Cepheids (V340 Ara, AV Sgr, VY Sgr, UZ Sct, Z Sct, V367 Sct, WZ Sgr, XX Sgr, KQ Sco, RY Sco, V500 Sco) were used as a control sample since we have collected from four to six spectra each and with both the instrumental configurations (with the exception of V500 Sco, which has 4 spectra collected only with the second instrument setting). The S/N ratios are typically better than ~ 100 for all the échelle orders in the case of the first instrumental configuration (see examples in Fig. 1), and ranges from ~ 50 to roughly 300 for the second one. All the spectra were reduced using the ESO UVES pipeline Reflex v2.1 (Ballester et al. 2011).

The stars BB Gem and GQ Ori were initially present in the sample of G14. BB Gem still has an uncertain status as it is classified either as a classical or as a type II Cepheid in different catalogs (see e.g. Harris 1985; Loomis et al. 1988; Bersier et al. 1997). It has been excluded from the current investigation, since its uncertain classification could lead to a wrong distance determination or to a wrong interpretation of the abundance pattern. The spectrum of GQ Ori has low S/N, it is not good enough to provide a reliable abundance determination, and it was also excluded.

2.2. Atmospheric parameters and abundances

We adopted the same iron abundances and atmospheric parameters derived by G14. The iron abundances are based on the equivalent widths (EW) of about 100–200 Fe I and about 20–40 Fe II lines, the number of lines depending on the spectral range used. The number of lines also varies according to the metallicity and to the spectral type of the star. To determine the atmospheric parameters, we set a limit of $EW < 120$ mÅ in order to remain in the linear part of the curve of growth. For the objects where the number of weak lines was too small, we increased the limit to 180 mÅ. This slightly increases the uncertainties affecting the correlated atmospheric parameters, namely the effective temperature and the microturbulent velocity. For more details on the impact that typical uncertainties on effective temperature, surface gravity, and microturbulent velocity have on the iron abundances, see Table 2 of G14.

The effective temperature (T_{eff}) of individual spectra was estimated using the line depth ratio (LDR) method (Kovtyukh & Gorlova 2000). The estimated values of T_{eff} were validated to make sure that the Fe I abundances do not depend on the excitation potential (χ_{ex}), i.e., the slope of [Fe I/H] vs. χ_{ex} should be as close to zero. The surface gravity ($\log g$) was derived through the ionization equilibrium between Fe I and Fe II lines, and the microturbulent velocity (v_t) by minimizing the slope in the [Fe I/H] vs. EW plot.

Concerning the Na, Al, and α (Mg, Si, Ca) elements, we used the linelist provided by Lemasle et al. (2013), with the same atomic parameters (χ_{ex} and $\log g f$) listed in their Table A.1, but with small differences in the number of lines. We used the six Al I lines, two lines for Na I instead of three (the line at 5688.21 Å is often too strong), the nine Ca I lines (the Ca II line was not included), and 14 Si I lines (5665.56 Å was included but used only for the P89 stars). For magnesium, we preferred to adopt only the abundances provided by the line Mg I at 5711.09 Å because those at 8712.69 and 8736.02 Å are not available in the wavelength range of the 11 control sample stars. Note that the line at 5711.09 Å is affected by non-LTE effects. However, Merle et al. (2011) found that the non-LTE correction to the EWs is smaller than 10% in the quoted stellar parameter regime.

To minimize any systematic bias in the continuum estimate due to the subjectivity of the operator, three of us have independently performed EW measurements on a sample of selected lines. The EWs for several elements were also measured using the *Automatic Routine for line Equivalent widths in stellar Spectra* (ARES, Sousa et al. 2007), and double-checked using the *splot* task of IRAF³. The internal dispersion is smaller than 6 mÅ and there is no evidence of systematics.

The abundances were derived with *calrai*, a spectrum synthesis code originally developed by Spite (1967) and regularly improved since then. The code computes synthetic spectra over a large grid of stellar atmospheres in which we can interpolate, using 1-D, hydrostatic, plane-parallel, and spherical LTE model atmospheres (MARCS, Gustafsson et al. 2008). For all the elements studied here, we assumed the standard solar abundances provided by Grevesse et al. (1996), namely $A(\text{Fe})_{\odot} = 7.50$, $A(\text{Na})_{\odot} = 6.33$, $A(\text{Al})_{\odot} = 6.47$, $A(\text{Mg})_{\odot} = 7.58$, $A(\text{Si})_{\odot} = 7.55$, and $A(\text{Ca})_{\odot} = 6.36$.

Table 1 lists the abundances obtained from individual spectra. Columns 3 and 4 show the iron abundances and the number of Fe I and Fe II lines used by G14. The other columns show our results for the abundances of Na, Al, and α elements, together with the number of lines used. In Table 2 we list the mean abundances computed for the stars with multiple spectra.

2.3. Data available in the literature

We compared our abundance estimates with the results provided by similar studies available in the literature: Lemasle et al. (2013, hereafter LEM), Luck et al. (2011, LII), Luck & Lambert (2011, LIII), and Yong et al. (2006, YON). By comparing the stars in common among the different data sets, we evaluated the systematic difference among them. The mean difference between our measurements and those of LEM, LII, and LIII are quite small, about 0.13 dex in modulus or smaller for all the elements investigated here. The difference for Mg is on average 0.23 dex more abundant in our study than in LII's. The differences are larger in the comparison with YON's measurements,

¹ 081.D-0928(A) and 082.D-0901(A), PI: S. Pedicelli

² 089.D-0767(C), PI: K. Genovali

³ *Image Reduction and Analysis Facility*, distributed by the National Optical Astronomy Observatories (NOAO), USA.

which have abundances systematically smaller than ours and range from 0.18 dex for Mg up to 0.31 dex for Fe. The details on these comparisons are listed in Table 3, where we show the zero-point differences obtained by G14 for the iron abundance ratios together with our determinations for the other elements. Each pair of data sets was chosen aiming to maximize the number of stars in common between them. In order to provide a homogeneous abundance scale for Galactic Cepheids, we applied these zero-point differences to the quoted data sets, putting them in the same scale of our current sample. The element abundances available in the literature and the rescaled values are listed in columns from 2 to 15 of Table 5.

The priority in using the abundances from the literature follows the same approach adopted by G14: firstly, we adopt the abundances provided by our group, i.e., this study and then results from LEM, and finally those provided by the other studies, namely LIII, LII, and YON in this order. We ended up with a sample of 439 Cepheids, with a homogeneous abundance scale for Fe, Na, Al, Mg, Si, and Ca.

3. α -element gradients

In this section we investigate the radial gradients of Na, Al, and three α elements (Mg, Ca, Si) across the Galactic disk using our sample of 75 classical Cepheids plus a sample of 364 Cepheids available in literature. The iron gradient for our sample was provided by G14 together with a homogenous iron scale for the remaining objects. The current approach when compared with similar investigations available in the literature has two indisputable advantages: *i*) We use accurate elemental abundances based on high-resolution, high signal-to-noise spectra. Moreover, the approach to constrain the intrinsic parameters (surface gravity, effective temperature, microturbulent velocity) is identical and we also use similar line lists; *ii*) The individual Cepheid distances were estimated using the same near-infrared Period-Wesenheit relations. The key advantages of distances based on this diagnostic is that they are independent of uncertainties affecting reddening corrections and minimally affected by the metallicity dependence (Inno et al. 2013).

Figure 2 shows the abundances scaled to hydrogen of Na, Al, and of the three α elements as a function of R_G for the final sample. Objects plotted in this figure include the current 75 Cepheids (filled blue circles) plus 38 Cepheids from LEM (red triangles), 263 from LIII (open green circles), 61 from LII (magenta crosses), and two from YON (cyan asterisks). The individual Galactocentric distances of the Cepheids in the total sample have been estimated by G14. They adopt the Near-Infrared Period-Wesenheit relations derived by Inno et al. (2013) and assume a solar Galactocentric distance of $7.94 \pm 0.37 \pm 0.26$ kpc (see Groenewegen et al. 2008; Matsunaga et al. 2013, and references therein). The R_G values are listed in our Table 2 and in their Table 4. The typical final uncertainty on the distances is $\sim 5\%$ and is mainly due to the Period-Wesenheit zero-point calibration (for more details see Inno et al. 2013).

The abundances from the literature plotted in Fig. 2 were corrected by adopting the zero-point differences listed in Table 3. This figure also shows the linear Least Squares fits to the current sample of 75 Cepheids (blue solid line) and to the entire sample (439, black dashed line). A *biweight* procedure (Beers et al. 1990) was adopted to remove outliers from the data fitted. The slopes and the zero-points of these two radial gradients are labeled in the panels. The slopes and the zero-points of the fits based on the entire sample together with their uncertainties and standard deviations are listed in columns 2 to 4 of Table 4.

A glance at the data plotted in this figure shows that the occurrence of a radial gradient is solid for the five investigated elements. The main difference is that the standard deviations scale with the number of lines adopted to estimate the abundances. Indeed, the dispersion of the Mg gradient, based on a single line, is almost a factor of two larger than the dispersion of the Si gradient, based on 14 lines. The radial gradients of the five investigated elements attain, within the errors, similar slopes. This finding supports similar results by Lemasle et al. (2007, 2013) and by LII+LIII. The above result becomes even more compelling if we take account of the similarity with the iron radial gradient (-0.060 ± 0.002 dex kpc $^{-1}$) showed by the same Cepheids (G14). The abundances of Na, Al and of the three α -elements seem to show a flattening for distances larger than ~ 13 kpc. Thus supporting a similar trend found using open clusters (Yong et al. 2012). However, firm conclusions are hampered by the increased spread in abundance and by the paucity of the sample in the outermost disk regions.

The current slopes also agree, within 1σ , with similar estimates available in the literature. In our results the slopes range from -0.055 ± 0.003 for [Al/H] to -0.039 ± 0.002 dex kpc $^{-1}$ for [Ca/H]. The slopes estimated by LII+LIII for the same elements range from -0.053 ± 0.004 to -0.040 ± 0.004 dex kpc $^{-1}$, while those estimated by LEM range from -0.046 ± 0.013 to -0.044 ± 0.012 dex kpc $^{-1}$. The reader interested in a more detailed analysis of the difference among the different data sets is referred to columns 6 to 9 of Table 4.

3.1. Comparisons with independent radial gradients

Figure 3 shows the comparison between the slopes of the α -element gradients based on Cepheids and similar abundances for Galactic field stars. We focussed our attention on the α -element abundances provided by Davies et al. (2009a,b) for two red supergiants (RSGs) located in the Galactic center and two RSGs in the Scutum cluster, plus two Luminous Blue Variables belonging to the Quintuplet cluster measured by Najarro et al. (2009). Note that their α -element and iron abundances were rescaled to the abundances of the solar mixture adopted in the current investigation (Grevesse et al. 1996). Data plotted in this figure indicate that young stellar tracers located in the innermost Galactic regions attain α -element abundances that are, at fixed Galactocentric distance, lower than the radial gradients of Galactic Cepheids. To further constrain this difference we extrapolated the Cepheids gradient to the Galactocentric distance of the above targets. We found that the difference $\Delta[\frac{1}{3}([{\rm Mg/H}]+[{\rm Si/H}]+[{\rm Ca/H}])]$ between the expected Cepheid gradient and the Scutum stars is 0.3–0.6 dex and becomes of the order of 0.1–0.4 dex for the targets located in the Galactic center.

Note that α -element abundances provided by these authors are based on a different approach (spectrum-synthesis vs. EWs). To constrain the possible occurrence of systematic differences in the abundances we also plotted the α -element abundances recently provided by Origlia et al. (2013) using high spectral resolution ($R \sim 50\,000$) NIR (Y,J,H,K) spectra collected with GIANO at the Telescopio Nazionale Galileo (TNG). Note that these authors observed the same targets observed by Davies et al. (2009b). The comparison shows, once again, that RSGs located in the near end of the Galactic bar have α abundances lower than classical Cepheids located in the inner edge of the Galactic thin disk.

Figure 3 also shows the comparison with the radial gradients provided by Mikolaitis et al. (2014, hereafter M14) using thin

(solid black line) and thick (dotted black line) disk field stars observed within the Gaia-ESO survey. We adopted their *clean* sample, which only includes dwarfs, with $\log g > 3.5$. To overcome possible differences between Cepheid and spectroscopic distances of field dwarfs, in plotting their radial gradients we adopted the zero-points of our gradients at the solar Galactocentric distance. The comparison shows that the slopes agree quite well over the entire range of Galactocentric distances covered by the Gaia-ESO survey (4–12 kpc).

3.2. Age dependence of the $[\alpha/H]$ ratios

The above findings rely on the Galactocentric distance as independent variable. This is a crucial parameter to identify possible radial trends. However, one of the key issues in dealing with the chemical enrichment history of the thin disk is the age dependence. Detailed chemo-dynamical models suggest a strong dependence of the metallicity gradients for ages older than 1–3 Gyr (Kubryk et al. 2014a,b; Minchev et al. 2013, 2014). This means a steady decrease in the metallicity with increasing age. Moreover, they also predict a strong dependence on stellar migrations.

Classical Cepheids can play a crucial role in this context, since there are solid theoretical and empirical arguments suggesting that the pulsation period is strongly anti-correlated with age (Bono et al. 2005). An increase in stellar mass causes, for intermediate-mass stars during central helium burning phases, an increase in the mean luminosity of the blue loop. Plain physical arguments rooted on the Stefan-Boltzman relation, on the fundamental pulsation relation and on the mass-luminosity relation indicate that the increase in luminosity causes a decrease in surface gravity, and in turn, an increase in the pulsation period.

To constrain the age dependence of the metallicity gradients, Fig. 4 shows the same elemental abundances plotted in Fig. 2, but as a function of the logarithmic period. Data plotted in this figure show a well defined positive gradient as a function of the pulsation period. The slopes of the α -elements attain similar values, while for Na and Al they are systematically larger (see labelled values). This evidence further supports the hydrostatic nature of both Na and Al due to their steady increase with pulsation period (stellar mass). This finding agrees quite well with yields predicted by nucleosynthesis models (Arnett 1971; Limongi & Chieffi 2012).

3.3. Radial gradient of [element/Fe]

The similarity of the slopes between iron and the current elements suggested to investigate the [element/Fe] radial gradients as a function of the Galactocentric distance. Data plotted in Fig. 5 show that the ratio is on average quite flat across the entire thin disk. We performed a *biweight* linear Least Squares fit over the entire sample and we found that the slopes are vanishing for Na, Al, and Si. There is a mild evidence of positive slope for Mg and Ca. However, the standard deviation of the former element is a factor of two larger than for Si (0.15 vs. 0.06 dex). Thus suggesting that the slope has to be cautiously treated. The positive slope for Ca appears more solid (see values in Table 3), and indeed, the slope attains the largest value among the investigated elements.

The above findings bring forward a few interesting consequences:

i) The radial gradients of the [element/Fe] ratios are slightly positive if not zero. This evidence indicates that the chemical enrichment history of iron and of the other five elements has

been quite similar across the Galactic thin disk. This finding is also supported by the small standard deviations of the quoted ratios. The standard deviation of Si, the element with the most accurate measurements, can be explained as the consequence of the intrinsic error. These results become even more compelling if we take account of the range in iron abundance covered by Galactic Cepheids (~ 1 dex).

ii) The $[\alpha/\text{Fe}]$ ratios are typically considered as tracers of the star formation activity. This means that the $[\alpha/\text{Fe}]$ ratios are also tracers of stellar mass, and in particular, of gas and dust mass. The lack of a clear negative gradient, between the high (inner) and the low (outer) density regions of the thin disk, is suggesting that the $[\alpha/\text{Fe}]$ radial gradients are affected by other parameters such as radial migration of stars or radial gas flows.

iii) There is evidence of a mild enhancement in the investigated elements and of an increase in the intrinsic scatter when moving toward the outer disk. The synthesis of Na, Al and Mg takes mainly place in massive stars during hydrostatic central He, C or Ne burning phases and current prediction suggest that their production is metallicity dependent (Woosley & Weaver 1995; Limongi & Chieffi 2012). However, these findings further support the evidence that the ratios $[\text{Na}/\text{Fe}]$ and $[\text{Al}/\text{Fe}]$ are constant across the Galactic thin disk (McWilliam et al. 2013).

However, the number of Cepheids with Galactocentric distance larger than 13 kpc is limited. New identifications of classical Cepheids in the outer disk from the ongoing long-term photometric surveys are clearly required to further constrain the trend in the outer disk. The same applies for new homogenous spectroscopic measurements.

3.4. Comparisons with independent radial gradients

To validate the above findings concerning the flat trend of $[\alpha/\text{Fe}]$ radial gradients, Fig. 6 shows the comparison with similar data available in the literature. The magenta, cyan, red and yellow symbols mark the same young stars plotted in Fig. 3. Interestingly enough, $[\alpha/\text{Fe}]$ is solar and quite similar to the mean ratio of the entire Cepheid sample. This evidence further supports the working hypothesis that the Galactic thin disk experienced a homogeneous chemical enrichment history during the last 300 Myr. The lack of a clear enhancement in the innermost Galactic regions is also supporting the mild correlation of the $[\alpha/\text{Fe}]$ ratio with the star formation rate. Indeed, recent NIR (Matsunaga et al. 2011) and MIR/FIR (Ramírez et al. 2008; Gerin et al. 2015) investigations indicate that the Galactic bar and the Galactic center are very efficient star forming regions.

A comparison with radial gradients provided by M14, for thin (solid black line) and thick (dotted black line) disk field stars in the Gaia-ESO survey further supports the above conclusions. Indeed, there is a very good agreement with the $[\alpha/\text{Fe}]$ ratios of both thin and thick disk stars. Once again, in plotting their radial gradients we adopted the zero-points of our gradients at the solar Galactocentric distance.

The above figure also shows the comparison with the α -element abundances for open clusters provided by Yong et al. (2012). The green and the orange dashed lines show the gradients for inner ($R_G < 13$ kpc) and outer ($R_G > 13$ kpc) disk objects, respectively. In plotting these gradients we adopted the zero-points of our gradients at the solar Galactocentric distance. The agreement is quite good over the entire range of distances. This finding becomes even more compelling if we account for the fact that the open clusters adopted by Yong et al. cover the entire range of ages typical of thin disk stellar populations, namely from ~ 0.5 to ~ 10 Gyr (see their figures 25 and 26).

3.5. Age dependence of the $[\alpha/\text{Fe}]$ ratios

To constrain the age dependence of the $[\alpha/\text{Fe}]$ abundance ratios, Fig. 7 shows the same elemental abundances plotted in Fig. 5, but as a function of the logarithmic period. A glance at the data plotted in this figure shows that the ratios are approximately constant over the entire period range. Note that the difference in age between short ($\log P \sim 0.3$) and long-period ($\log P \sim 1.8$) is of the order of 300 Myr (Bono et al. 2000; Anderson et al. 2014). These findings strongly suggest that the chemical enrichment of Galactic Cepheids has been homogenous both in space and in time.

To constrain the period/age dependence on a more quantitative basis, we performed *biweight* linear Least Squares fits to the above data. The zero-points, the slopes, their uncertainties, and the standard deviations are listed in the bottom lines of Table 4. We found that Na, Al, Mg, and Si either do not show evidence of a slope or the slope is marginal (see Fig. 7). On the other hand, Ca shows once again a (negative) gradient, suggesting that Ca is underabundant among youngest Cepheids. In passing we note that the nucleosynthesis of Si, Ca, and Fe mostly takes place during the SNe II explosive events (these elements, in particular Fe, are also produced in SNe Ia). This might explain the flat distribution of Si, but the negative trend showed by Ca when moving from older to younger Cepheids would remain unclear. Note that the occurrence of a negative gradient in Ca as a function of period and of a positive gradient of Ca as a function of Galactocentric distance are not correlated, since the Cepheids located in the outer disk have a canonical period distribution (mostly between 2 and 20 days).

4. Metallicity distribution

The range in age covered by Galactic Cepheids is too short to constrain a possible age dependence on the timescale of the order of a few Gyrs. To further investigate this effect we compared the current Cepheid metallicity distribution with the metallicity distribution of field dwarf stars (743) collected by Soubiran & Girard (2005, hereafter SG05). In their sample, 72% are thin disk stars and 28% are from the thick disk. Note that the sample collected by SG05 is based on spectroscopic data available in the literature. Their α -element and iron abundances were not rescaled to the solar mixture adopted in the current investigation (Grevesse et al. 1996). We also perform the same comparison with the results provided by the GAIA-ESO survey (Mikolaitis et al. 2014; Recio-Blanco et al. 2014). Data plotted in Fig. 8 shows that the agreement between Cepheids and thin disk dwarfs is quite good over the entire metallicity range covered by the current sample. This outcome applies to the α -elements and to Al. On the other hand, the Na in field stars attain values that are the lower envelope of the typical Na abundances of classical Cepheids. The same agreement for α -elements and for Al is also shared in the [element/Fe] plane (Fig. 9), in which the difference concerning Na is even more clear. This difference appears to be significant and may be caused by non-LTE effects. Indeed, the difference increases when moving from the metal-rich to the metal-poor regime, as expected for non-LTE effects (Fabrizio et al. 2012; Takeda & Takada-Hidai 2000). Recent empirical investigations (Johnson & Pilachowski 2012) are also suggesting an increase in Na enhancement when moving from the base to the tip of the RGB. Moreover, we also found evidence of a positive gradient (slope = 0.20 ± 0.03 dex kpc $^{-1}$) in [Na/H] versus the logarithmic period. This finding further supports an increase in the difference in Na abundance when moving

from long-periods (low surface gravity) to short-periods (high surface gravity).

In this context it is worth mentioning that Takeda et al. (2013) performed a detailed abundance analysis of ten Galactic Cepheids using high-resolution spectra. They investigated CNO plus Na elements, since they are solid tracers of induced mixing during advanced evolutionary phases of intermediate-mass stars. They found a well defined Na overabundance of the order of 0.2 dex over the entire period range covered by their targets (2–16 days). They suggested that the Na enhancement could be due to mixing events that dredge up Na-rich material, produced by the NeNa cycle, into the surface of classical Cepheids. A similar explanation was originally suggested by Sasselov (1986) and by Denissenkov (1994). We plan to address this specific issue, and in particular, the period (i.e. stellar mass) dependence in a forthcoming paper.

4.1. Al-Mg and Na-O correlations

To further constrain the recent chemical enrichment of the Galactic thin disk we also investigated the (anti-)correlation between Mg-Al and Na-O. Detailed spectroscopic investigations indicate that evolved and unevolved stars in the Local Group globular clusters display well defined anti-correlation between Na-O, and Mg-Al (e.g., Carretta et al. 2009, 2014). The left panel of Figure 10 show the comparison between the current abundances of Mg and Al for the Cepheid sample (blue dots plus grey dots for Cepheids in the literature) with similar abundances for F- and G-type field dwarf stars collected by Bensby et al. (2005, hereafter B05, 102 objects). The latter sample includes both thin (dark green) and thick (light green) disk stars. Moreover, we also included Mg-Al abundances for field dwarf stars collected by Reddy et al. (2003, hereafter R03). This sample includes 189 objects and a significant fraction of them are thin disk stars (magenta dots). Note that the α -element and iron abundances provided by these authors were rescaled to the abundances of the solar mixture adopted in the current investigation (Grevesse et al. 1996). Data plotted in this figure disclose a very good agreement between field dwarfs and Cepheids. However, the sample by R03 shows, at fixed [Mg/Fe] abundance, a well defined underabundance in [Al/Fe]. There are some plausible reasons that could explain the difference. The Mg abundances provided by R03 are based on three lines (4730.04, 6318.71, 7657.61 Å) while we only use the line at 5711.09 Å. The agreement with the Mg abundances provided by B05 is due to the fact that they adopted eight different lines including the current one, but not the three Mg lines adopted by R03. The difference may also be caused by different values of $\log g f$ adopted by these studies. Nevertheless, Galactic Cepheids display, at fixed [Al/Fe] abundance, a large dispersion in [Mg/Fe] abundances when compared with field dwarfs. However, they clearly follow the Mg-Al correlation typical of field stars.

To confirm the above similarity, the middle panel of Figure 10 shows the same comparison, but with the thin (black crosses) and thick (orange pluses) disk field dwarf stars measured by M14. The agreement is once again very good over the entire abundance range covered by the two samples. Data plotted in this panel display that Cepheids, thin and thick disk dwarf stars have similar [Al/Fe] and [Mg/Fe] distributions. This is an interesting finding, since according to R03, B05 and M14 their samples include both old (~12 Gyr) and intermediate-age (0.5–7 Gyr) field dwarf stars.

The right panel of Figure 10 shows the comparison between the abundances of Na and O for the current sample of Cepheids with the same sample of field stars we adopted in the left panel of the same figure. Note that in plotting Cepheid abundances we are using the current Na abundances, but the O abundances for the same objects provided by LII and LIII. To overcome problems introduced by non-LTE effects, we only used oxygen abundances based on the O I triplet at 6156 Å and on the [O I] forbidden line at 6300 Å, the mean values of both provided by LIII, and the triplet-based ones provided by LII. A glance at the data plotted in this panel shows the well defined offset in Na abundances between field dwarfs and Cepheids. The sample by R03 appears to be located between the B05 and the Cepheids. This mild difference might be due to their larger uncertainties in O abundances (see their Sect. 7.2), or to different assumptions on the adopted $\log g f$ values.

4.2. Hydrostatic and explosive elements

The chemical enrichment history of the Galactic thin disk can also be constrained by investigating the ratio between hydrostatic and explosive elements. The left panel of Fig. 11 shows [Mg/Ca] as a function of the iron abundance. The Cepheids display typical solar abundances of [Mg/Ca] for iron abundances more metal-poor than the Sun. For iron abundances more metal-rich than the Sun, the spread in [Mg/Ca] abundances increases and becomes of the order of 0.5–0.7 dex. On the other hand, the abundances of thin and thick disk dwarf stars collected either by B05 or by M14 display the typical decreasing trend when moving from metal-poor to more metal-rich objects⁴. The same outcome applies to the metal-rich regime, and indeed the metal-rich objects (green diamonds) collected by B05 display a mild increase in the [Mg/Ca] abundance ratio for $[Fe/H] \geq 0.15$.

The reasons for the above difference are not clear, therefore we investigated a possible radial dependence. The middle panel of Fig. 11 shows both the Cepheid and the M14 [Mg/Ca] abundances as a function of Galactocentric distance. Data plotted in this figure display that a significant fraction of the spread in [Mg/Ca] abundance (~ 0.7 dex) showed by metal-rich Cepheids is evident among objects that are located either across or inside the solar circle (~ 8 kpc). Evidence for a mild increase in the spread in [Mg/Ca] seems to be also present in the outer disk.

The thin disk stars by M14 display a flat distribution over the entire range of Galactocentric distances they cover. On the other hand, the thick disk stars display a larger spread (~ 0.3 dex) in a limited range of Galactocentric distances ($6 \leq R_G \leq 8$ kpc). Note that in this panel we did not plot the sample by B05, since individual distances are not available. This evidence appears slightly counter intuitive, since the increase in iron typical of the innermost disk regions should also be followed by a steady increase in Ca abundance, since they are explosive elements. This means a steady decrease in the [Mg/Ca] abundance ratio. Oddly enough, we found that the [Mg/Ca] ratio increases when moving towards the inner disk.

To further constrain this effect we also investigated the age dependence. The right panel of Fig. 11 shows the [Mg/Ca] abundances of the Cepheid sample as a function of the logarithmic period. Data plotted in this figure show no clear trend. The spread in the [Mg/Ca] abundance ratio is almost constant over the entire period range, and therefore, no solid evidence of a dependence on stellar mass.

⁴ The thin disk stars by M14 appear to have a flat distribution, but we performed a test and we found that the negative slope is significant.

5. Summary and final remarks

We present accurate and homogeneous measurements of Na, Al and three α -elements (Mg, Si, Ca) for 75 classical Galactic Cepheids. The current abundances are based on high spectral resolution ($R \sim 38\,000$) and high signal-to-noise ratio ($S/N \sim 50$ –300) spectra collected with UVES at ESO VLT. The iron abundance of the same Cepheids was already discussed in Genovali et al. (2013, 2014). The current sample covers a broad range in pulsation periods ($0.36 \leq \log P \leq \sim 1.54$) and in Galactocentric distances ($4.6 \leq R_G \leq 14.3$ kpc).

The current spectroscopic measurements were complemented with Cepheid abundances available in the literature and based on similar spectra and on a similar approach in performing the abundance analysis. We ended up with a sample of 439 Galactic Cepheids. Among them 140 have measurements estimated by our group (current plus LEM), while the others come from LII, LIII, and YON. The samples have from 16 to 55 Cepheids in common, which allow us to calibrate a homogeneous abundance scale for the quoted five elements plus iron (G14).

The use of homogeneous abundance scales, and accurate and homogenous individual distances based on NIR photometry allowed us to investigate the radial gradients across a significant portion of the Galactic inner and outer disk ($4.1 \leq R_G \leq 18.4$ kpc). The main findings of the current analysis are the following:

i) *Radial gradients*: The five investigated elements display a well defined radial gradient. The slopes range from -0.058 for [Al/H] to -0.038 dex kpc $^{-1}$ for [Ca/H]. The negative slopes are linear over the entire range of Galactocentric distances covered by the current sample. Moreover they agree, within the errors, with similar estimates available in the literature. The main difference is that the current gradients display standard deviations on average smaller than 0.16 dex.

ii) *Environmental effects*: The comparison of current abundances with similar measurements for young stars located in the near end of the bar and in the nuclear bulge indicates that the latter attain, within the errors, solar abundances. This means that inner disk Cepheids attain higher α abundances when compared with young stars of the quoted regions. Thus suggesting that the bar plus the nuclear bulge and the inner disk underwent different chemical enrichment histories. However, the above regions attain similar solar [α/Fe] ratios.

iii) *Spatial homogeneity*: The [element/Fe] ratios are constant across the entire thin disk with no evidence of radial gradient. This applies to Na, Al, and Si. The radial distribution of Mg and Ca display marginal positive slopes, but they should be treated with caution. The Mg abundances display, at fixed Galactocentric distance, a large spread mainly driven by measurement errors.

The above results indicate that the chemical enrichment history of iron and of the other five elements has been quite similar across the Galactic thin disk. Moreover, since the [α/Fe] ratios are typically considered tracers of star formation, the lack of a clear negative gradient suggests that the [α/Fe] radial gradients are also affected by other parameters. There is also evidence for a mild abundance enhancement for the five elements and of an increase in the intrinsic scatter in the outer disk. However, the number of Cepheids with $R_G > 13$ kpc is limited, and new identifications of classical Cepheids in this region are clearly required.

iv) *Temporal homogeneity*: The ratios [element/Fe] vs. $\log P$ are constant over the entire period range for Na, Al, Mg. This empirical evidence together with the well established anti-

correlation between age and pulsation period indicates that the chemical enrichment of Galactic Cepheids has also been very homogenous during the last 300 Myr. On the other hand, Ca shows a significant negative gradient, being underabundant among youngest Cepheids.

v) *Comparison between giants and dwarfs:* The comparison between the metallicity distribution of Galactic Cepheids and field dwarf stars shows that the current Al, Mg, Si, and Ca abundances agree quite well with those of the thin disk dwarfs over the entire metallicity range. On the other hand, the Na abundances in field stars are the lower envelope of the typical Na abundances of classical Cepheids. This effect appears real and caused by non-LTE effects, since the difference increases when moving from the metal-rich to metal-poor Cepheids. More recent investigations suggest that an increase in Na abundance in evolved intermediate-mass stars might also be caused by mixing events that dredge up Na-rich material, produced by the NeNa cycle, into the surface of classical Cepheids.

vi) *Mg-Al and Na-O correlations:* Evolved and unevolved stars in the Local Group globular clusters show a well defined anti-correlation between Mg-Al and Na-O. On the other hand, classical Cepheid follow the same correlation typical of field stars. However, Cepheid Na abundances show a well defined enhancement when compared with Na abundances for field dwarfs. The difference is mainly caused by evolutionary effects (dredge-up into the surface of Na-rich material) and by non-LTE effects. Moreover, Cepheids, thin and thick disk dwarf stars display very similar [Al/Fe] and [Mg/Fe] abundance distributions. This is an interesting finding, since the different samples of field dwarfs and Cepheids cover a large range in age (0.5–12 Gyr).

vii) *Hydrostatic and explosive elements:* Cepheids in the [Mg/Ca] vs. [Fe/H] plane display a flat solar abundance for iron abundances more metal-poor than the Sun. For iron abundances more metal-rich than the Sun, the spread in [Mg/Ca] abundances increases and becomes of the order of 0.5–0.7 dex. Thin and thick disk stars display in the quoted iron regimes similar trends. The [Mg/Ca] abundance ratio decreases approaching solar iron abundances and increases in the more metal rich regime. Simple chemical enrichment histories would imply a steady decrease in [Mg/Ca] for higher Fe abundances, since Ca and Fe are explosive elements. This trend is mainly caused by objects located either across or inside the solar circle and does not show a clear dependence on the pulsation period (i.e. stellar mass).

The above results bring forward two interesting consequences concerning the chemical enrichment of the Galactic thin disk. The flat and homogeneous trend of the five investigated elements as a function of the Galactocentric distances and of the pulsation period. This suggests similar trends when moving from the inner to the outer disk. Moreover, there is mounting evidence of a marginal difference between young (Cepheids), intermediate- and old age field dwarfs. This means minor spatial and temporal variations across the Galactic thin, and possibly thick, disk. More solid empirical constraints are required to further support the above trends. No doubts that *s*- and *r*-elements are good diagnostics to constrain possible differences in chemical enrichment between different stellar populations (Cescutti et al. 2008; Matteucci et al. 2014).

The wealth of new results concerning iron and α -elements is also opening the path to new empirical constraints on the initial mass function. In particular, the steady increase of the hydrostatic-to-explosive [Mg/Ca] abundance ratio in the innermost, more metal-rich regions of the inner disk is suggesting a more complex relation between the IMF and the nucleosynthesis of SNe Ia and SNe II (McWilliam et al. 2013). More recently,

Kudritzki et al. (2015) called attention to the chemical enrichment of star forming galaxies using analytical chemical evolution models. They found that their sample can be split into three groups according to the rate either of the galactic wind mass loss or of the accretion mass gain to the star formation rate. They applied their model to the Galaxy and they found that the actual iron gradient would imply a modest accretion rate and a moderate mass-loading factor. The homogeneity of the above α -element gradients can provide new firm constraints on the role that the IMF and the infall rate played in the star formation history of the Galactic thin disk.

Acknowledgements. This work was partially supported by PRIN-MIUR (2010 LY5N2T) "Chemical and dynamical evolution of the Milky Way and Local Group galaxies" (P.I.: F. Matteucci). M.F. acknowledges the financial support from the PO FSE Abruzzo 2007-2013 through the grant "Spectro-photometric characterization of stellar populations in Local Group dwarf galaxies" prot. 89/2014/OACTe/D (P.I.: S. Cassisi). We also acknowledge an anonymous referee for his/her positive opinions concerning this experiment and for the very pertinent suggestions that improved the content and the readability of the paper.

References

- Anderson, R.I., Ekström, S., Georgy, C., et al. 2014, A&A, 564, A100
 Andrievsky, S.M., Luck, R.E., Martin, P., & Lépine, J.R.D. 2004, A&A, 413, 159
 Arnett, W.D. 1971, ApJ, 166, 153
 Ballester, P., Bramich, D., Forchi, V., et al. 2011, Astronomical Data Analysis Software and Systems XX, 442, 261
 Balser, D.S., Rood, R.T., Bania, T.M., & Anderson, L.D. 2011, ApJ, 738, 27
 Beers, T.C., Flynn, K., & Gebhardt, K. 1990, AJ, 100, 32
 Bensby, T., Feltzing, S., & Lundström, I. 2003, A&A, 410, 527 (B05)
 Bersier, D., Burki, G., & Kurucz, R.L. 1997, A&A, 320, 228
 Bono, G., Caputo, F., Cassini, S., et al. 2000, ApJ, 543, 955
 Bono, G., Marconi, M., Cassini, S., et al. 2005, ApJ, 621, 966
 Bragaglia, A., Sestito, P., Villanova, S., et al. 2008, A&A, 480, 79
 Bresolin, F. 2011, ApJ, 729, 56
 Calura, F., Recchi, S., Matteucci, F., & Kroupa, P. 2010, MNRAS, 406, 1985
 Carraro, G., de La Fuente Marcos, R., Villanova, S., et al. 2007a, A&A, 466, 931
 Carraro, G., Geisler, D., Villanova, S., Frinchaboy, P.M., & Majewski, S.R. 2007b, A&A, 476, 217
 Carretta, E., Bragaglia, A., Gratton, R.G., & Lucatello, S. 2009, A&A, 505, 139
 Carretta, E., Bragaglia, A., Gratton, R.G., et al. 2014, A&A, 564, A60
 Cescutti, G., Matteucci, F., François, P., & Chiappini, C. 2007, A&A, 462, 943
 Cescutti, G., Matteucci, F., Lanfranchi, G.A., & McWilliam, A. 2008, A&A, 491, 401
 Chen, L., Hou, J.L., & Wang, J.J. 2003, AJ, 125, 1397
 Chiappini, C., Matteucci, F., & Padoan, P. 1997, From Quantum Fluctuations to Cosmological Structures, 126, 545
 Chiappini, C., Matteucci, F., & Romano, D. 2001, ApJ, 554, 1044
 Colavitti, E., Matteucci, F., & Murante, G. 2008, A&A, 483, 401
 Costa, R.D.D., Uchida, M.M.M., & Maciel, W.J. 2004, A&A, 423, 199
 Crowther, P.A. 2007, ARA&A, 45, 177
 Daflon, S., & Cunha, K. 2004, ApJ, 617, 1115
 Davies, B., Origlia, L., Kudritzki, R.-P., et al. 2009a, ApJ, 694, 46 (D09a)
 Davies, B., Origlia, L., Kudritzki, R.-P., et al. 2009b, ApJ, 696, 2014 (D09b)
 Decressin, T., Meynet, G., Charbonnel, C., Prantzos, N., & Ekström, S. 2007, A&A, 464, 1029
 Denissenkov, P.A. 1994, A&A, 287, 113
 Edmunds, M.G., & Roy, J.-R. 1993, MNRAS, 261, L17
 Evans, C.J., Davies, B., Kudritzki, R.-P., et al. 2011, A&A, 527, 50
 Fabrizio, M., Merle, T., Thévenin, F., et al. 2012, PASP, 124, 519
 François, P., Matteucci, F., Cayrel, R., Spite, M., Spite, F., & Chiappini, C. 2004, A&A, 421, 613
 Friel, E.D., Janes, K.A., Tavarez, M., et al. 2002, AJ, 124, 2693
 Friel, E.D., Jacobson, H.R., & Pilachowski, C.A. 2010, AJ, 139, 1942
 Fu, J., Hou, J.L., Yin, J., & Chang, R.X. 2009, ApJ, 696, 668
 Genovali, K., Lemasse, B., Bono, G., et al. 2013, A&A, 554, A132
 Genovali, K., Lemasse, B., Bono, G., et al. 2014, A&A, 566, A37 (G14)
 Gerin, M., Ruaud, M., Goicoechea, J.R., et al. 2015, A&A, 573, A30
 Grevesse, N., Noels, A., & Sauval, A.J. 1996, Cosmic Abundances, 99, 117
 Groenewegen, M.A.T., Udalski, A., & Bono, G. 2008, A&A, 481, 441
 Gustafsson, B., Edvardsson, B., Eriksson, K., et al. 2008, A&A, 486, 951
 Harris, H.C. 1985, AJ, 90, 756
 Henry, R.B.C., Kwinter, K.B., & Balick, B. 2004, AJ, 127, 2284
 Henry, R.B.C., Kwinter, K.B., Jaskot, A.E., et al. 2010, ApJ, 724, 748

- Inno, L., Matsunaga, N., Bono, G. 2013, ApJ, 764, 84
- Jacobson, H.R., Friel, E.D., & Pilachowski, C.A. 2008, AJ, 135, 2341
- Jacobson, H.R., Friel, E.D., & Pilachowski, C.A. 2009, AJ, 137, 4753
- Jacobson, H.R., Friel, E.D., & Pilachowski, C.A. 2011a, AJ, 141, 58
- Jacobson, H.R., Pilachowski, C.A., & Friel, E.D. 2011b, AJ, 142, 59
- Johnson, C.I., & Pilachowski, C.A. 2012, ApJ, 754, L38
- Karakas, A.I., García-Hernández, D.A., & Lugaro, M. 2012, ApJ, 751, 8
- Korotin, S.A., Andrievsky, S.M., Luck, R.E., et al. 2014, MNRAS, 444, 3301
- Kovtyukh, V.V., & Gorlova, N.I. 2000, A&A, 358, 587
- Kubryk, M., Prantzos, N., Athanassoula, E., 2014a [arXiv:1412.0585]
- Kubryk, M., Prantzos, N., Athanassoula, E., 2014b [arXiv:1412.4859]
- Kudritzki, R.-P., Urbaneja, M.A., Bresolin, F., et al. 2008, ApJ, 681, 269
- Kudritzki, R.-P., Urbaneja, M.A., Gazak, Z., et al. 2012, ApJ, 747, A15
- Kudritzki, R.-P., Urbaneja, M.A., Bresolin, F., et al. 2014, ApJ, 788, A56
- Kudritzki, R.-P., Ho, I.-T., Schruba, A., et al. 2015, MNRAS, accepted [arXiv:1503.01503]
- Lemasle, B., François, P., Bono, G., et al. 2007, A&A, 467, 283
- Lemasle, B., François, P., Genovali, K., et al. 2013, A&A, 558, A31 (LEM)
- Lépine, J.R.D., Cruz, P., Scarano, S., Jr., et al. 2011, MNRAS, 417, 698
- Limongi, M., & Chieffi, A. 2012, ApJS, 199, 38
- Loomis, C., Schmidt, E.G., & Simon, N.R. 1988, MNRAS, 235, 1059
- Luck, R.E., Andrievsky, S.M., Kovtyukh, V.V., Gieren, W., & Graczyk, D. 2011, AJ, 142, 51 (LII)
- Luck, R.E., & Lambert, D.L. 2011, AJ, 142, 136 (LIII)
- Maciel, W.J., & Quireza, C. 1999, A&A, 345, 629
- Maeder, A. 2009, in Physics, Formation, and Evolution of Rotating Stars, Astronomy and Astrophysics Library, Springer Berlin Heidelberg, 2009
- Magrini, L., Stanghellini, L., & Villaver, E. 2009, ApJ, 696, 729
- Magrini, L., Stanghellini, L., Corbelli, E., et al. 2010a, A&A, 512, A63
- Magrini, L., Randich, S., Zoccali, M., et al. 2010b, A&A, 523, A11
- Marino, R.A., Gil de Paz, A., Castillo-Morales, A., et al. 2012, ApJ, 754, A61
- Martin, P., & Roy, J.-R. 1994, ApJ, 424, 599
- Matsunaga, N., Kawadu, T., Nishiyama, S., et al. 2011, Nature, 477, 188
- Matsunaga, N., Feast, M.W., Kawadu, T., et al. 2013, MNRAS, 429, 385
- Matteucci, F., & François, P. 1989, MNRAS, 239, 885
- Matteucci, F. 2003, Ap&SS, 284, 539
- Matteucci, F., Romano, D., Arcones, A., Korobkin, O., & Rosswog, S. 2014, MNRAS, 438, 2177
- McWilliam, A., Wallerstein, G., & Mottini, M. 2013, ApJ, 778, 149
- Merle, T., Thévenin, F., Pichon, B., & Bigot, L. 2011, MNRAS, 418, 863
- Mikolaitis, Š., Hill, V., Recio-Blanco, A., et al. 2014, A&A, 572, A33 (M14)
- Minchev, I., Chiappini, C., & Martig, M. 2013, A&A558, A9
- Minchev, I., Chiappini, C., & Martig, M. 2014, A&A, 572, A92
- Mollá, M., & Díaz, A.I. 2005, MNRAS, 358, 521
- Najarro, F., Figer, D.F., Hillier, D.J., Geballe, T.R., Kudritzki, R.P. 2009, ApJ, 691, 1816 (N09)
- Origlia, L., Oliva, E., Maiolino, R., et al. 2013, A&A, 560, A46 (O13)
- Pancino, E., Carrera, R., Rossetti, E., & Gallart, C. 2010, A&A, 511, A56
- Perinotto, M., & Morbidelli, L. 2006, MNRAS, 372, 45
- Pilyugin, L.S., Grebel, E.K., & Kniazev, A.Y. 2014a, AJ, 147, 131
- Pilyugin, L.S., Grebel, E.K., Zinchenko, I.A., & Kniazev, A.Y. 2014b, AJ, 148, 134
- Pottasch, S.R., & Bernard-Salas, J. 2006, A&A, 457, 189
- Prantzos, N., & Boissier, S. 2000, MNRAS, 313, 338
- Quireza, C., Rood, R.T., Bania, T.M., Balser, D.S., & Maciel, W.J. 2006, ApJ, 653, 1226
- Ramírez, S.V., Arendt, R.G., Sellgren, K., et al. 2008, ApJS, 175, 147
- Reddy, B.E., Tomkin, J., Lambert, D.L., & Prieto, C.A. 2003, MNRAS, 340, 304 (R03)
- Recio-Blanco, A., de Laverny, P., Kordopatis, G., et al. 2014, A&A, 567, A5
- Rolleston, W.R.J., Smartt, S.J., Dufton, P.L., & Ryans, R.S.I. 2000, A&A, 363, 537
- Rudolph, A.L., Fich, M., Bell, G.R., et al. 2006, ApJS, 162, 346
- Sánchez, S.F., Rosales-Ortega, F.F., Iglesias-Páramo, J., et al. 2014, A&A, 563, A49
- Sanders, N., Caldwell, N., & McDowell, J. 2012, ApJ, 758, 133
- Sasselov, D.D. 1986, PASP, 98, 561
- Sestito, P., Bragaglia, A., Randich, S., et al. 2006, A&A, 458, 121
- Sestito, P., Randich, S., & Bragaglia, A. 2007, A&A, 465, 185
- Smartt, S.J., & Rolleston, W.R.J. 1997, ApJ, 481, L47
- Soubiran, C., & Girard, P. 2005, A&A, 438, 139 (SG05)
- Sousa, S.G., Santos, N.C., Israelian, G., Mayor, M., & Monteiro, J.P.F.G. 2007, A&A, 469, 783
- Spite, M. 1967, Annales d'Astrophysique, 30, 211
- Spitoni, E., Matteucci, F., Recchi, S., Cescutti, G., & Pipino, A. 2013, A&A, 504, 87
- Spitoni, E., Matteucci, F., & Marcon-Uchida, M.M. 2013, A&A, 551, A123
- Stanghellini, L., Guerrero, M.A., Cunha, K., Manchado, A., & Villaver, E. 2006, ApJ, 651, 898
- Stanghellini, L., Magrini, L., Casasola, V., et al. 2014, A&A, 567, A88
- Stasinska, G., Peña, M., Bresolin, F., et al. 2013, A&A, 552, A12
- Takeda, Y., & Takada-Hidai, M. 2000, PASJ, 52, 113
- Takeda, Y., Kang, D.-I., Han, I., Lee, B.-C., & Kim, K.-M. 2013, MNRAS, 432, 769
- Tinsley, B.M. 1979, ApJ, 229, 1046
- Twarog, B.A., Ashman, K.M., & Anthony-Twarog, B.J. 1997, AJ, 114, 2556
- Urbaneja, M.A., Herrero, A., Bresolin, F., et al. 2005, ApJ, 622, 862
- Ventura, P., D'Antona, F., & Mazzitelli, I. 2002, A&A, 393, 215
- Vila-Costas, M.B., & Edmunds, M.G. 1992, MNRAS, 259, 121
- Woosley, S.E., & Weaver, T.A. 1995, ApJS, 101, 181
- Yong, D., Carney, B.W., & Teixera de Almeida, M.L. 2005, AJ, 130, 597
- Yong, D., Carney, B.W., Teixera de Almeida, M.L., & Pohl, B.L. 2006, AJ, 131, 2256 (YON)
- Yong, D., Carney, B.W., & Friel, E.D. 2012, AJ, 144, 95
- Zaritsky, D., Kennicutt, R.C., Jr., & Huchra, J.P. 1994, ApJ, 420, 87
- Zurita, A., & Bresolin, F. 2012, MNRAS, 427, 1463

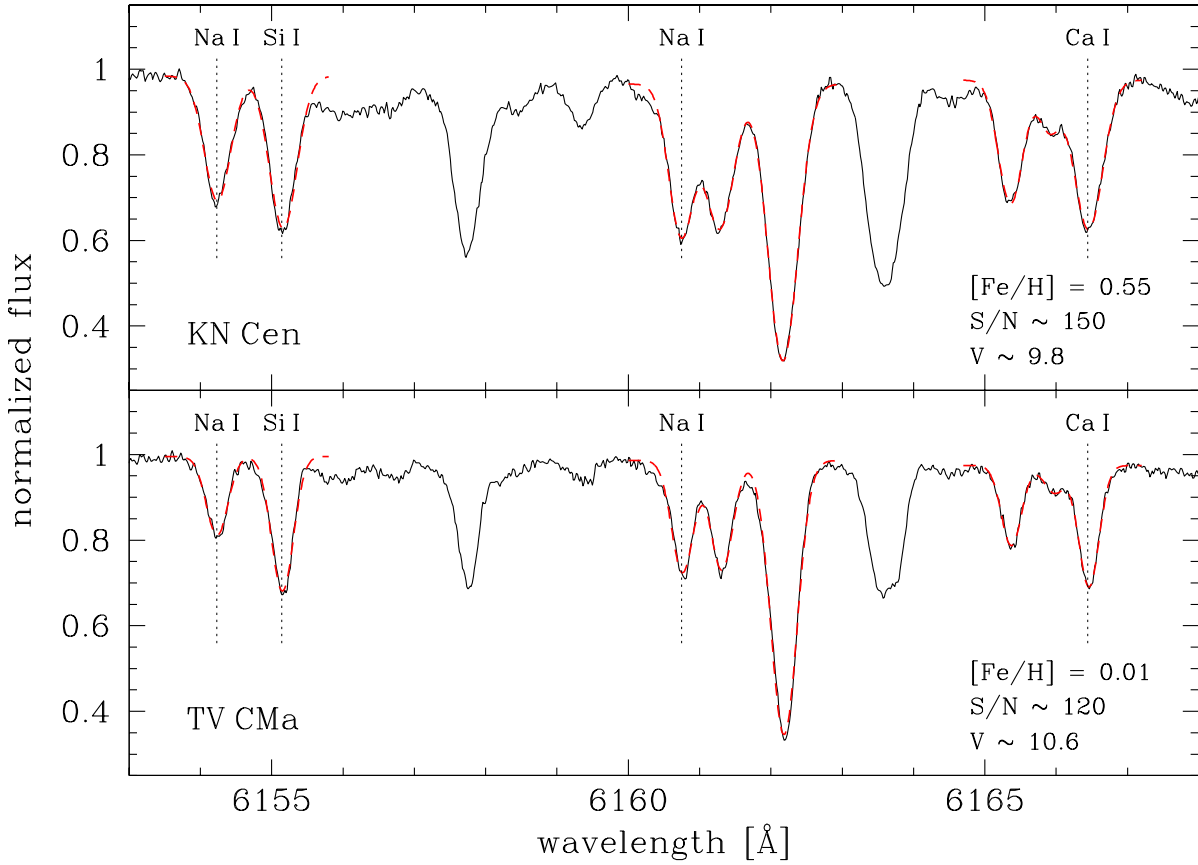


Fig. 1. High-resolution ($R \sim 38\,000$) UVES spectrum of KN Cen and TV CMa. The apparent visual magnitude and the S/N in the spectral range $\lambda \sim 5650 - 7500 \text{ \AA}$ are also labeled. The vertical dashed lines display some of the spectral lines (Na I 6154.23, Si I 6155.14, Na I 6160.75, Ca I 6166.44 \AA) adopted to estimate the abundances.

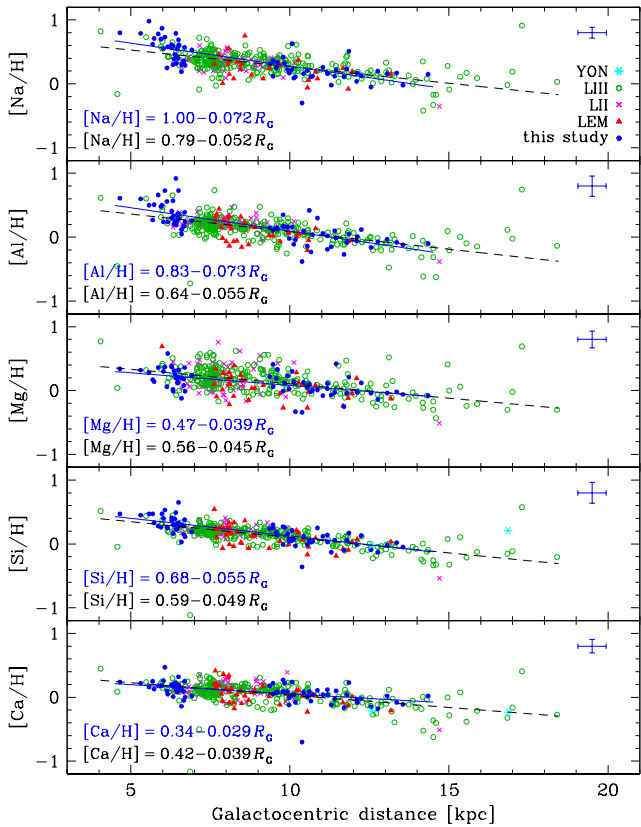


Fig. 2. Abundances of Na, Al, and α elements as a function of R_G . Our results (filled blue circles) are compared with those of Yong et al. (2006, YON, cyan asterisks), Luck et al. (2011, LII, magenta crosses), Luck & Lambert (2011, LIII, open green circles), and Lemasle et al. (2013, LEM, red triangles). The blue solid line shows the linear regression of our Cepheid sample, while the black dashed line the linear regression of the entire Cepheid sample. The blue error bars display the mean spectroscopic error of the current sample. The abundances available in the literature have similar errors.

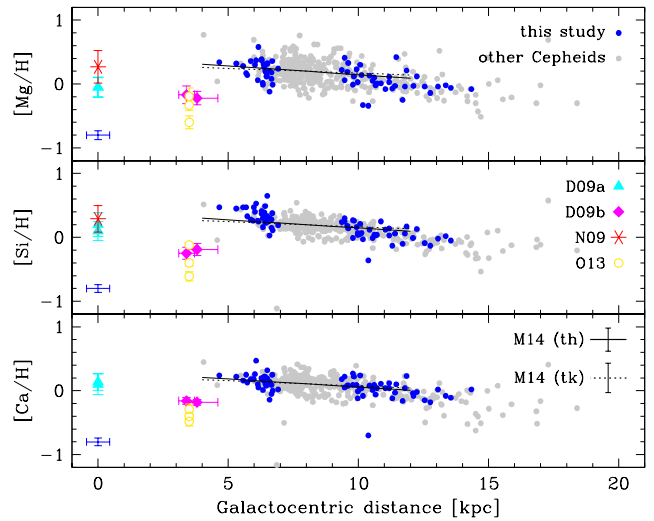


Fig. 3. Abundances of α elements as a function R_G . Cepheid stars (filled circles) are compared with RSGs in the Galactic center analyzed by Davies et al. (2009a, D09a, cyan triangles), RSGs in the Scutum cluster analyzed by Davies et al. (2009b, D09b, magenta diamonds) and by Origlia et al. (2013, O13, yellow open circles), and with the mean abundance of two Luminous Blue Variables (LBVs) in the Quintuplet cluster measured by Najarro et al. (2009, N09, red asterisk). The radial gradients derived by Mikolaitis et al. (2014, M14) for thin (solid line) and thick (dotted line) disk stars in the Gaia-ESO survey are also shown.

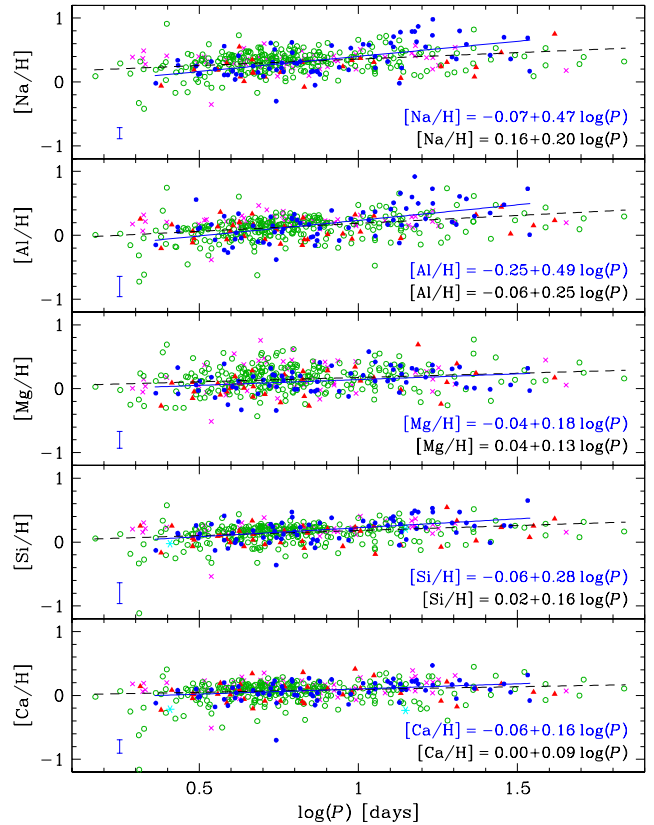


Fig. 4. Abundances of Na, Al, and α elements as a function of the pulsation period. Symbols and colors are the same as in Fig. 2.

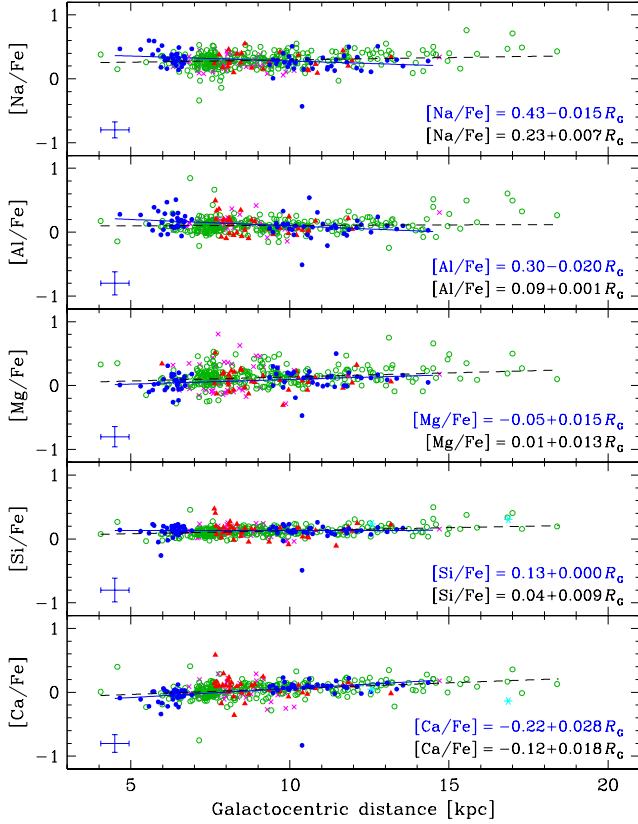


Fig. 5. The same as Fig. 2, but the abundances are scaled to iron.

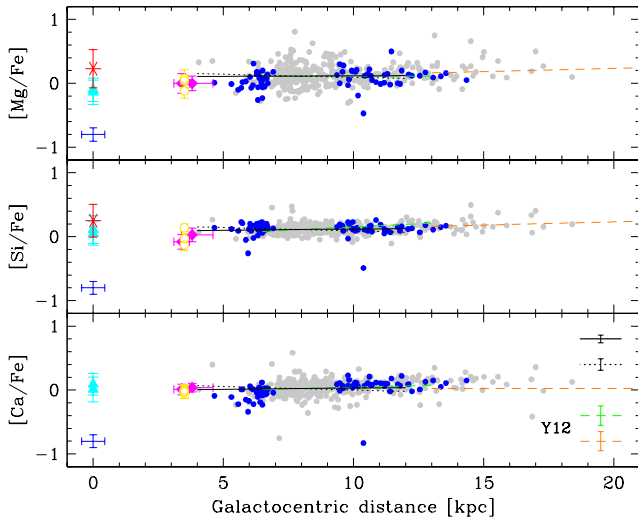


Fig. 6. The same as Fig. 3, but the abundances are scaled to iron. The abundance trends derived by Yong et al. (2012, Y12) for open clusters (green and orange dashed lines) are also shown.

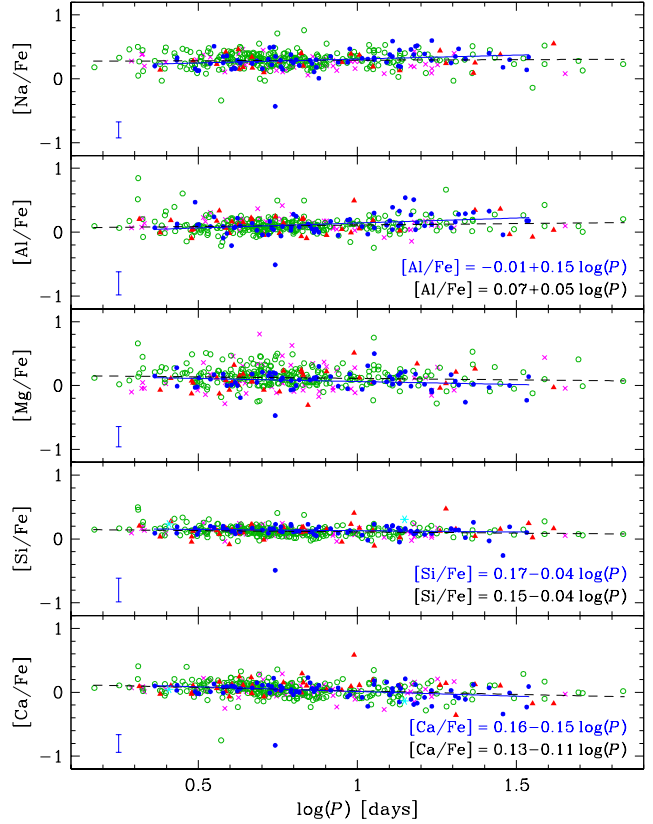


Fig. 7. Abundances of Na, Al, and α elements scaled to iron as a function of the logarithmic pulsation period. For Na and Mg the equations are not shown because the slopes have no statistical significance. Symbols and colors are the same as in Fig. 2.

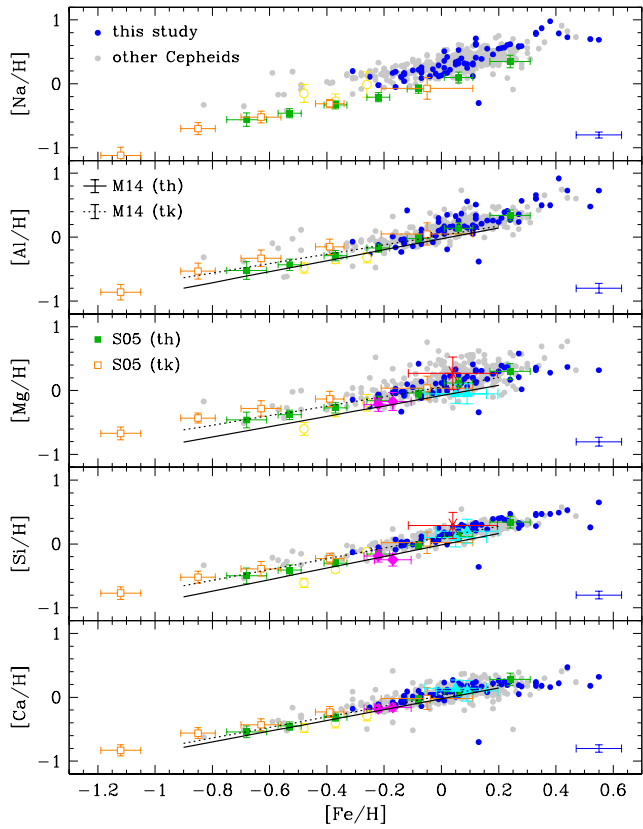


Fig. 8. Abundances of Na, Al, and α elements as a function of the metallicity. Cepheid stars (filled circles) are compared with thin disk (filled green squares) and thick disk (open orange squares) field dwarfs from Soubiran & Girard (2005, S05). The abundances of red supergiants and LBVs are also plotted when available (symbols and colors are the same as in Fig. 3). The gradients derived by Mikolaitis et al. (2014, M14) for thin (solid line) and thick (dotted line) disk stars in the Gaia-ESO survey are also shown.

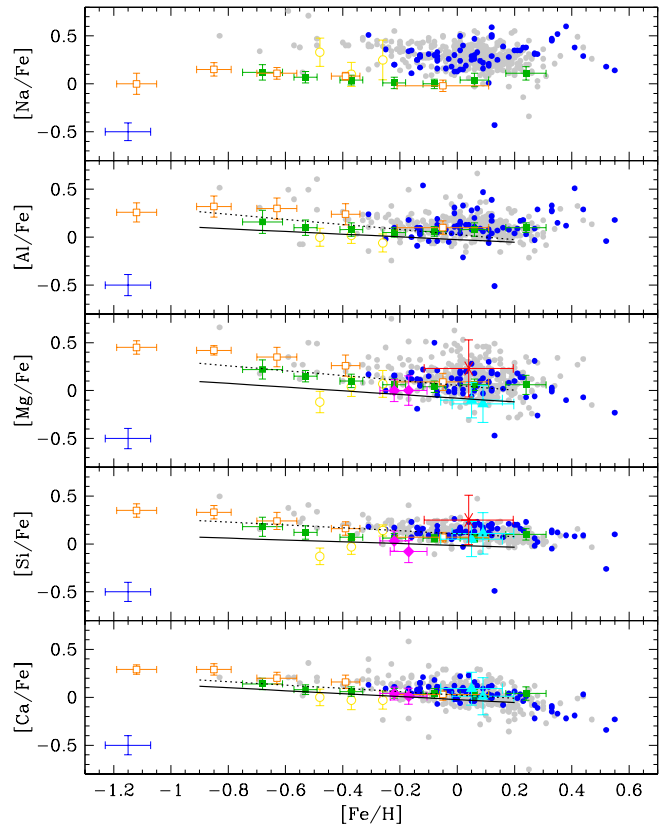


Fig. 9. The same as Fig. 8, but the abundances are scaled to iron.

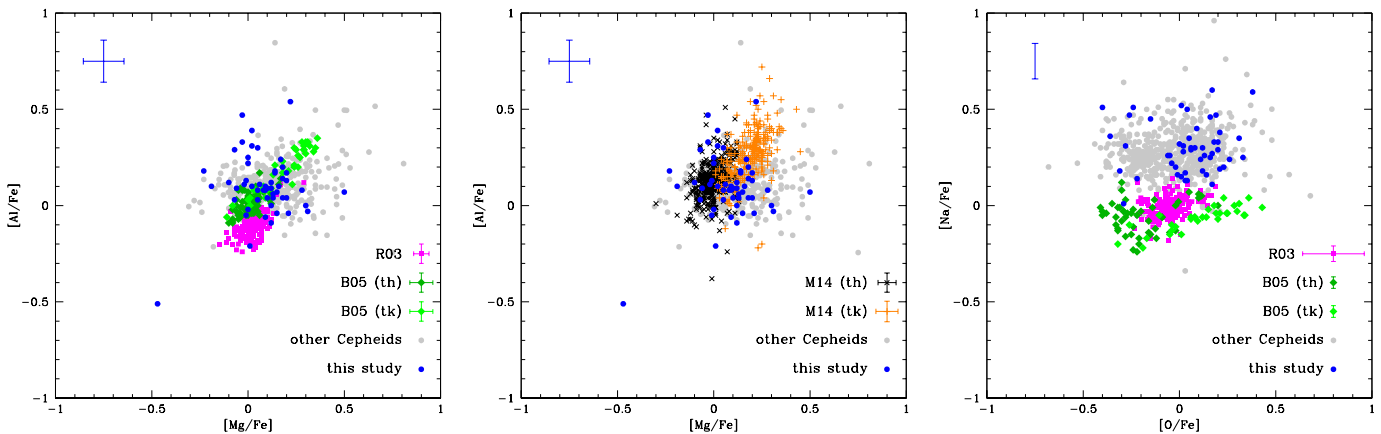


Fig. 10. Correlations between Al–Mg (left and middle panels) and between Na–O (right panel). Cepheid stars (filled circles) are compared with field dwarfs from the thin disk analyzed by Reddy et al. (2003, R03, magenta squares), from the thin (dark green diamonds) and thick (light green diamonds) disks analyzed by Bensby et al. (2005, B05), and from the thin (black crosses) and thick (orange pluses) disks analyzed by Mikolaitis et al. (2014, M14).

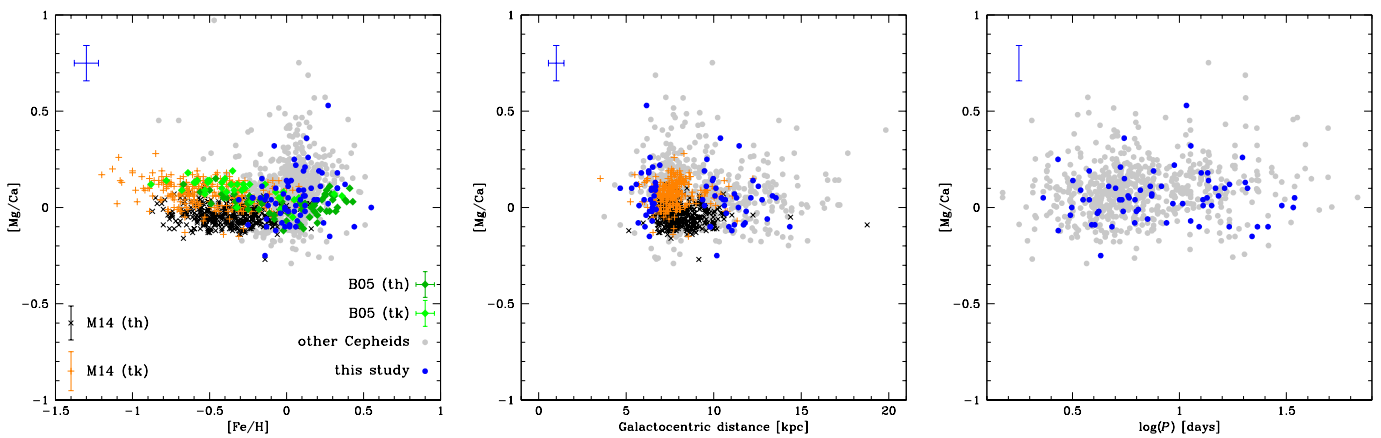


Fig. 11. Abundance ratios between Mg and Ca as a function of metallicity (left panel), Galactocentric distance (middle panel), and logarithmic pulsation period (right panel). Symbols and colors are the same as in Fig. 10.

Table 1. Abundances of Fe, Na, Al, and α elements for our sample of classical Cepheids derived based on individual spectra.

Name	MJD	[Fe/H]	N_L (Fe I, Fe II)	[Na/H]	N_L	[Al/H]	N_L	[Mg/H]	N_L	[Si/H]	N_L	[Ca/H]	N_L
V340 Ara	56137.137	0.27 ± 0.10	(23, 2)	0.72 ± 0.05	1	0.71 ± 0.08	1	0.28 ± 0.08	2	0.17 ± 0.04	2
V340 Ara	54708.065	0.53 ± 0.09	(53, 4)	0.98 ± 0.01	2	0.59 ± 0.14	4	0.55 ± 0.01	1	0.67 ± 0.14	10	0.41 ± 0.12	2
V340 Ara	54709.079	0.53 ± 0.16	(26, 3)	0.95 ± 0.01	2	0.71 ± 0.06	3	0.47 ± 0.07	1	0.61 ± 0.15	10	0.36 ± 0.12	2
V340 Ara	56138.094	0.32 ± 0.09	(41, 2)	0.77 ± 0.13	2	0.55 ± 0.18	2	0.24 ± 0.07	1	0.33 ± 0.01	2	0.17 ± 0.05	2
V340 Ara	56139.185	0.22 ± 0.01	(51, 2)	0.59 ± 0.05	1	0.50 ± 0.12	2	0.10 ± 0.07	1	0.30 ± 0.11	3	0.14 ± 0.06	5
V340 Ara	56152.054	0.24 ± 0.18	(15, 2)	0.62 ± 0.06	1	0.17 ± 0.06	1
AS Aur	54845.136	0.00 ± 0.08	(74, 8)	0.13 ± 0.05	1	0.12 ± 0.40	2	0.12 ± 0.18	1	0.13 ± 0.25	10	-0.02 ± 0.17	3
KN Cen	54862.355	0.55 ± 0.12	(14, 3)	0.69 ± 0.04	2	0.73 ± 0.17	4	0.32 ± 0.17	1	0.65 ± 0.24	10	0.32 ± 0.26	2
MZ Cen	54584.280	0.27 ± 0.10	(45, 4)	0.59 ± 0.05	1	0.36 ± 0.18	4	0.21 ± 0.36	1	0.33 ± 0.19	7	0.19 ± 0.12	2
OO Cen	54585.060	0.20 ± 0.06	(30, 4)	0.55 ± 0.05	1	0.24 ± 0.19	5	0.30 ± 0.10	1	0.40 ± 0.23	6	0.26 ± 0.12	2
TX Cen	54862.363	0.44 ± 0.12	(78, 7)	0.73 ± 0.05	1	0.73 ± 0.16	2	0.37 ± 0.16	1	0.53 ± 0.27	9	0.47 ± 0.11	2
V339 Cen	54584.304	0.06 ± 0.03	(39, 3)	0.53 ± 0.23	2	0.26 ± 0.11	5	0.24 ± 0.19	1	0.19 ± 0.18	10	0.02 ± 0.07	2
VW Cen	54862.359	0.41 ± 0.08	(43, 2)	0.79 ± 0.05	1	0.92 ± 0.08	1	0.49 ± 0.20	3	0.22 ± 0.01	2
AO CMa	54839.053	0.01 ± 0.06	(75, 5)	0.16 ± 0.03	2	0.10 ± 0.15	6	0.13 ± 0.02	1	0.12 ± 0.14	14	0.08 ± 0.10	3
RW CMa	54839.138	-0.07 ± 0.08	(83, 5)	0.22 ± 0.08	2	0.05 ± 0.04	12	0.03 ± 0.08	2
SS CMa	54839.066	0.06 ± 0.04	(57, 5)	0.32 ± 0.04	2	0.17 ± 0.15	6	0.12 ± 0.17	1	0.26 ± 0.18	14	0.22 ± 0.14	3
TV CMa	54847.246	0.01 ± 0.07	(89, 6)	0.25 ± 0.02	2	0.15 ± 0.12	6	0.19 ± 0.07	1	0.18 ± 0.14	13	0.08 ± 0.09	3
TW CMa	54839.077	0.04 ± 0.09	(38, 4)	0.17 ± 0.23	2	0.27 ± 0.16	11	0.27 ± 0.31	2
AA Gem	54846.149	-0.08 ± 0.05	(74, 5)	0.22 ± 0.03	2	-0.01 ± 0.15	6	0.42 ± 0.20	1	0.10 ± 0.22	5
AD Gem	54846.221	-0.14 ± 0.06	(70, 7)	0.11 ± 0.13	2	-0.23 ± 0.23	4	-0.02 ± 0.12	1	0.03 ± 0.19	12	-0.06 ± 0.13	2
BB Gem	54846.187	-0.09 ± 0.04	(70, 9)
BW Gem	54845.122	-0.22 ± 0.09	(99, 6)	-0.02 ± 0.00	2	-0.15 ± 0.19	6	-0.07 ± 0.04	1	-0.13 ± 0.14	12	-0.12 ± 0.12	2
DX Gem	54846.196	-0.01 ± 0.09	(72, 6)	0.12 ± 0.00	2	0.10 ± 0.16	3	-0.03 ± 0.15	1	0.06 ± 0.11	11	-0.03 ± 0.06	2
RZ Gem	54845.094	-0.16 ± 0.03	(44, 5)	0.19 ± 0.16	2	0.03 ± 0.07	1	0.07 ± 0.15	12	-0.12 ± 0.06	2
BE Mon	54846.201	0.05 ± 0.09	(78, 5)	0.34 ± 0.13	2	0.13 ± 0.24	6	0.33 ± 0.22	1	0.14 ± 0.16	12	0.08 ± 0.12	3
CV Mon	54846.182	0.09 ± 0.09	(52, 2)	0.31 ± 0.20	2	0.15 ± 0.16	4	0.22 ± 0.04	1	0.24 ± 0.27	11	0.18 ± 0.24	3
FT Mon	54845.104	-0.13 ± 0.08	(61, 8)	0.15 ± 0.19	2	-0.10 ± 0.17	5	-0.08 ± 0.01	1	0.02 ± 0.01	2
SV Mon	54845.119	0.12 ± 0.08	(54, 8)	0.63 ± 0.04	2	0.16 ± 0.06	6	0.30 ± 0.17	1	0.21 ± 0.16	14	0.24 ± 0.20	3
TW Mon	54796.347	-0.13 ± 0.07	(75, 6)	0.16 ± 0.06	2	-0.03 ± 0.31	6	-0.04 ± 0.07	1	-0.02 ± 0.14	13	0.02 ± 0.12	3
TX Mon	54798.345	-0.03 ± 0.05	(76, 4)	0.23 ± 0.06	2	-0.08 ± 0.11	4	-0.04 ± 0.08	1	0.06 ± 0.13	11	0.04 ± 0.10	2
TY Mon	54846.139	0.02 ± 0.08	(85, 6)	0.17 ± 0.09	2	-0.19 ± 0.07	3	0.03 ± 0.11	1	0.14 ± 0.23	11	0.12 ± 0.15	3
TZ Mon	54847.237	-0.02 ± 0.07	(94, 6)	0.16 ± 0.01	2	0.02 ± 0.08	6	0.11 ± 0.05	1	0.03 ± 0.12	12	0.04 ± 0.18	3
V465 Mon	54847.241	-0.07 ± 0.07	(107, 6)	0.26 ± 0.08	2	0.06 ± 0.17	6	-0.08 ± 0.17	1	0.12 ± 0.18	12	0.04 ± 0.08	3
V495 Mon	54846.167	-0.13 ± 0.07	(73, 4)	0.04 ± 0.08	2	-0.06 ± 0.30	6	-0.01 ± 0.18	12	-0.04 ± 0.12	3
V508 Mon	54847.232	-0.04 ± 0.10	(118, 7)	0.12 ± 0.01	2	0.04 ± 0.28	5	0.01 ± 0.05	1	0.04 ± 0.20	13	0.04 ± 0.21	2
V510 Mon	54846.153	-0.16 ± 0.06	(80, 3)	-0.05 ± 0.03	2	-0.16 ± 0.15	5	-0.04 ± 0.06	1	-0.09 ± 0.15	12	-0.15 ± 0.03	3
XX Mon	54798.335	0.01 ± 0.08	(55, 2)	0.51 ± 0.37	2	0.05 ± 0.22	4	0.21 ± 0.07	1	0.17 ± 0.23	12	0.23 ± 0.06	2
GU Nor	54667.205	0.08 ± 0.06	(80, 7)	0.32 ± 0.04	2	0.17 ± 0.10	6	0.18 ± 0.19	1	0.28 ± 0.15	13	0.09 ± 0.04	2
IQ Nor	54584.299	0.22 ± 0.07	(63, 7)	0.57 ± 0.07	2	0.39 ± 0.13	5	0.36 ± 0.13	1	0.38 ± 0.16	11	0.25 ± 0.06	3
QZ Nor	54863.366	0.18 ± 0.08	(81, 3)	0.56 ± 0.01	2	0.30 ± 0.18	6	0.38 ± 0.11	1	0.41 ± 0.16	14	0.17 ± 0.15	3
QZ Nor	54923.345	0.23 ± 0.07	(86, 2)	0.55 ± 0.05	2	0.30 ± 0.18	6	0.40 ± 0.16	1	0.40 ± 0.19	14	0.23 ± 0.16	3
RS Nor	54863.361	0.18 ± 0.08	(82, 5)	0.57 ± 0.07	2	0.39 ± 0.13	5	0.36 ± 0.13	1	0.38 ± 0.16	11	0.25 ± 0.06	3
SY Nor	54708.061	0.27 ± 0.10	(46, 5)	0.73 ± 0.25	2	0.45 ± 0.14	5	0.37 ± 0.01	1	0.39 ± 0.15	9	0.20 ± 0.13	2
SY Nor	54709.075	0.20 ± 0.09	(58, 4)	0.50 ± 0.01	2	0.36 ± 0.11	5	0.37 ± 0.09	1	0.35 ± 0.14	11	0.18 ± 0.15	3
TW Nor	54666.127	0.27 ± 0.10	(69, 7)	0.58 ± 0.11	2	0.24 ± 0.07	2	0.58 ± 0.60	1	0.25 ± 0.10	10	0.05 ± 0.06	2
V340 Nor	54873.376	0.07 ± 0.07	(47, 4)	0.40 ± 0.05	1	0.37 ± 0.08	1	0.12 ± 0.11	1	0.30 ± 0.21	9	0.19 ± 0.18	3
CS Ori	54845.085	-0.25 ± 0.06	(68, 6)	0.11 ± 0.06	2	-0.27 ± 0.14	4	-0.25 ± 0.12	1	-0.10 ± 0.13	11	-0.16 ± 0.04	2
GQ Ori	54845.082	0.20 ± 0.08	(92, 14)
RS Ori	54845.100	0.11 ± 0.09	(71, 5)	0.12 ± 0.16	2	0.11 ± 0.22	5	0.41 ± 0.17	1	0.30 ± 0.20	11	0.22 ± 0.19	4
AQ Pup	54839.075	0.06 ± 0.05	(14, 2)	0.36 ± 0.05	1	0.06 ± 0.04	1	0.25 ± 0.22	6	0.05 ± 0.00	2
BC Pup	54839.147	-0.31 ± 0.07	(57, 3)	0.20 ± 0.05	2	-0.07 ± 0.22	6	-0.14 ± 0.21	1	-0.13 ± 0.17	12	-0.18 ± 0.06	3
BM Pup	54839.086	-0.07 ± 0.08	(61, 7)	0.17 ± 0.15	2	-0.02 ± 0.18	5	0.04 ± 0.18	11	-0.01 ± 0.03	3
BN Pup	54839.109	0.03 ± 0.05	(69, 4)	0.22 ± 0.02	2	0.16 ± 0.10	6	0.23 ± 0.07	1	0.16 ± 0.14	14	0.09 ± 0.17	3
CK Pup	54839.113	-0.15 ± 0.08	(72, 4)	0.17 ± 0.06	2	-0.12 ± 0.20	5	0.00 ± 0.08	1	0.00 ± 0.21	12	-0.10 ± 0.06	2
CK Pup	54839.173	-0.12 ± 0.08	(78, 11)	0.16 ± 0.01	2	-0.05 ± 0.29	6	-0.02 ± 0.02	1	0.02 ± 0.20	12	-0.05 ± 0.06	1
HW Pup	54792.249	-0.22 ± 0.09	(70, 3)	-0.02 ± 0.01	2	-0.12 ± 0.12	6	-0.06 ± 0.14	1	-0.05 ± 0.24	13	-0.11 ± 0.12	3
LS Pup	54839.081	-0.12 ± 0.11	(18, 1)	0.42 ± 0.08	1	0.10 ± 0.10	1	0.04 ± 0.09	7	0.09 ± 0.06	1
VW Pup	54832.331	-0.14 ± 0.06	(50, 4)	0.11 ± 0.03	2	-0.04 ± 0.17	5	-0.33 ± 0.21	1	-0.03 ± 0.14	12	-0.08 ± 0.09	3
VZ Pup	54839.096	-0.01 ± 0.04	(27, 2)	0.30 ± 0.39	3	0.01 ± 0.16	1	0.25 ± 0.16	11	0.11 ± 0.01	2
WW Pup	54839.091	0.13 ± 0.16	(18, 1)	-0.30 ± 0.11	2	-0.38 ± 0.24	6	-0.34 ± 0.29	1	-0.36 ± 0.22	14	-0.70 ± 0.04	2
WY Pup	54839.100	-0.10 ± 0.08	(49, 6)	0.21 ± 0.05	1	-0.14 ± 0.29	3	0.05 ± 0.08	1	-0.01 ± 0.10	11	0.01 ± 0.05	2

continued on next page

Notes. Column 3 lists the weighted mean and standard deviation of the Fe I and Fe II abundances derived by Genovali et al. (2014). Column 4 lists the respective number (N_L) of iron lines used. The other N_L values indicate the number of lines used for the other elements to derive their abundances. For these elements, the quoted errors represent either the dispersion around the mean if two or more lines were measured, or the mean dispersion computed for the eleven calibrating stars if only one line was available.

Table 1. continued.

Name	MJD	[Fe/H]	N_L (Fe I, Fe II)	[Na/H]	N_L	[Al/H]	N_L	[Mg/H]	N_L	[Si/H]	N_L	[Ca/H]	N_L
WZ Pup	54839.104	-0.07 ± 0.06	(72, 7)	0.09 ± 0.01	2	-0.11 ± 0.07	4	0.14 ± 0.09	1	0.07 ± 0.17	13	0.04 ± 0.07	3
X Pup	54839.070	0.02 ± 0.08	(15, 2)	0.42 ± 0.05	1	0.35 ± 0.08	1	-0.01 ± 0.01	1	-0.01 ± 0.21	4	0.09 ± 0.02	2
KQ Sco	56139.021	0.26 ± 0.15	(32, 0)	0.69 ± 0.05	1	0.59 ± 0.08	1	0.18 ± 0.06	1	0.16 ± 0.06	1
KQ Sco	54873.379	0.52 ± 0.08	(51, 4)	0.17 ± 0.24	2	0.23 ± 0.06	1
KQ Sco	56152.097	0.30 ± 0.21	(16, 1)	0.72 ± 0.05	2	0.38 ± 0.02	2	0.47 ± 0.06	1	0.15 ± 0.11	2
KQ Sco	56163.004	0.22 ± 0.27	(20, 1)	0.23 ± 0.06	1
KQ Sco	56166.004	0.21 ± 0.28	(15, 1)	0.70 ± 0.05	1	0.24 ± 0.06	1
RY Sco	56140.187	0.06 ± 0.01	(74, 2)	0.31 ± 0.01	2	0.14 ± 0.04	2	0.00 ± 0.07	1	0.19 ± 0.13	3	-0.01 ± 0.14	7
RY Sco	54599.412	0.06 ± 0.02	(34, 5)	0.46 ± 0.06	2	0.11 ± 0.10	6	0.25 ± 0.14	1	0.19 ± 0.11	12	0.02 ± 0.10	3
RY Sco	56152.143	0.01 ± 0.03	(75, 3)	0.32 ± 0.06	2	0.22 ± 0.01	2	-0.01 ± 0.07	1	0.15 ± 0.18	3	-0.06 ± 0.12	7
RY Sco	56162.170	-0.03 ± 0.05	(66, 2)	0.29 ± 0.00	2	0.14 ± 0.04	2	0.01 ± 0.07	1	0.12 ± 0.09	3	-0.02 ± 0.14	7
RY Sco	56167.085	-0.04 ± 0.08	(45, 2)	0.40 ± 0.16	2	0.22 ± 0.12	2	0.00 ± 0.07	1	0.09 ± 0.08	3	-0.17 ± 0.11	3
V470 Sco	54708.073	0.16 ± 0.06	(66, 4)	0.55 ± 0.11	2	0.26 ± 0.13	5	0.18 ± 0.01	1	0.23 ± 0.09	8	0.08 ± 0.10	3
V500 Sco	56140.191	-0.01 ± 0.05	(86, 3)	0.16 ± 0.04	2	0.13 ± 0.03	2	-0.18 ± 0.07	1	0.00 ± 0.16	3	-0.17 ± 0.09	7
V500 Sco	56152.092	0.00 ± 0.10	(67, 3)	0.17 ± 0.02	2	0.03 ± 0.04	2	-0.04 ± 0.07	1	0.03 ± 0.08	3	-0.10 ± 0.11	7
V500 Sco	56162.998	-0.03 ± 0.12	(53, 3)	0.26 ± 0.08	2	0.17 ± 0.03	2	-0.05 ± 0.07	1	0.04 ± 0.07	3	-0.09 ± 0.07	5
V500 Sco	56167.077	-0.11 ± 0.07	(97, 5)	0.16 ± 0.05	2	0.14 ± 0.02	2	-0.19 ± 0.07	1	0.01 ± 0.23	3	-0.21 ± 0.12	7
EV Sct	54708.086	0.09 ± 0.07	(57, 3)	0.25 ± 0.05	1	0.56 ± 0.08	1	0.06 ± 0.14	1	0.26 ± 0.21	9	0.10 ± 0.18	2
RU Sct	54906.414	0.16 ± 0.05	(95, 7)	0.43 ± 0.11	2	0.24 ± 0.15	6	0.31 ± 0.18	1	0.35 ± 0.19	12	0.21 ± 0.25	3
RU Sct	54923.375	0.09 ± 0.07	(45, 5)	0.35 ± 0.01	2	0.17 ± 0.08	5	0.31 ± 0.12	1	0.25 ± 0.12	10	0.14 ± 0.22	3
UZ Sct	56137.160	0.28 ± 0.12	(17, 4)	0.32 ± 0.06	1	0.14 ± 0.06	1
UZ Sct	54906.400	0.36 ± 0.10	(34, 5)	0.83 ± 0.08	2	0.66 ± 0.25	5	0.36 ± 0.21	1	0.58 ± 0.15	10	0.42 ± 0.20	3
UZ Sct	54923.366	0.45 ± 0.07	(63, 7)	0.92 ± 0.08	2	0.55 ± 0.12	4	0.31 ± 0.21	1	0.48 ± 0.13	11	0.28 ± 0.16	2
UZ Sct	56152.064	0.25 ± 0.28	(8, 0)	0.41 ± 0.06	1	0.09 ± 0.06	1
UZ Sct	56160.167	0.36 ± 0.10	(47, 2)	0.72 ± 0.03	2	0.31 ± 0.07	1	0.40 ± 0.05	3	0.22 ± 0.10	5
UZ Sct	56175.049	0.31 ± 0.21	(36, 2)	0.67 ± 0.13	2	0.30 ± 0.07	1	0.48 ± 0.13	2	0.19 ± 0.05	4
V367 Sct	56137.147	0.13 ± 0.07	(72, 3)	0.28 ± 0.01	2	0.33 ± 0.08	1	-0.02 ± 0.07	1	0.17 ± 0.19	3	0.04 ± 0.18	7
V367 Sct	54709.128	-0.04 ± 0.04	(56, 4)	0.26 ± 0.02	2	0.19 ± 0.26	6	0.01 ± 0.29	1	0.14 ± 0.10	10	-0.06 ± 0.07	3
V367 Sct	56175.105	0.14 ± 0.06	(50, 3)	0.36 ± 0.05	1	0.37 ± 0.08	1	0.00 ± 0.07	1	0.18 ± 0.19	2	0.07 ± 0.15	5
V367 Sct	56184.000	0.03 ± 0.07	(84, 4)	0.31 ± 0.11	2	0.44 ± 0.08	1	0.00 ± 0.07	1	0.15 ± 0.24	2	-0.02 ± 0.10	7
X Sct	54709.122	0.12 ± 0.09	(72, 9)	0.41 ± 0.25	2	0.34 ± 0.26	5	0.12 ± 0.12	1	0.32 ± 0.27	11	0.14 ± 0.14	3
Z Sct	56137.123	0.10 ± 0.16	(20, 0)	0.77 ± 0.05	1	0.58 ± 0.08	1	-0.21 ± 0.07	1	0.13 ± 0.01	2
Z Sct	54678.090	0.18 ± 0.09	(41, 3)	0.68 ± 0.05	1	0.41 ± 0.08	1	-0.08 ± 0.23	1	0.07 ± 0.14	4	0.06 ± 0.06	1
Z Sct	56152.073	0.11 ± 0.02	(49, 2)	0.49 ± 0.05	1	0.40 ± 0.08	1	-0.06 ± 0.07	1	0.18 ± 0.14	3	-0.05 ± 0.07	4
Z Sct	56159.186	0.26 ± 0.08	(45, 2)	0.74 ± 0.14	2	0.53 ± 0.08	1	0.20 ± 0.07	1	0.38 ± 0.12	3	0.08 ± 0.04	2
Z Sct	56175.038	0.00 ± 0.30	(25, 0)	0.55 ± 0.05	1	0.44 ± 0.08	1	0.03 ± 0.06	1	-0.08 ± 0.03	2
AA Ser	54708.040	0.38 ± 0.20	(24, 1)	0.98 ± 0.05	1	0.50 ± 0.08	1	0.28 ± 0.07	1	0.47 ± 0.10	6	0.16 ± 0.06	1
CR Ser	54709.116	0.12 ± 0.08	(53, 5)	0.61 ± 0.29	2	0.29 ± 0.19	6	0.32 ± 0.22	1	0.28 ± 0.21	10	0.11 ± 0.10	3
AV Sgr	56136.169	0.40 ± 0.15	(29, 2)	0.85 ± 0.00	2	0.54 ± 0.08	1	0.48 ± 0.06	1	0.22 ± 0.01	2
AV Sgr	56136.192	0.44 ± 0.15	(31, 2)	0.93 ± 0.03	2	0.59 ± 0.08	1	0.50 ± 0.06	1	0.24 ± 0.07	2
AV Sgr	54923.348	0.53 ± 0.17	(16, 2)	0.90 ± 0.05	1	0.03 ± 0.08	1	0.35 ± 0.02	2	0.05 ± 0.06	1
AV Sgr	56152.082	0.42 ± 0.17	(24, 2)	0.77 ± 0.01	2	0.61 ± 0.04	2	0.53 ± 0.06	1	0.17 ± 0.02	2
AV Sgr	56168.049	0.30 ± 0.22	(19, 1)	0.88 ± 0.05	1	0.75 ± 0.13	2	0.49 ± 0.06	1	0.21 ± 0.04	2
AY Sgr	54599.398	0.11 ± 0.06	(58, 5)	0.32 ± 0.06	2	0.19 ± 0.17	6	0.20 ± 0.06	1	0.23 ± 0.15	14	0.11 ± 0.10	3
V1954 Sgr	54599.389	0.24 ± 0.10	(61, 4)	0.62 ± 0.06	2	0.27 ± 0.14	5	0.17 ± 0.29	1	0.47 ± 0.22	13	0.25 ± 0.08	3
V773 Sgr	54669.207	0.11 ± 0.06	(58, 8)	0.30 ± 0.05	1	0.05 ± 0.08	1	0.20 ± 0.00	1	0.30 ± 0.17	10	0.14 ± 0.02	2
VY Sgr	56160.179	0.27 ± 0.25	(14, 1)	0.73 ± 0.05	1	0.71 ± 0.08	1	0.17 ± 0.06	1	0.08 ± 0.06	1
VY Sgr	54923.356	0.42 ± 0.14	(30, 6)	0.94 ± 0.09	2	0.54 ± 0.11	6	0.53 ± 0.13	1	0.54 ± 0.16	11	0.32 ± 0.10	2
VY Sgr	56162.162	0.32 ± 0.27	(17, 1)	0.85 ± 0.05	1	0.72 ± 0.08	1	0.06 ± 0.06	1	0.09 ± 0.11	2
VY Sgr	56168.062	0.31 ± 0.05	(51, 2)	0.61 ± 0.06	2	0.19 ± 0.07	1	0.34 ± 0.08	3	0.22 ± 0.08	5
WZ Sgr	56132.190	0.18 ± 0.08	(56, 2)	0.56 ± 0.12	2	0.51 ± 0.08	1	0.04 ± 0.07	1	0.24 ± 0.11	3	0.08 ± 0.11	5
WZ Sgr	54599.395	0.35 ± 0.08	(42, 2)	0.78 ± 0.05	1	0.72 ± 0.07	2	0.48 ± 0.28	3	0.23 ± 0.06	1
WZ Sgr	56136.213	0.24 ± 0.01	(48, 2)	0.41 ± 0.05	2	0.03 ± 0.07	1	0.31 ± 0.07	3	0.18 ± 0.07	5
WZ Sgr	56152.044	0.28 ± 0.12	(28, 2)	0.56 ± 0.05	1	0.56 ± 0.08	1	0.00 ± 0.07	1	0.13 ± 0.06	1	0.13 ± 0.01	2
WZ Sgr	56159.125	0.37 ± 0.06	(44, 2)	0.65 ± 0.16	2	0.48 ± 0.33	2	-0.02 ± 0.07	1	0.36 ± 0.07	3	0.23 ± 0.09	5
XX Sgr	56054.234	-0.01 ± 0.10	(100, 5)	0.22 ± 0.05	2	0.25 ± 0.01	2	-0.05 ± 0.07	1	0.04 ± 0.13	3	-0.06 ± 0.16	7
XX Sgr	54599.404	-0.07 ± 0.07	(59, 4)	0.29 ± 0.03	2	0.02 ± 0.15	5	0.06 ± 0.05	1	0.23 ± 0.21	13	-0.03 ± 0.09	2
XX Sgr	56136.223	-0.05 ± 0.05	(101, 6)	0.20 ± 0.08	2	0.21 ± 0.08	1	-0.10 ± 0.07	1	0.07 ± 0.13	3	-0.06 ± 0.11	6
XX Sgr	56152.047	0.05 ± 0.03	(43, 3)	0.35 ± 0.11	2	0.41 ± 0.01	2	0.08 ± 0.07	1	0.14 ± 0.14	3	0.17 ± 0.20	6
XX Sgr	56159.128	-0.02 ± 0.12	(64, 4)	0.40 ± 0.29	2	0.30 ± 0.01	2	-0.04 ± 0.07	1	0.08 ± 0.05	3	-0.02 ± 0.09	5
EZ Vel	54759.348	-0.17 ± 0.15	(23, 1)	0.17 ± 0.28	2	0.01 ± 0.18	4	-0.03 ± 0.28	1	-0.08 ± 0.16	2

Table 2. Mean abundances of Fe, Na, Al, and α elements for our sample of classical Cepheids.

Name	$\log P$ [days]	R_G [pc]	[Fe/H]	[Na/H]	[Al/H]	[Mg/H]	[Si/H]	[Ca/H]	N_S
V340 Ara	1.3183	4657 ± 427	0.33 ± 0.09	0.80 ± 0.03	0.61 ± 0.10	0.34 ± 0.00	0.47 ± 0.08	0.24 ± 0.07	6
QZ Nor	0.5782	6283 ± 447	0.21 ± 0.06	0.56 ± 0.03	0.30 ± 0.18	0.39 ± 0.14	0.41 ± 0.17	0.20 ± 0.15	2
SY Nor	1.1019	6286 ± 446	0.23 ± 0.07	0.61 ± 0.13	0.41 ± 0.12	0.37 ± 0.05	0.37 ± 0.15	0.19 ± 0.14	2
CK Pup	0.8703	13357 ± 423	-0.13 ± 0.06	0.17 ± 0.03	-0.08 ± 0.24	-0.02 ± 0.02	0.02 ± 0.20	-0.08 ± 0.03	2
KQ Sco	1.4577	5948 ± 451	0.52 ± 0.08	0.70 ± 0.02	0.48 ± 0.01	...	0.26 ± 0.05	0.18 ± 0.04	5
RY Sco	1.3078	6663 ± 453	0.01 ± 0.06	0.36 ± 0.06	0.17 ± 0.06	0.08 ± 0.05	0.15 ± 0.12	-0.05 ± 0.12	5
V500 Sco	0.9693	6590 ± 453	-0.07 ± 0.08	0.19 ± 0.05	0.12 ± 0.03	-0.12 ± 0.00	0.03 ± 0.13	-0.14 ± 0.10	4
RU Sct	1.2945	6361 ± 449	0.14 ± 0.04	0.39 ± 0.06	0.21 ± 0.11	0.31 ± 0.15	0.30 ± 0.15	0.17 ± 0.23	2
UZ Sct	1.1686	5309 ± 448	0.33 ± 0.08	0.79 ± 0.08	0.60 ± 0.18	0.32 ± 0.10	0.45 ± 0.08	0.22 ± 0.09	6
V367 Sct	0.7989	6332 ± 451	0.05 ± 0.08	0.30 ± 0.04	0.33 ± 0.07	-0.01 ± 0.14	0.16 ± 0.18	0.01 ± 0.12	4
Z Sct	1.1106	5733 ± 445	0.12 ± 0.09	0.71 ± 0.05	0.51 ± 0.05	0.14 ± 0.08	0.33 ± 0.09	0.13 ± 0.06	5
AV Sgr	1.1879	5980 ± 455	0.35 ± 0.17	0.87 ± 0.01	0.50 ± 0.03	...	0.47 ± 0.00	0.18 ± 0.03	5
VY Sgr	1.1322	5862 ± 453	0.33 ± 0.12	0.78 ± 0.04	0.66 ± 0.04	0.36 ± 0.07	0.28 ± 0.06	0.18 ± 0.07	4
WZ Sgr	1.3394	6326 ± 453	0.28 ± 0.08	0.59 ± 0.07	0.57 ± 0.10	0.02 ± 0.00	0.30 ± 0.11	0.17 ± 0.06	5
XX Sgr	0.8078	6706 ± 453	-0.01 ± 0.06	0.29 ± 0.11	0.24 ± 0.04	-0.01 ± 0.01	0.11 ± 0.13	0.00 ± 0.13	5
AS Aur	0.5017	12244 ± 469	0.00 ± 0.08	0.13 ± 0.00	0.12 ± 0.40	0.12 ± 0.18	0.13 ± 0.25	-0.02 ± 0.17	1
KN Cen	1.5321	6498 ± 417	0.55 ± 0.12	0.69 ± 0.04	0.73 ± 0.17	0.32 ± 0.17	0.65 ± 0.24	0.32 ± 0.26	1
MZ Cen	1.0151	6501 ± 391	0.27 ± 0.10	0.59 ± 0.00	0.36 ± 0.18	0.21 ± 0.36	0.33 ± 0.19	0.19 ± 0.12	1
OO Cen	1.1099	6025 ± 389	0.20 ± 0.06	0.55 ± 0.00	0.24 ± 0.19	0.30 ± 0.10	0.40 ± 0.23	0.26 ± 0.12	1
TX Cen	1.2328	6070 ± 419	0.44 ± 0.12	0.73 ± 0.00	0.73 ± 0.16	0.37 ± 0.16	0.53 ± 0.27	0.47 ± 0.11	1
V339 Cen	0.9762	6917 ± 446	0.06 ± 0.03	0.53 ± 0.23	0.26 ± 0.11	0.24 ± 0.19	0.19 ± 0.18	0.02 ± 0.07	1
VW Cen	1.1771	6417 ± 405	0.41 ± 0.08	0.79 ± 0.00	0.92 ± 0.00	...	0.49 ± 0.20	0.22 ± 0.01	1
AO CMa	0.7646	10430 ± 433	0.01 ± 0.06	0.16 ± 0.03	0.10 ± 0.15	0.13 ± 0.02	0.12 ± 0.14	0.08 ± 0.10	1
RW CMa	0.7581	10057 ± 445	-0.07 ± 0.08	0.22 ± 0.08	0.05 ± 0.04	0.03 ± 0.08	1
SS CMa	1.0921	9829 ± 439	0.06 ± 0.04	0.32 ± 0.04	0.17 ± 0.15	0.12 ± 0.17	0.26 ± 0.18	0.22 ± 0.14	1
TV CMa	0.6693	9575 ± 447	0.01 ± 0.07	0.25 ± 0.02	0.15 ± 0.12	0.19 ± 0.07	0.18 ± 0.14	0.08 ± 0.09	1
TW CMa	0.8448	9788 ± 445	0.04 ± 0.09	...	0.17 ± 0.23	...	0.27 ± 0.16	0.27 ± 0.31	1
AA Gem	1.0532	11454 ± 459	-0.08 ± 0.05	0.22 ± 0.03	-0.01 ± 0.15	0.42 ± 0.20	...	0.10 ± 0.22	1
AD Gem	0.5784	10662 ± 455	-0.14 ± 0.06	0.11 ± 0.13	-0.23 ± 0.23	-0.02 ± 0.12	0.03 ± 0.19	-0.06 ± 0.13	1
BG Gem	0.3633	11199 ± 460	-0.09 ± 0.04
BW Gem	0.3633	11302 ± 463	-0.22 ± 0.09	-0.02 ± 0.00	-0.15 ± 0.19	-0.07 ± 0.04	-0.13 ± 0.14	-0.12 ± 0.12	1
DX Gem	0.4966	11407 ± 473	-0.01 ± 0.09	0.12 ± 0.00	0.10 ± 0.16	-0.03 ± 0.15	0.06 ± 0.11	-0.03 ± 0.06	1
RZ Gem	0.7427	9973 ± 454	-0.16 ± 0.03	0.19 ± 0.16	...	0.03 ± 0.00	0.07 ± 0.15	-0.12 ± 0.06	1
BE Mon	0.4322	9609 ± 452	0.05 ± 0.09	0.34 ± 0.13	0.13 ± 0.24	0.33 ± 0.22	0.14 ± 0.16	0.08 ± 0.12	1
CV Mon	0.7307	9362 ± 452	0.09 ± 0.09	0.31 ± 0.20	0.15 ± 0.16	0.22 ± 0.04	0.24 ± 0.27	0.18 ± 0.24	1
FT Mon	0.6843	14344 ± 468	-0.13 ± 0.08	0.15 ± 0.19	-0.10 ± 0.17	-0.08 ± 0.01	...	0.02 ± 0.01	1
SV Mon	1.1828	10070 ± 453	0.12 ± 0.08	0.63 ± 0.04	0.16 ± 0.06	0.30 ± 0.17	0.21 ± 0.16	0.24 ± 0.20	1
TW Mon	0.8511	13059 ± 457	-0.13 ± 0.07	0.16 ± 0.06	-0.03 ± 0.31	-0.04 ± 0.07	-0.02 ± 0.14	0.02 ± 0.12	1
TX Mon	0.9396	11790 ± 452	-0.03 ± 0.05	0.23 ± 0.06	-0.08 ± 0.11	-0.04 ± 0.08	0.06 ± 0.13	0.04 ± 0.10	1
TY Mon	0.6045	11180 ± 451	0.02 ± 0.08	0.17 ± 0.09	-0.19 ± 0.07	0.03 ± 0.11	0.14 ± 0.23	0.12 ± 0.15	1
TZ Mon	0.8709	11183 ± 451	-0.02 ± 0.07	0.16 ± 0.01	0.02 ± 0.08	0.11 ± 0.05	0.03 ± 0.12	0.04 ± 0.18	1
V465 Mon	0.4335	11037 ± 450	-0.07 ± 0.07	0.26 ± 0.08	0.06 ± 0.17	-0.08 ± 0.17	0.12 ± 0.18	0.04 ± 0.08	1
V495 Mon	0.6124	12098 ± 453	-0.13 ± 0.07	0.04 ± 0.08	-0.06 ± 0.30	...	-0.01 ± 0.18	-0.04 ± 0.12	1
V508 Mon	0.6163	10714 ± 452	-0.04 ± 0.10	0.12 ± 0.01	0.04 ± 0.28	0.01 ± 0.05	0.04 ± 0.20	0.04 ± 0.21	1
V510 Mon	0.8637	12550 ± 456	-0.16 ± 0.06	-0.05 ± 0.03	-0.16 ± 0.15	-0.04 ± 0.06	-0.09 ± 0.15	-0.15 ± 0.03	1
XX Mon	0.7369	11854 ± 451	0.01 ± 0.08	0.51 ± 0.37	0.05 ± 0.22	0.21 ± 0.07	0.17 ± 0.23	0.23 ± 0.06	1
GU Nor	0.5382	6663 ± 450	0.08 ± 0.06	0.32 ± 0.04	0.17 ± 0.10	0.18 ± 0.19	0.28 ± 0.15	0.09 ± 0.04	1
IQ Nor	0.9159	6691 ± 448	0.22 ± 0.07	0.57 ± 0.07	0.39 ± 0.13	0.36 ± 0.13	0.38 ± 0.16	0.25 ± 0.06	1
RS Nor	0.7923	6385 ± 449	0.18 ± 0.08	0.57 ± 0.07	0.39 ± 0.13	0.36 ± 0.13	0.38 ± 0.16	0.25 ± 0.06	1
TW Nor	1.0329	6160 ± 447	0.27 ± 0.10	0.58 ± 0.11	0.24 ± 0.07	0.58 ± 0.60	0.25 ± 0.10	0.05 ± 0.06	1
V340 Nor	1.0526	6483 ± 449	0.07 ± 0.07	0.40 ± 0.00	0.37 ± 0.00	0.12 ± 0.11	0.30 ± 0.21	0.19 ± 0.18	1
CS Ori	0.5899	11701 ± 458	-0.25 ± 0.06	0.11 ± 0.06	-0.27 ± 0.14	-0.25 ± 0.12	-0.10 ± 0.13	-0.16 ± 0.04	1
GQ Ori	0.9353	10129 ± 453	0.20 ± 0.08
RS Ori	0.8789	9470 ± 453	0.11 ± 0.09	0.12 ± 0.16	0.11 ± 0.22	0.41 ± 0.17	0.30 ± 0.20	0.22 ± 0.19	1
AQ Pup	1.4786	9472 ± 436	0.06 ± 0.05	0.36 ± 0.00	...	0.06 ± 0.04	0.25 ± 0.22	0.05 ± 0.00	1
BC Pup	0.5495	12763 ± 426	-0.31 ± 0.07	0.20 ± 0.05	-0.07 ± 0.22	-0.14 ± 0.21	-0.13 ± 0.17	-0.18 ± 0.06	1
BM Pup	0.8572	9981 ± 435	-0.07 ± 0.08	0.17 ± 0.15	-0.02 ± 0.18	...	0.04 ± 0.18	-0.01 ± 0.03	1
BN Pup	1.1359	9930 ± 428	0.03 ± 0.05	0.22 ± 0.02	0.16 ± 0.10	0.23 ± 0.07	0.16 ± 0.14	0.09 ± 0.17	1
HW Pup	1.1289	13554 ± 436	-0.22 ± 0.09	-0.02 ± 0.01	-0.12 ± 0.12	-0.06 ± 0.14	-0.05 ± 0.24	-0.11 ± 0.12	1
LS Pup	1.1506	10610 ± 423	-0.12 ± 0.11	...	0.42 ± 0.00	0.10 ± 0.10	0.04 ± 0.09	0.09 ± 0.00	1
VW Pup	0.6320	10175 ± 443	-0.14 ± 0.06	0.11 ± 0.03	-0.04 ± 0.17	-0.33 ± 0.21	-0.03 ± 0.14	-0.08 ± 0.09	1
VZ Pup	1.3649	10867 ± 425	-0.01 ± 0.04	...	0.30 ± 0.39	0.01 ± 0.16	0.25 ± 0.16	0.11 ± 0.01	1
WW Pup	0.7417	10382 ± 436	0.13 ± 0.16	-0.30 ± 0.11	-0.38 ± 0.24	-0.34 ± 0.29	-0.36 ± 0.22	-0.70 ± 0.04	1
WY Pup	0.7202	10549 ± 430	-0.10 ± 0.08	0.21 ± 0.00	-0.14 ± 0.29	0.05 ± 0.08	-0.01 ± 0.10	0.01 ± 0.05	1
WZ Pup	0.7013	10123 ± 437	-0.07 ± 0.06	0.09 ± 0.01	-0.11 ± 0.07	0.14 ± 0.09	0.07 ± 0.17	0.04 ± 0.07	1
X Pup	1.4143	9788 ± 441	0.02 ± 0.08	0.42 ± 0.00	0.35 ± 0.00	-0.01 ± 0.01	-0.01 ± 0.21	0.09 ± 0.02	1
V470 Sco	1.2112	6461 ± 454	0.16 ± 0.06	0.55 ± 0.11	0.26 ± 0.13	0.18 ± 0.01	0.23 ± 0.09	0.08 ± 0.10	1
EV Sct	0.4901	6135 ± 449	0.09 ± 0.07	0.25 ± 0.00	0.56 ± 0.00	0.06 ± 0.14	0.26 ± 0.21	0.10 ± 0.18	1
X Sct	0.6230	6464 ± 452	0.12 ± 0.09	0.41 ± 0.25	0.34 ± 0.26	0.12 ± 0.12	0.32 ± 0.27	0.14 ± 0.14	1
AA Ser	1.2340	5572 ± 437	0.38 ± 0.20	0.98 ± 0.00	0.50 ± 0.00	0.28 ± 0.00	0.47 ± 0.10	0.16 ± 0.00	1
CR Ser	0.7244	6510 ± 452	0.12 ± 0.08	0.61 ± 0.29	0.29 ± 0.19	0.32 ± 0.22	0.28 ± 0.21	0.11 ± 0.10	1
AY Sgr	0.8175	6429 ± 452	0.11 ± 0.06	0.32 ± 0.06	0.19 ± 0.17	0.20 ± 0.06	0.23 ± 0.15	0.11 ± 0.10	1
V1954 Sgr	0.7909	5687 ± 456	0.24 ± 0.10	0.62 ± 0.06	0.27 ± 0.14	0.17 ± 0.29	0.47 ± 0.22	0.25 ± 0.08	1
V773 Sgr	0.7596	6595 ± 454	0.11 ± 0.06	0.30 ± 0.00	0.05 ± 0.00	0.20 ± 0.00	0.30 ± 0.17	0.14 ± 0.02	1
EZ Vel	1.5383	12119 ± 358	-0.17 ± 0.15	0.17 ± 0.28	0.01 ± 0.18	-0.03 ± 0.28	...	-0.08 ± 0.16	1

Notes. The weighted (in the case of iron) or the arithmetic (for the other elements) mean abundances of the stars with multiple spectra (Table 1) are listed first. Columns 2 and 3 shows the logarithmic of the pulsation period and the Galactocentric distance (R_G), respectively. The N_S values indicate the number of spectra available for each star.

Table 3. Abundance difference of stars in common among the current sample and other data sets.

Abundance ratio	Data sets ¹	Zero-point difference	N_{Common}
[Fe/H]	LII–G14	-0.05 ± 0.11	45
[Fe/H]	LIII–G14	0.03 ± 0.08	33
[Fe/H]	LII–LEM	0.08 ± 0.12	51
[Fe/H]	LIII–YON	0.34 ± 0.20	20
[Na/H]	LII–TS	-0.13 ± 0.14	38
[Na/H]	LIII–TS	-0.10 ± 0.13	34
[Na/H]	LII–LEM	-0.11 ± 0.17	36
[Al/H]	LII–TS	-0.08 ± 0.16	36
[Al/H]	LIII–TS	-0.03 ± 0.14	33
[Al/H]	LII–LEM	-0.03 ± 0.16	41
[Mg/H]	LII–TS	-0.23 ± 0.24	26
[Mg/H]	LIII–TS	-0.10 ± 0.17	30
[Mg/H]	LII–LEM	-0.27 ± 0.24	35
[Mg/H]	LIII–YON	0.08 ± 0.15	16
[Si/H]	LII–TS	-0.11 ± 0.12	41
[Si/H]	LIII–TS	-0.06 ± 0.11	33
[Si/H]	LII–LEM	-0.06 ± 0.11	55
[Si/H]	LIII–YON	0.12 ± 0.08	18
[Ca/H]	LII–TS	-0.11 ± 0.17	42
[Ca/H]	LIII–TS	-0.08 ± 0.15	32
[Ca/H]	LII–LEM	-0.06 ± 0.17	54
[Ca/H]	LIII–YON	0.14 ± 0.11	19

Notes. ⁽¹⁾ G14: Genovali et al. (2014); TS: this study; LII: Luck et al. (2011); LIII: Luck & Lambert (2011); LEM: Lemasle et al. (2013); YON: Yong et al. (2006). The quoted errors represent the dispersion around the mean.

Table 4. Slopes and zero-points of the abundance gradients as a function of the Galactocentric distance and of the pulsation period.

Abundance ratio	Slope ^a	Zero-point [dex]	σ [dex]	N	Slope ^a (TS)	Slope ^a (LEM)	Slope ^a (LII)	Slope ^a (LIII)
as a function of R_G								
[Na/H]	-0.052 ± 0.003	0.79 ± 0.03	0.14	428	-0.072 ± 0.007	-0.066 ± 0.015	-0.044 ± 0.004	-0.047 ± 0.003
[Al/H]	-0.055 ± 0.003	0.64 ± 0.03	0.13	426	-0.073 ± 0.007	-0.046 ± 0.013	-0.053 ± 0.004	-0.049 ± 0.003
[Mg/H]	-0.045 ± 0.004	0.56 ± 0.03	0.17	417	-0.039 ± 0.007	-0.050 ± 0.013	-0.048 ± 0.006	-0.048 ± 0.004
[Si/H]	-0.049 ± 0.002	0.59 ± 0.02	0.09	432	-0.055 ± 0.005	-0.068 ± 0.009	-0.049 ± 0.003	-0.048 ± 0.002
[Ca/H]	-0.039 ± 0.002	0.42 ± 0.02	0.11	434	-0.029 ± 0.005	-0.044 ± 0.012	-0.040 ± 0.004	-0.041 ± 0.003
[Na/Fe]	0.007 ± 0.002	0.23 ± 0.02	0.11	428	-0.015 ± 0.005	-0.026 ± 0.011	0.011 ± 0.003	0.015 ± 0.002
[Al/Fe]	0.001 ± 0.002	0.09 ± 0.02	0.10	425	-0.020 ± 0.006	0.001 ± 0.012	0.004 ± 0.002	0.012 ± 0.002
[Mg/Fe]	0.013 ± 0.003	0.01 ± 0.03	0.15	415	0.015 ± 0.006	0.003 ± 0.010	0.008 ± 0.005	0.010 ± 0.003
[Si/Fe]	0.009 ± 0.001	0.04 ± 0.01	0.06	432	0.000 ± 0.003	-0.011 ± 0.007	0.006 ± 0.002	0.012 ± 0.001
[Ca/Fe]	0.018 ± 0.002	-0.12 ± 0.02	0.10	433	0.028 ± 0.004	0.010 ± 0.010	0.017 ± 0.002	0.020 ± 0.002
as a function of $\log P$								
[Na/H]	0.20 ± 0.03	0.16 ± 0.02	0.17	427	0.47 ± 0.09	0.23 ± 0.08	0.18 ± 0.03	0.10 ± 0.03
[Al/H]	0.25 ± 0.03	-0.06 ± 0.02	0.17	427	0.49 ± 0.09	0.19 ± 0.07	0.23 ± 0.03	0.13 ± 0.03
[Mg/H]	0.13 ± 0.03	0.04 ± 0.03	0.19	417	0.18 ± 0.07	0.24 ± 0.09	0.09 ± 0.04	0.07 ± 0.04
[Si/H]	0.16 ± 0.02	0.02 ± 0.02	0.14	435	0.28 ± 0.06	0.17 ± 0.07	0.14 ± 0.03	0.06 ± 0.02
[Ca/H]	0.09 ± 0.02	0.00 ± 0.02	0.13	432	0.16 ± 0.05	0.05 ± 0.07	0.05 ± 0.03	0.07 ± 0.03
[Al/Fe]	0.05 ± 0.02	0.07 ± 0.02	0.10	423	0.15 ± 0.05	0.03 ± 0.07	0.04 ± 0.02	0.06 ± 0.02
[Si/Fe]	-0.04 ± 0.01	0.15 ± 0.01	0.07	431	-0.04 ± 0.03	-0.02 ± 0.04	-0.05 ± 0.01	-0.04 ± 0.01
[Ca/Fe]	-0.11 ± 0.02	0.13 ± 0.02	0.11	436	-0.15 ± 0.04	-0.10 ± 0.05	-0.04 ± 0.02	-0.10 ± 0.02

Notes. ^(a) In units of dex kpc⁻¹ if in function of R_G , and dex per logarithmic day if in function of $\log P$. Columns from 2 to 5 shows the results for all the different samples fitted together. We also list the standard deviation (σ) of the residuals and the number of data points (N) used in the fit. The slopes using only the stars of our sample (TS: this study) and of previous studies (LEM, LII, and LIII) are shown for comparison.

Table 5. Galactic Cepheids for which the abundances of Na, Al, and α -elements was available in the literature.

Name	[Na/H] _{lit}	[Na/H]	Ref.	[Al/H] _{lit}	[Al/H]	Ref.	[Mg/H] _{lit}	[Mg/H]	Ref.	[Si/H] _{lit}	[Si/H]	Ref.	[Ca/H] _{lit}	[Ca/H]	Ref.
T Ant	-0.04	0.06	LIII	-0.09	-0.06	LIII	-0.20	-0.10	LIII	-0.09	-0.03	LIII	-0.18	-0.10	LIII
BC Aql	-0.26	-0.16	LIII	-0.48	-0.45	LIII	-0.06	0.04	LIII	-0.10	-0.04	LIII	0.01	0.09	LIII
EV Aql	0.16	0.26	LIII	0.10	0.13	LIII	0.03	0.13	LIII	0.05	0.11	LIII	-0.15	-0.07	LIII
FF Aql	0.23	0.36	LII	0.12	0.20	LII	-0.26	-0.03	LII	0.05	0.16	LII	-0.01	0.10	LII
FM Aql	0.28	0.38	LIII	0.27	0.30	LIII	0.28	0.38	LIII	0.19	0.25	LIII	0.04	0.12	LIII
FN Aql	0.19	0.29	LIII	0.01	0.04	LIII	-0.10	0.00	LIII	-0.03	0.03	LIII	-0.13	-0.05	LIII
KL Aql	0.46	0.56	LIII	0.32	0.35	LIII	0.28	0.38	LIII	0.28	0.34	LIII	0.13	0.21	LIII
SZ Aql	0.25	0.38	LII	0.31	0.39	LII	-0.08	0.15	LII	0.16	0.27	LII	0.10	0.21	LII
TT Aql	0.37	0.47	LIII	0.24	0.27	LIII	0.27	0.37	LIII	0.24	0.30	LIII	0.02	0.10	LIII
U Aql	0.32	0.42	LIII	0.27	0.30	LIII	0.09	0.19	LIII	0.16	0.22	LIII	-0.01	0.07	LIII
V1162 Aql	0.13	0.26	LII	0.13	0.21	LII	-0.19	0.04	LII	0.06	0.17	LII	-0.03	0.08	LII
V1344 Aql	0.21	0.31	LIII	0.21	0.24	LIII	0.03	0.13	LIII	0.12	0.18	LIII	-0.04	0.04	LIII
V1359 Aql	-0.19	-0.09	LIII	0.01	0.04	LIII	-0.03	0.07	LIII	0.32	0.38	LIII	-0.58	-0.50	LIII
V336 Aql	0.26	0.36	LIII	0.25	0.28	LIII	0.11	0.21	LIII	0.18	0.24	LIII	0.04	0.12	LIII
V493 Aql	0.32	0.42	LIII	0.01	0.04	LIII	0.14	0.24	LIII	0.07	0.13	LIII	0.01	0.09	LIII
V496 Aql	0.24	0.37	LII	0.10	0.18	LII	-0.12	0.11	LII	0.11	0.22	LII	-0.03	0.08	LII
V526 Aql	0.63	0.73	LIII	0.58	0.61	LIII	0.22	0.32	LIII	0.38	0.44	LIII	0.16	0.24	LIII
V600 Aql	0.30	0.43	LII	0.15	0.23	LII	0.20	0.43	LII	0.08	0.19	LII	0.06	0.17	LII
V733 Aql	0.19	0.32	LII	0.08	0.16	LII	0.22	0.45	LII	0.09	0.20	LII	-0.02	0.09	LII
V916 Aql	0.55	0.65	LIII	0.63	0.66	LIII	0.41	0.51	LIII	0.39	0.45	LIII	0.22	0.30	LIII
η Aql	0.20	0.33	LII	0.15	0.23	LII	-0.05	0.18	LII	0.12	0.23	LII	-0.02	0.09	LII
V340 Ara	0.80	0.80	TS	0.61	0.61	TS	0.34	0.34	TS	0.47	0.47	TS	0.24	0.24	TS
AN Aur	0.07	0.17	LIII	-0.08	-0.05	LIII	-0.11	-0.01	LIII	-0.09	-0.03	LIII	-0.19	-0.11	LIII
AO Aur	-0.10	-0.08	LEM	-0.11	-0.07	LEM	-0.08	-0.12	LEM	-0.15	-0.10	LEM	-0.18	-0.13	LEM
AS Aur	0.13	0.13	TS	0.12	0.12	TS	0.12	0.12	TS	0.13	0.13	TS	-0.02	-0.02	TS
AX Aur	0.17	0.19	LEM	-0.09	-0.05	LEM	-0.01	-0.05	LEM	-0.02	0.03	LEM	-0.04	0.01	LEM
BK Aur	0.51	0.61	LIII	-0.03	0.01	LEM	0.32	0.28	LEM	0.16	0.21	LEM	0.05	0.10	LEM
CO Aur	0.19	0.29	LIII	0.00	0.03	LIII	-0.12	-0.02	LIII	0.07	0.13	LIII	-0.01	0.07	LIII
CY Aur	0.06	0.16	LIII	-0.04	-0.01	LIII	-0.16	-0.06	LIII	-0.10	-0.04	LIII	-0.20	-0.12	LIII
ER Aur	-0.01	0.09	LIII	-0.17	-0.14	LIII	-0.31	-0.21	LIII	-0.18	-0.12	LIII	-0.29	-0.21	LIII
EW Aur	-0.27	-0.17	LIII	-0.20	-0.17	LIII	-0.40	-0.30	LIII	-0.31	-0.25	LIII	-0.44	-0.36	LIII
FF Aur	-0.52	-0.42	LIII	-0.64	-0.61	LIII	-0.37	-0.27	LIII	-0.33	-0.27	LIII	-0.60	-0.52	LIII
GT Aur	0.01	0.11	LIII	-0.02	0.01	LIII	-0.04	0.06	LIII	0.05	0.11	LIII	0.00	0.08	LIII
GV Aur	0.04	0.14	LIII	-0.03	-0.00	LIII	-0.09	0.01	LIII	-0.05	0.01	LIII	-0.09	-0.01	LIII
IN Aur	-0.02	0.08	LIII	-0.13	-0.10	LIII	-0.18	-0.08	LIII	-0.18	-0.12	LIII	-0.11	-0.03	LIII
RT Aur	0.37	0.47	LIII	0.14	0.17	LIII	0.17	0.27	LIII	0.19	0.25	LIII	0.09	0.17	LIII
RX Aur	0.27	0.37	LIII	0.10	0.13	LIII	0.22	0.32	LIII	0.15	0.21	LIII	0.06	0.14	LIII
SY Aur	0.35	0.37	LEM	0.01	0.05	LEM	0.16	0.12	LEM	0.12	0.17	LEM	0.06	0.11	LEM
V335 Aur	0.05	0.15	LIII	-0.12	-0.09	LIII	-0.16	-0.06	LIII	-0.08	-0.02	LIII	-0.22	-0.14	LIII
V637 Aur	-0.04	0.06	LIII	-0.19	-0.16	LIII	-0.18	-0.08	LIII	-0.13	-0.07	LIII	-0.24	-0.16	LIII
Y Aur	0.27	0.29	LEM	-0.11	-0.07	LEM	-0.01	-0.05	LEM	-0.01	0.04	LEM	-0.17	-0.12	LEM
YZ Aur	0.22	0.24	LEM	-0.14	-0.11	LIII	-0.20	-0.24	LEM	-0.13	-0.08	LEM	-0.14	-0.09	LEM
AOC Ma	0.16	0.16	TS	0.10	0.10	TS	0.13	0.13	TS	0.12	0.12	TS	0.08	0.08	TS
RW CMa	0.22	0.22	TS	0.05	0.05	TS	0.03	0.03	TS
RY CMa	0.12	0.14	LEM	0.12	0.16	LEM	0.07	0.03	LEM	0.07	0.12	LEM	0.02	0.07	LEM
RZ CMa	0.06	0.08	LEM	-0.12	-0.04	LII	0.12	0.08	LEM	0.06	0.17	LII	0.12	0.17	LEM
SS CMa	0.32	0.32	TS	0.17	0.17	TS	0.12	0.12	TS	0.26	0.26	TS	0.22	0.22	TS
TV CMa	0.25	0.25	TS	0.15	0.15	TS	0.19	0.19	TS	0.18	0.18	TS	0.08	0.08	TS
TW CMa	-0.03	0.10	LII	0.17	0.17	TS	-0.23	-0.27	LEM	0.27	0.27	TS	0.27	0.27	TS
VZ CMa	0.16	0.29	LII	0.00	0.11	LII	-0.06	0.05	LII
XZ CMa	-0.20	-0.02	YON	-0.43	-0.21	YON
AB Cam	0.09	0.19	LIII	-0.05	-0.02	LIII	-0.11	-0.01	LIII	-0.05	0.01	LIII	-0.15	-0.07	LIII
AC Cam	0.18	0.28	LIII	-0.01	0.02	LIII	-0.15	-0.05	LIII	-0.02	0.04	LIII	-0.03	0.05	LIII
AD Cam	0.07	0.17	LIII	-0.07	-0.04	LIII	-0.06	0.04	LIII	-0.15	-0.09	LIII	-0.20	-0.12	LIII
AM Cam	0.08	0.18	LIII	-0.10	-0.07	LIII	-0.01	0.09	LIII	-0.02	0.04	LIII	-0.01	0.07	LIII
CK Cam	0.19	0.29	LIII	0.10	0.13	LIII	0.15	0.25	LIII	0.12	0.18	LIII	0.07	0.15	LIII
LO Cam	0.12	0.22	LIII	-0.14	-0.11	LIII	-0.06	0.04	LIII	-0.07	-0.01	LIII	-0.19	-0.11	LIII
MN Cam	0.18	0.28	LIII	0.04	0.07	LIII	0.01	0.11	LIII	0.02	0.08	LIII	-0.08	-0.00	LIII
MQ Cam	0.18	0.28	LIII	-0.01	0.02	LIII	0.00	0.10	LIII	-0.09	-0.03	LIII	-0.18	-0.10	LIII
OX Cam	0.02	0.12	LIII	-0.06	-0.03	LIII	-0.16	-0.06	LIII	-0.07	-0.01	LIII	-0.26	-0.18	LIII
PV Cam	-0.06	0.04	LIII	-0.13	-0.10	LIII	-0.19	-0.09	LIII	-0.09	-0.03	LIII	-0.15	-0.07	LIII
QS Cam	-0.07	0.03	LIII	0.07	0.10	LIII	0.29	0.39	LIII	0.07	0.13	LIII	-0.07	0.01	LIII
RW Cam	0.07	0.17	LIII	0.33	0.36	LIII	0.13	0.23	LIII	0.13	0.19	LIII	-0.28	-0.20	LIII
RX Cam	0.22	0.32	LIII	0.16	0.19	LIII	0.20	0.30	LIII	0.11	0.17	LIII	0.03	0.11	LIII
TV Cam	0.19	0.29	LIII	-0.03	-0.00	LIII	-0.07	0.03	LIII	0.02	0.08	LIII	-0.05	0.03	LIII
V359 Cam	0.08	0.18	LIII	-0.12	-0.09	LIII	-0.02	0.08	LIII	-0.07	-0.01	LIII	-0.07	0.01	LIII
AQ Car	0.15	0.25	LIII	0.28	0.32	LEM	0.38	0.34	LEM	0.18	0.23	LEM	0.36	0.41	LEM
CN Car	0.42	0.52	LIII	0.10	0.13	LIII	0.18	0.28	LIII	0.20	0.26	LIII	0.14	0.22	LIII
CY Car	0.25	0.35	LIII	0.17	0.20	LIII	0.08	0.18	LIII	0.13	0.19	LIII	0.05	0.13	LIII
DY Car	0.28	0.38	LIII	0.08	0.11	LIII	0.11	0.21	LIII	0.09	0.15	LIII	-0.05	0.03	LIII
ER Car	0.22	0.32	LIII	0.17	0.20	LIII	0.21	0.31	LIII	0.13	0.19	LIII	0.05	0.13	LIII
FI Car	0.21	0.31	LIII	0.28	0.31	LIII	0.24	0.34	LIII	0.28	0.34	LIII	0.14	0.22	LIII
FR Car	0.14	0.24	LIII	0.11	0.14	LIII	0.00	0.10	LIII	0.08	0.14	LIII	-0.08	-0.00	LIII
GH Car	0.41	0.51	LIII	0.15	0.18	LIII	0.23	0.33	LIII	0.21	0.27	LIII	0.11	0.19	LIII
GX Car	0.19	0.29	LIII	0.15	0.18	LIII	0.33	0.43	LIII	0.17	0.23	LIII	0.07	0.15	LIII

continued on next page

Table 5. continued.

Name	[Na/H] _{lit}	[Na/H]	Ref.	[Al/H] _{lit}	[Al/H]	Ref.	[Mg/H] _{lit}	[Mg/H]	Ref.	[Si/H] _{lit}	[Si/H]	Ref.	[Ca/H] _{lit}	[Ca/H]	Ref.
HQ Car	0.03	0.21	YON	-0.45	-0.23	YON
HW Car	0.24	0.34	LIII	0.09	0.12	LIII	-0.04	0.06	LIII	0.05	0.11	LIII	-0.08	-0.00	LIII
IO Car	0.15	0.25	LIII	0.05	0.08	LIII	-0.09	0.01	LIII	0.04	0.10	LIII	-0.17	-0.09	LIII
IT Car	0.36	0.46	LIII	0.25	0.28	LIII	0.25	0.35	LIII	0.19	0.25	LIII	0.13	0.21	LIII
L Car	-0.01	0.09	LIII	0.11	0.15	LEM	0.01	0.11	LIII	0.20	0.25	LEM	0.00	0.05	LEM
SX Car	0.29	0.39	LIII	0.02	0.05	LIII	0.24	0.34	LIII	0.14	0.20	LIII	0.01	0.09	LIII
U Car	0.43	0.53	LIII	0.41	0.44	LIII	0.22	0.45	LII	0.23	0.29	LIII	0.10	0.18	LIII
UW Car	0.18	0.28	LIII	0.05	0.08	LIII	0.26	0.36	LIII	0.14	0.20	LIII	0.09	0.17	LIII
UX Car	0.27	0.37	LIII	0.32	0.36	LEM	-0.06	-0.10	LEM	0.05	0.10	LEM	0.14	0.19	LEM
UY Car	0.23	0.33	LIII	0.12	0.15	LIII	0.46	0.56	LIII	0.19	0.25	LIII	0.17	0.25	LIII
UZ Car	0.20	0.30	LIII	0.17	0.20	LIII	0.38	0.48	LIII	0.21	0.27	LIII	0.19	0.27	LIII
V Car	0.20	0.30	LIII	0.23	0.27	LEM	0.31	0.27	LEM	0.20	0.25	LEM	0.31	0.36	LEM
V397 Car	0.22	0.32	LIII	0.21	0.25	LEM	0.14	0.24	LIII	0.20	0.25	LEM	0.09	0.14	LEM
VY Car	0.29	0.31	LEM	0.71	0.74	LIII	0.14	0.10	LEM	0.49	0.54	LEM	0.16	0.21	LEM
WW Car	0.20	0.30	LIII	0.12	0.15	LIII	0.04	0.14	LIII	0.05	0.11	LIII	0.00	0.08	LIII
WZ Car	0.43	0.53	LIII	0.19	0.22	LIII	0.45	0.55	LIII	0.10	0.16	LIII	0.06	0.14	LIII
XX Car	0.36	0.46	LIII	0.31	0.34	LIII	0.17	0.27	LIII	0.19	0.25	LIII	0.08	0.16	LIII
XY Car	0.20	0.30	LIII	0.16	0.19	LIII	0.11	0.21	LIII	0.13	0.19	LIII	0.01	0.09	LIII
XZ Car	0.44	0.54	LIII	0.29	0.32	LIII	0.28	0.38	LIII	0.27	0.33	LIII	0.22	0.30	LIII
YZ Car	0.16	0.26	LIII	0.12	0.15	LIII	0.15	0.25	LIII	0.07	0.13	LIII	-0.03	0.05	LIII
AP Cas	0.24	0.34	LIII	0.11	0.14	LIII	-0.02	0.08	LIII	0.05	0.11	LIII	-0.06	0.02	LIII
AS Cas	0.12	0.22	LIII	-0.10	-0.07	LIII	0.38	0.48	LIII	0.07	0.13	LIII	0.11	0.19	LIII
AW Cas	0.06	0.16	LIII	0.02	0.05	LIII	0.05	0.15	LIII	0.03	0.09	LIII	-0.04	0.04	LIII
AY Cas	0.13	0.23	LIII	0.07	0.10	LIII	0.09	0.19	LIII	0.08	0.14	LIII	0.03	0.11	LIII
BF Cas	0.11	0.21	LIII	-0.04	-0.01	LIII	-0.13	-0.03	LIII	0.10	0.16	LIII	-0.02	0.06	LIII
BP Cas	0.24	0.34	LIII	0.06	0.09	LIII	0.03	0.13	LIII	0.09	0.15	LIII	0.02	0.10	LIII
BV Cas	0.09	0.19	LIII	0.12	0.15	LIII	0.05	0.15	LIII	0.06	0.12	LIII	-0.02	0.06	LIII
BY Cas	0.26	0.36	LIII	0.11	0.14	LIII	0.18	0.28	LIII	0.21	0.27	LIII	0.09	0.17	LIII
CD Cas	0.29	0.39	LIII	0.11	0.14	LIII	0.21	0.27	LIII	0.06	0.14	LIII
CF Cas	0.20	0.30	LIII	0.16	0.19	LIII	0.10	0.20	LIII	0.06	0.12	LIII	0.01	0.09	LIII
CG Cas	0.28	0.38	LIII	0.03	0.06	LIII	0.21	0.31	LIII	0.13	0.19	LIII	0.04	0.12	LIII
CH Cas	0.28	0.41	LII	0.14	0.25	LII	-0.04	0.07	LII
CT Cas	0.26	0.36	LIII	0.04	0.07	LIII	-0.08	0.02	LIII	0.02	0.08	LIII	-0.01	0.07	LIII
CY Cas	0.08	0.16	LII	0.11	0.22	LII	-0.01	0.10	LII
CZ Cas	0.16	0.26	LIII	0.09	0.12	LIII	0.09	0.19	LIII	0.09	0.15	LIII	0.00	0.08	LIII
DD Cas	0.30	0.43	LII	0.10	0.18	LII	0.20	0.43	LII	0.10	0.21	LII	0.00	0.11	LII
DF Cas	0.16	0.29	LII	-0.33	-0.10	LII	0.03	0.14	LII	-0.18	-0.07	LII
DL Cas	0.11	0.24	LII	0.14	0.22	LII	0.11	0.34	LII	0.02	0.13	LII	0.01	0.12	LII
DW Cas	0.25	0.35	LIII	0.15	0.18	LIII	0.23	0.33	LIII	0.12	0.18	LIII	0.04	0.12	LIII
EX Cas	0.28	0.38	LIII	0.13	0.16	LIII	0.01	0.11	LIII	0.07	0.13	LIII	0.15	0.23	LIII
FM Cas	0.17	0.30	LII	0.30	0.38	LII	0.20	0.43	LII	0.09	0.20	LII	0.14	0.25	LII
FO Cas	0.07	0.17	LIII	-0.12	-0.09	LIII	-0.34	-0.24	LIII	-0.27	-0.21	LIII	-0.46	-0.38	LIII
FW Cas	-0.03	0.07	LIII	0.02	0.05	LIII	-0.16	-0.06	LIII	-0.07	-0.01	LIII	-0.05	0.03	LIII
GL Cas	0.32	0.42	LIII	0.19	0.22	LIII	0.37	0.47	LIII	0.07	0.13	LIII	0.15	0.23	LIII
GM Cas	0.15	0.25	LIII	-0.18	-0.15	LIII	-0.18	-0.08	LIII	-0.10	-0.04	LIII	-0.10	-0.02	LIII
GO Cas	0.33	0.43	LIII	0.09	0.12	LIII	0.01	0.11	LIII	0.19	0.25	LIII	0.13	0.21	LIII
HK Cas	0.81	0.91	LIII	0.72	0.75	LIII	0.59	0.69	LIII	0.52	0.58	LIII	0.33	0.41	LIII
IO Cas	0.09	0.19	LIII	-0.05	-0.02	LIII	-0.12	-0.02	LIII	-0.17	-0.11	LIII	-0.24	-0.16	LIII
KK Cas	0.34	0.44	LIII	0.17	0.20	LIII	0.04	0.14	LIII	0.15	0.21	LIII	0.14	0.22	LIII
LT Cas	-0.09	0.01	LIII	-0.23	-0.20	LIII	-0.29	-0.19	LIII	-0.28	-0.22	LIII	-0.35	-0.27	LIII
NP Cas	0.07	0.17	LIII	0.01	0.04	LIII	0.01	0.11	LIII	0.07	0.13	LIII	0.04	0.12	LIII
NY Cas	-0.12	-0.02	LIII	0.09	0.12	LIII	-0.40	-0.30	LIII	-0.21	-0.15	LIII	-0.40	-0.32	LIII
OP Cas	0.49	0.59	LIII	0.27	0.30	LIII	0.14	0.24	LIII	0.19	0.25	LIII	0.15	0.23	LIII
OZ Cas	0.07	0.17	LIII	0.03	0.06	LIII	-0.07	0.03	LIII	0.13	0.19	LIII	0.07	0.15	LIII
PW Cas	0.12	0.22	LIII	-0.06	-0.03	LIII	-0.04	0.06	LIII	-0.03	0.03	LIII	-0.14	-0.06	LIII
RS Cas	0.36	0.46	LIII	0.10	0.13	LIII	0.11	0.21	LIII	0.19	0.25	LIII	0.13	0.21	LIII
RW Cas	0.05	0.13	LII	0.13	0.24	LII	0.28	0.39	LII
RY Cas	0.26	0.39	LII	0.15	0.23	LII	0.22	0.33	LII	-0.07	0.04	LII
SU Cas	0.26	0.39	LII	0.10	0.18	LII	-0.22	0.01	LII	0.09	0.20	LII	0.07	0.18	LII
SW Cas	0.26	0.39	LII	0.22	0.30	LII	0.12	0.23	LII	0.04	0.15	LII
SY Cas	0.16	0.29	LII	0.15	0.23	LII	0.32	0.55	LII	0.07	0.18	LII	0.10	0.21	LII
SZ Cas	0.34	0.44	LIII	0.08	0.11	LIII	0.20	0.30	LIII	0.14	0.20	LIII	0.07	0.15	LIII
TU Cas	0.15	0.28	LII	0.14	0.22	LII	-0.19	0.04	LII	0.10	0.21	LII	-0.02	0.09	LII
UZ Cas	0.22	0.32	LIII	0.01	0.04	LIII	-0.23	-0.13	LIII	-0.02	0.04	LIII	-0.03	0.05	LIII
V1017 Cas	0.05	0.15	LIII	-0.14	-0.11	LIII	-0.21	-0.11	LIII	-0.16	-0.10	LIII	-0.25	-0.17	LIII
V1019 Cas	0.22	0.32	LIII	0.08	0.11	LIII	0.12	0.22	LIII	0.11	0.17	LIII	0.08	0.16	LIII
V1020 Cas	0.29	0.39	LIII	0.25	0.28	LIII	0.20	0.30	LIII	0.17	0.23	LIII	0.09	0.17	LIII
V1100 Cas	0.11	0.21	LIII	-0.28	-0.25	LIII	0.04	0.14	LIII	-0.06	-0.00	LIII	-0.16	-0.08	LIII
V1154 Cas	0.10	0.20	LIII	-0.07	-0.04	LIII	0.10	0.20	LIII	-0.09	-0.03	LIII	-0.27	-0.19	LIII
V1206 Cas	0.10	0.20	LIII	0.03	0.06	LIII	0.08	0.18	LIII	-0.01	0.05	LIII	-0.15	-0.07	LIII
V342 Cas	0.17	0.27	LIII	0.09	0.12	LIII	-0.08	0.02	LIII	0.08	0.14	LIII	0.04	0.12	LIII
V379 Cas	0.21	0.34	LII	0.23	0.31	LII	0.19	0.30	LII	0.18	0.29	LII
V395 Cas	0.28	0.38	LII	0.16	0.19	LII	0.07	0.17	LII	0.11	0.17	LII	0.01	0.09	LII
V407 Cas	0.36	0.46	LIII	0.20	0.23	LIII	-0.01	0.09	LIII	0.11	0.17	LIII	0.06	0.14	LIII
V556 Cas	0.24	0.34	LIII	0.06	0.09	LIII	0.05	0.15	LIII	0.02	0.08	LIII	-0.05	0.03	LIII

continued on next page

Table 5. continued.

Name	[Na/H] _{lit}	[Na/H]	Ref.	[Al/H] _{lit}	[Al/H]	Ref.	[Mg/H] _{lit}	[Mg/H]	Ref.	[Si/H] _{lit}	[Si/H]	Ref.	[Ca/H] _{lit}	[Ca/H]	Ref.
V636 Cas	0.28	0.41	LII	0.12	0.20	LII	-0.14	0.09	LII	0.06	0.17	LII	0.06	0.17	LII
VV Cas	0.15	0.25	LIII	0.00	0.03	LIII	-0.15	-0.05	LIII	0.04	0.10	LIII	-0.09	-0.01	LIII
VW Cas	0.20	0.30	LIII	0.21	0.24	LIII	0.24	0.34	LIII	0.14	0.20	LIII	0.10	0.18	LIII
XY Cas	0.37	0.47	LIII	0.12	0.15	LIII	0.16	0.26	LIII	0.14	0.20	LIII	0.10	0.18	LIII
AY Cen	0.26	0.36	LIII	0.12	0.15	LIII	-0.01	0.09	LIII	0.08	0.14	LIII	0.00	0.08	LIII
AZ Cen	0.24	0.34	LIII	0.03	0.06	LIII	0.02	0.12	LIII	0.10	0.16	LIII	-0.03	0.05	LIII
BB Cen	0.30	0.40	LIII	0.18	0.21	LIII	0.11	0.21	LIII	0.19	0.25	LIII	0.01	0.09	LIII
KK Cen	0.52	0.62	LIII	0.27	0.30	LIII	0.18	0.28	LIII	0.24	0.30	LIII	0.16	0.24	LIII
KN Cen	0.69	0.69	TS	0.73	0.73	TS	0.32	0.32	TS	0.65	0.65	TS	0.32	0.32	TS
MZ Cen	0.59	0.59	TS	0.36	0.36	TS	0.21	0.21	TS	0.33	0.33	TS	0.19	0.19	TS
OO Cen	0.55	0.55	TS	0.24	0.24	TS	0.30	0.30	TS	0.40	0.40	TS	0.26	0.26	TS
QY Cen	0.41	0.51	LIII	0.21	0.24	LIII	-0.17	-0.07	LIII	0.24	0.30	LIII	0.11	0.19	LIII
TX Cen	0.73	0.73	TS	0.73	0.73	TS	0.37	0.37	TS	0.53	0.53	TS	0.47	0.47	TS
V Cen	0.28	0.38	LIII	0.10	0.13	LIII	0.02	0.12	LIII	0.09	0.15	LIII	-0.07	0.01	LIII
V339 Cen	0.53	0.53	TS	0.26	0.26	TS	0.24	0.24	TS	0.19	0.19	TS	0.02	0.02	TS
V378 Cen	0.25	0.35	LIII	0.06	0.09	LIII	-0.05	0.05	LIII	0.07	0.13	LIII	-0.09	-0.01	LIII
V381 Cen	0.20	0.30	LIII	0.08	0.11	LIII	0.00	0.10	LIII	0.08	0.14	LIII	-0.03	0.05	LIII
V419 Cen	0.36	0.46	LIII	0.33	0.36	LIII	0.42	0.52	LIII	0.20	0.26	LIII	0.16	0.24	LIII
V496 Cen	0.36	0.46	LIII	0.13	0.16	LIII	0.12	0.22	LIII	0.14	0.20	LIII	0.06	0.14	LIII
V659 Cen	0.19	0.29	LIII	0.14	0.17	LIII	0.00	0.10	LIII	0.09	0.15	LIII	-0.05	0.03	LIII
V737 Cen	0.25	0.35	LIII	0.16	0.19	LIII	0.01	0.11	LIII	0.11	0.17	LIII	-0.04	0.04	LIII
VW Cen	0.79	0.79	TS	0.92	0.92	TS	0.49	0.49	TS	0.22	0.22	TS
XX Cen	0.24	0.34	LIII	0.21	0.24	LIII	0.10	0.20	LIII	0.17	0.23	LIII	0.01	0.09	LIII
AK Cep	0.08	0.18	LIII	0.08	0.11	LIII	0.21	0.31	LIII	0.12	0.18	LIII	0.03	0.11	LIII
CN Cep	0.29	0.39	LIII	-0.15	-0.12	LIII	0.12	0.22	LIII	0.06	0.12	LIII	-0.03	0.05	LIII
CP Cep	0.13	0.26	LII	0.07	0.15	LII	0.10	0.33	LII	0.10	0.21	LII	0.14	0.25	LII
CR Cep	0.09	0.22	LII	0.19	0.27	LII	0.39	0.62	LII	0.02	0.13	LII	0.02	0.13	LII
DR Cep	0.02	0.12	LIII	-0.06	-0.03	LIII	-0.36	-0.26	LIII	-0.10	-0.04	LIII	-0.47	-0.39	LIII
IR Cep	0.36	0.49	LII	0.24	0.32	LII	-0.08	0.15	LII	0.19	0.30	LII	0.08	0.19	LII
IY Cep	0.19	0.29	LIII	0.14	0.17	LIII	0.01	0.11	LIII	0.07	0.13	LIII	-0.02	0.06	LIII
MU Cep	0.20	0.30	LIII	-0.03	-0.00	LIII	0.46	0.56	LIII	0.11	0.17	LIII	-0.01	0.07	LIII
V901 Cep	0.12	0.22	LIII	-0.03	-0.00	LIII	0.16	0.26	LIII	0.07	0.13	LIII	0.04	0.12	LIII
V911 Cep	0.35	0.45	LIII	-0.11	-0.08	LIII	0.24	0.34	LIII	0.09	0.15	LIII	0.02	0.10	LIII
δ Cep	0.28	0.38	LIII	0.19	0.22	LIII	0.10	0.20	LIII	0.14	0.20	LIII	0.01	0.09	LIII
AV Cir	0.21	0.31	LIII	0.13	0.16	LIII	0.09	0.19	LIII	0.15	0.21	LIII	-0.01	0.07	LIII
AX Cir	0.17	0.27	LIII	0.03	0.06	LIII	-0.08	0.02	LIII	0.01	0.07	LIII	-0.12	-0.04	LIII
BP Cir	0.12	0.22	LIII	-0.05	-0.02	LIII	0.11	0.21	LIII	0.10	0.16	LIII	-0.06	0.02	LIII
AD Cru	0.31	0.41	LIII	0.07	0.10	LIII	0.24	0.34	LIII	0.14	0.20	LIII	0.09	0.17	LIII
AG Cru	0.31	0.41	LIII	-0.03	-0.00	LIII	0.14	0.24	LIII	0.14	0.20	LIII	0.04	0.12	LIII
BG Cru	-0.13	-0.03	LIII	0.13	0.16	LIII	0.30	0.40	LIII	-0.07	-0.01	LIII	-0.16	-0.08	LIII
R Cru	0.23	0.33	LIII	0.14	0.17	LIII	0.09	0.19	LIII	0.14	0.20	LIII	0.05	0.13	LIII
S Cru	0.23	0.33	LIII	0.10	0.13	LIII	0.15	0.25	LIII	0.16	0.22	LIII	0.07	0.15	LIII
T Cru	0.22	0.32	LIII	0.17	0.20	LIII	0.02	0.12	LIII	0.11	0.17	LIII	-0.01	0.07	LIII
VW Cru	0.29	0.39	LIII	0.18	0.21	LIII	0.07	0.17	LIII	0.15	0.21	LIII	0.01	0.09	LIII
X Cru	0.36	0.46	LIII	0.22	0.25	LIII	0.18	0.28	LIII	0.16	0.22	LIII	0.08	0.16	LIII
BZ Cyg	0.38	0.51	LII	0.24	0.32	LII	0.29	0.40	LII	0.17	0.28	LII
CD Cyg	0.34	0.44	LIII	0.34	0.37	LIII	0.18	0.28	LIII	0.27	0.33	LIII	0.22	0.30	LIII
DT Cyg	0.28	0.41	LII	0.13	0.21	LII	-0.05	0.18	LII	0.12	0.23	LII	0.09	0.20	LII
EP Cyg	0.12	0.22	LIII	0.01	0.04	LIII	-0.07	0.03	LIII	-0.01	0.05	LIII	-0.01	0.07	LIII
EU Cyg	0.01	0.11	LIII	0.07	0.10	LIII	-0.10	0.00	LIII	-0.04	0.02	LIII	-0.17	-0.09	LIII
EX Cyg	0.44	0.54	LIII	0.21	0.24	LIII	-0.13	-0.03	LIII	0.20	0.26	LIII	0.01	0.09	LIII
EZ Cyg	0.60	0.70	LIII	0.44	0.47	LIII	0.45	0.55	LIII	0.36	0.42	LIII	0.25	0.33	LIII
GH Cyg	0.24	0.34	LIII	0.14	0.17	LIII	-0.02	0.08	LIII	0.17	0.23	LIII	0.01	0.09	LIII
GI Cyg	0.34	0.44	LIII	0.32	0.35	LIII	0.49	0.59	LIII	0.22	0.28	LIII	0.21	0.29	LIII
GL Cyg	0.16	0.26	LIII	0.07	0.10	LIII	-0.14	-0.04	LIII	0.04	0.10	LIII	0.00	0.08	LIII
IY Cyg	0.08	0.18	LIII	0.03	0.06	LIII	-0.11	-0.01	LIII	-0.10	-0.04	LIII	-0.23	-0.15	LIII
KX Cyg	0.05	0.15	LIII	0.18	0.21	LIII	0.09	0.19	LIII	0.15	0.21	LIII	-0.05	0.03	LIII
MW Cyg	0.15	0.28	LII	0.18	0.26	LII	0.08	0.31	LII	0.06	0.17	LII	-0.01	0.10	LII
SU Cyg	0.21	0.34	LII	0.14	0.22	LII	-0.16	0.07	LII	0.04	0.15	LII	0.03	0.14	LII
SZ Cyg	0.44	0.57	LII	0.22	0.30	LII	0.03	0.26	LII	0.25	0.36	LII	0.19	0.30	LII
TX Cyg	0.32	0.45	LII	0.21	0.29	LII	0.22	0.33	LII	0.15	0.26	LII
V1020 Cyg	0.44	0.54	LIII	0.20	0.23	LIII	-0.08	0.02	LIII	0.18	0.24	LIII	0.12	0.20	LIII
V1025 Cyg	0.24	0.34	LIII	0.25	0.28	LIII	0.16	0.26	LIII	0.20	0.26	LIII	0.06	0.14	LIII
V1033 Cyg	-0.01	0.09	LIII	0.14	0.17	LIII	0.12	0.22	LIII	0.14	0.20	LIII	0.06	0.14	LIII
V1046 Cyg	0.37	0.47	LIII	0.24	0.27	LIII	0.28	0.38	LIII	0.23	0.29	LIII	0.08	0.16	LIII
V1154 Cyg	0.11	0.24	LII	0.09	0.17	LII	0.53	0.76	LII	0.04	0.15	LII	0.13	0.24	LII
V1334 Cyg	0.19	0.32	LII	0.17	0.25	LII	-0.29	-0.06	LII	0.06	0.17	LII	-0.02	0.09	LII
V1364 Cyg	0.42	0.52	LIII	0.38	0.41	LIII	0.28	0.38	LIII	0.31	0.37	LIII	0.10	0.18	LIII
V1397 Cyg	0.17	0.27	LIII	0.15	0.18	LIII	0.30	0.40	LIII	0.11	0.17	LIII	0.01	0.09	LIII
V1726 Cyg	0.29	0.42	LII	0.07	0.15	LII	-0.12	0.11	LII	0.11	0.22	LII	-0.16	-0.05	LII
V347 Cyg	0.36	0.46	LIII	0.14	0.17	LIII	0.30	0.40	LIII	0.22	0.28	LIII	0.12	0.20	LIII
V356 Cyg	0.33	0.43	LIII	0.22	0.25	LIII	0.02	0.12	LIII	0.19	0.25	LIII	0.09	0.17	LIII
V386 Cyg	0.23	0.36	LII	0.15	0.23	LII	0.14	0.25	LII	0.02	0.13	LII
V396 Cyg	0.30	0.40	LIII	0.32	0.35	LIII	0.19	0.29	LIII	0.17	0.23	LIII	0.29	0.37	LIII
V402 Cyg	0.40	0.53	LII	0.19	0.27	LII	0.15	0.38	LII	0.08	0.19	LII	0.12	0.23	LII

continued on next page

Table 5. continued.

Name	[Na/H] _{lit}	[Na/H]	Ref.	[Al/H] _{lit}	[Al/H]	Ref.	[Mg/H] _{lit}	[Mg/H]	Ref.	[Si/H] _{lit}	[Si/H]	Ref.	[Ca/H] _{lit}	[Ca/H]	Ref.
V438 Cyg	0.11	0.21	LIII	0.17	0.20	LIII	-0.27	-0.17	LIII	0.14	0.20	LIII	-0.03	0.05	LIII
V459 Cyg	0.38	0.48	LIII	0.28	0.31	LIII	0.26	0.36	LIII	0.24	0.30	LIII	0.10	0.18	LIII
V492 Cyg	0.32	0.42	LIII	0.23	0.26	LIII	0.18	0.28	LIII	0.17	0.23	LIII	0.05	0.13	LIII
V495 Cyg	0.44	0.54	LIII	0.20	0.23	LIII	LIII	0.26	0.32	LIII	0.11	0.19	LIII
V514 Cyg	0.32	0.42	LIII	0.13	0.16	LIII	0.18	0.28	LIII	0.17	0.23	LIII	0.07	0.15	LIII
V520 Cyg	0.26	0.36	LIII	0.24	0.27	LIII	-0.05	0.05	LIII	0.17	0.23	LIII	0.10	0.18	LIII
V532 Cyg	0.26	0.39	LII	0.16	0.24	LII	0.14	0.37	LII	0.15	0.26	LII	0.12	0.23	LII
V538 Cyg	0.25	0.35	LIII	0.14	0.17	LIII	-0.06	0.04	LIII	0.13	0.19	LIII	0.03	0.11	LIII
V547 Cyg	0.26	0.36	LIII	0.24	0.27	LIII	0.24	0.34	LIII	0.16	0.22	LIII	0.05	0.13	LIII
V609 Cyg	0.32	0.42	LIII	0.21	0.24	LIII	0.04	0.14	LIII	0.20	0.26	LIII	0.02	0.10	LIII
V621 Cyg	0.31	0.41	LIII	0.11	0.14	LIII	0.22	0.32	LIII	0.15	0.21	LIII	0.02	0.10	LIII
V924 Cyg	-0.04	0.09	LII	0.09	0.17	LII	-0.38	-0.15	LII	-0.04	0.07	LII	-0.21	-0.10	LII
VX Cyg	0.41	0.54	LII	0.13	0.21	LII	-0.16	0.07	LII	0.18	0.29	LII	0.20	0.31	LII
VY Cyg	0.23	0.36	LII	0.15	0.23	LII	0.19	0.42	LII	0.06	0.17	LII	0.06	0.17	LII
VZ Cyg	0.26	0.39	LII	0.39	0.47	LII	0.21	0.44	LII	0.10	0.21	LII	0.03	0.14	LII
X Cyg	0.25	0.38	LII	0.25	0.33	LII	0.04	0.27	LII	0.09	0.20	LII	0.09	0.20	LII
EK Del	-1.62	-1.52	LIII	-0.75	-0.72	LIII	-1.53	-1.43	LIII	-1.17	-1.11	LIII	-1.24	-1.16	LIII
β Dor	0.07	0.20	LII	0.07	0.15	LII	-0.30	-0.07	LII	0.00	0.11	LII	-0.18	-0.07	LII
AA Gem	0.22	0.22	TS	-0.01	-0.01	TS	0.42	0.42	TS	-0.24	-0.19	LEM	0.10	0.10	TS
AD Gem	0.11	0.11	TS	-0.23	-0.23	TS	-0.02	-0.02	TS	0.03	0.03	TS	-0.06	-0.06	TS
BB Gem	0.09	0.19	LIII	0.05	0.08	LIII	0.02	0.12	LIII	0.01	0.07	LIII	-0.04	0.04	LIII
BW Gem	-0.02	-0.02	TS	-0.15	-0.15	TS	-0.07	-0.07	TS	-0.13	-0.13	TS	-0.12	-0.12	TS
DX Gem	0.12	0.12	TS	0.10	0.10	TS	-0.03	-0.03	TS	0.06	0.06	TS	-0.03	-0.03	TS
RZ Gem	0.19	0.19	TS	0.04	0.08	LEM	0.03	0.03	TS	0.07	0.07	TS	-0.12	-0.12	TS
W Gem	0.03	0.13	LIII	-0.08	-0.05	LIII	-0.16	-0.06	LIII	-0.07	-0.01	LIII	-0.14	-0.06	LIII
ζ Gem	0.31	0.41	LIII	0.17	0.20	LIII	0.06	0.16	LIII	0.07	0.13	LIII	-0.10	-0.02	LIII
BB Her	0.48	0.58	LIII	0.29	0.32	LIII	0.23	0.33	LIII	0.25	0.31	LIII	0.14	0.22	LIII
BG Lac	0.31	0.41	LIII	0.19	0.22	LIII	0.22	0.32	LIII	0.12	0.18	LIII	-0.04	0.04	LIII
DF Lac	0.23	0.33	LIII	0.12	0.15	LIII	0.06	0.16	LIII	0.10	0.16	LIII	0.01	0.09	LIII
FQ Lac	0.11	0.21	LIII	-0.50	-0.47	LIII	0.42	0.52	LIII	-0.05	0.01	LIII	0.04	0.12	LIII
RR Lac	0.21	0.31	LIII	0.18	0.21	LIII	-0.12	-0.02	LIII	0.07	0.13	LIII	0.02	0.10	LIII
V Lac	0.32	0.42	LIII	0.11	0.14	LIII	0.16	0.26	LIII	0.19	0.25	LIII	0.09	0.17	LIII
V411 Lac	0.34	0.44	LIII	0.08	0.11	LIII	0.08	0.18	LIII	0.04	0.10	LIII	-0.07	0.01	LIII
X Lac	0.36	0.46	LIII	0.11	0.14	LIII	0.12	0.22	LIII	0.16	0.22	LIII	0.08	0.16	LIII
Y Lac	0.15	0.25	LIII	0.09	0.12	LIII	0.16	0.26	LIII	0.14	0.20	LIII	0.13	0.21	LIII
Z Lac	0.50	0.60	LIII	0.22	0.25	LIII	0.19	0.29	LIII	0.19	0.25	LIII	0.14	0.22	LIII
GH Lup	0.25	0.35	LIII	0.23	0.26	LIII	0.12	0.22	LIII	0.15	0.21	LIII	-0.01	0.07	LIII
V473 Lyr	-0.01	0.09	LIII	-0.02	0.01	LIII	-0.07	0.03	LIII	0.00	0.06	LIII	-0.10	-0.02	LIII
AA Mon	0.21	0.31	LIII	-0.13	-0.10	LIII	-0.19	-0.09	LIII	-0.04	0.02	LIII	-0.17	-0.09	LIII
AC Mon	0.19	0.29	LIII	0.02	0.05	LIII	-0.05	0.05	LIII	0.03	0.09	LIII	-0.08	-0.00	LIII
BE Mon	0.34	0.34	TS	0.13	0.13	TS	0.33	0.33	TS	0.14	0.14	TS	0.08	0.08	TS
BV Mon	0.08	0.18	LIII	0.02	0.06	LEM	0.14	0.10	LEM	0.01	0.06	LEM	-0.03	0.02	LEM
CS Mon	0.06	0.16	LIII	-0.01	0.02	LIII	-0.07	0.03	LIII	-0.07	-0.01	LIII	-0.21	-0.13	LIII
CU Mon	0.03	0.13	LIII	-0.20	-0.17	LIII	-0.23	-0.13	LIII	-0.16	-0.10	LIII	-0.19	-0.11	LIII
CV Mon	0.31	0.31	TS	0.15	0.15	TS	0.22	0.22	TS	0.24	0.24	TS	0.18	0.18	TS
EE Mon	-0.27	-0.17	LIII	-0.65	-0.62	LIII	-0.53	-0.43	LIII	-0.38	-0.32	LIII	-0.48	-0.40	LIII
EK Mon	0.22	0.32	LIII	0.02	0.06	LEM	0.05	0.01	LEM	-0.06	-0.01	LEM	-0.04	0.01	LEM
FG Mon	0.04	0.14	LIII	0.01	0.04	LIII	0.05	0.15	LIII	-0.06	-0.00	LIII	-0.10	-0.02	LIII
FI Mon	-0.02	0.08	LIII	-0.10	-0.07	LIII	-0.24	-0.14	LIII	0.06	0.12	LIII	-0.08	-0.00	LIII
FT Mon	0.15	0.15	TS	-0.10	-0.10	TS	-0.08	-0.08	TS	-0.15	-0.09	LIII	0.02	0.02	TS
SV Mon	0.63	0.63	TS	0.16	0.16	TS	0.30	0.30	TS	0.21	0.21	TS	0.24	0.24	TS
T Mon	0.43	0.53	LIII	0.45	0.48	LIII	0.39	0.49	LIII	0.28	0.34	LIII	0.23	0.31	LIII
TW Mon	0.16	0.16	TS	-0.03	-0.03	TS	-0.04	-0.04	TS	-0.02	-0.02	TS	0.02	0.02	TS
TX Mon	0.23	0.23	TS	-0.08	-0.08	TS	-0.04	-0.04	TS	0.06	0.06	TS	0.04	0.04	TS
TY Mon	0.17	0.17	TS	-0.19	-0.19	TS	0.03	0.03	TS	0.14	0.14	TS	0.12	0.12	TS
TZ Mon	0.16	0.16	TS	0.02	0.02	TS	0.11	0.11	TS	0.03	0.03	TS	0.04	0.04	TS
UY Mon	-0.08	-0.06	LEM	-0.25	-0.21	LEM	-0.23	-0.27	LEM	-0.22	-0.17	LEM	-0.28	-0.23	LEM
V446 Mon	0.03	0.13	LIII	-0.18	-0.15	LIII	-0.35	-0.25	LIII	-0.24	-0.18	LIII	-0.33	-0.25	LIII
V447 Mon	-0.07	0.03	LIII	-0.16	-0.13	LIII	-0.40	-0.30	LIII	-0.26	-0.20	LIII	-0.35	-0.27	LIII
V465 Mon	0.26	0.26	TS	0.06	0.06	TS	-0.08	-0.08	TS	0.12	0.12	TS	0.04	0.04	TS
V484 Mon	-0.10	0.00	LIII	-0.01	0.02	LIII	-0.13	-0.03	LIII	-0.10	-0.04	LIII	-0.13	-0.05	LIII
V495 Mon	0.04	0.04	TS	-0.06	-0.06	TS	0.23	0.19	LEM	-0.01	-0.01	TS	-0.04	-0.04	TS
V504 Mon	0.07	0.17	LIII	0.04	0.07	LIII	-0.02	0.08	LIII	-0.02	0.04	LIII	-0.09	-0.01	LIII
V508 Mon	0.12	0.12	TS	0.04	0.04	TS	0.01	0.01	TS	0.04	0.04	TS	0.04	0.04	TS
V510 Mon	-0.05	-0.05	TS	-0.16	-0.16	TS	-0.04	-0.04	TS	-0.09	-0.09	TS	-0.15	-0.15	TS
V526 Mon	0.05	0.15	LIII	-0.21	-0.18	LIII	-0.14	-0.04	LIII	-0.06	-0.00	LIII	-0.16	-0.08	LIII
V911 Mon	0.20	0.30	LIII	0.04	0.07	LIII	0.16	0.26	LIII	0.06	0.12	LIII	-0.03	0.05	LIII
VZ Mon	0.11	0.21	LIII	-0.02	0.01	LIII	0.01	0.11	LIII	-0.12	-0.06	LIII	-0.21	-0.13	LIII
WW Mon	0.13	0.15	LEM	-0.11	-0.08	LIII	-0.09	-0.13	LEM	-0.02	0.03	LEM	-0.26	-0.21	LEM
XX Mon	0.51	0.51	TS	0.05	0.05	TS	0.21	0.21	TS	0.17	0.17	TS	0.23	0.23	TS
YY Mon	-0.19	-0.09	LIII	-0.23	-0.20	LIII	-0.10	0.00	LIII	-0.38	-0.32	LIII	-0.36	-0.28	LIII
R Mus	0.37	0.47	LIII	0.18	0.21	LIII	0.23	0.33	LIII	0.14	0.20	LIII	0.03	0.11	LIII
RT Mus	0.20	0.30	LIII	0.07	0.10	LIII	0.04	0.14	LIII	0.14	0.20	LIII	0.03	0.11	LIII
S Mus	0.29	0.39	LIII	0.15	0.18	LIII	0.03	0.13	LIII	0.08	0.14	LIII	-0.04	0.04	LIII
TZ Mus	0.14	0.24	LIII	0.05	0.08	LIII	0.43	0.53	LIII	0.17	0.23	LIII	0.05	0.13	LIII

continued on next page

Table 5. continued.

Name	[Na/H] _{lit}	[Na/H]	Ref.	[Al/H] _{lit}	[Al/H]	Ref.	[Mg/H] _{lit}	[Mg/H]	Ref.	[Si/H] _{lit}	[Si/H]	Ref.	[Ca/H] _{lit}	[Ca/H]	Ref.
UU Mus	0.27	0.37	LIII	0.16	0.19	LIII	0.19	0.29	LIII	0.17	0.23	LIII	0.06	0.14	LIII
GU Nor	0.32	0.32	TS	0.17	0.17	TS	0.18	0.18	TS	0.28	0.28	TS	0.09	0.09	TS
IQ Nor	0.57	0.57	TS	0.39	0.39	TS	0.36	0.36	TS	0.38	0.38	TS	0.25	0.25	TS
QZ Nor	0.56	0.56	TS	0.30	0.30	TS	0.39	0.39	TS	0.41	0.41	TS	0.20	0.20	TS
RS Nor	0.46	0.46	TS	0.26	0.26	TS	0.26	0.26	TS	0.39	0.39	TS	0.22	0.22	TS
S Nor	0.35	0.45	LIII	0.20	0.23	LIII	0.14	0.24	LIII	0.16	0.22	LIII	0.05	0.13	LIII
SY Nor	0.61	0.61	TS	0.41	0.41	TS	0.37	0.37	TS	0.37	0.37	TS	0.19	0.19	TS
TW Nor	0.58	0.58	TS	0.24	0.24	TS	0.58	0.58	TS	0.25	0.25	TS	0.05	0.05	TS
U Nor	0.31	0.41	LIII	0.15	0.18	LIII	0.08	0.18	LIII	0.14	0.20	LIII	-0.06	0.02	LIII
V340 Nor	0.40	0.40	TS	0.37	0.37	TS	0.12	0.12	TS	0.30	0.30	TS	0.19	0.19	TS
BF Oph	0.31	0.41	LIII	0.07	0.10	LIII	0.05	0.15	LIII	0.18	0.24	LIII	0.04	0.12	LIII
Y Oph	0.07	0.20	LII	0.14	0.22	LII	-0.27	-0.04	LII	0.02	0.13	LII	-0.07	0.04	LII
CR Ori	0.23	0.33	LIII	-0.10	-0.07	LIII	-0.32	-0.22	LIII	-0.14	-0.08	LIII	-0.18	-0.10	LIII
CS Ori	0.11	0.11	TS	-0.27	-0.27	TS	-0.25	-0.25	TS	-0.10	-0.10	TS	-0.16	-0.16	TS
DF Ori	0.00	0.10	LIII	-0.23	-0.20	LIII	-0.25	-0.15	LIII	-0.16	-0.10	LIII	-0.21	-0.13	LIII
GQ Ori	0.20	0.33	LII	0.17	0.25	LII	0.21	0.44	LII	0.05	0.16	LII	-0.14	-0.03	LII
RS Ori	0.12	0.12	TS	0.11	0.11	TS	0.41	0.41	TS	0.30	0.30	TS	0.22	0.22	TS
AS Per	0.32	0.42	LIII	0.17	0.20	LIII	0.46	0.56	LIII	0.17	0.23	LIII	0.11	0.19	LIII
AW Per	0.39	0.49	LIII	0.20	0.23	LIII	0.12	0.22	LIII	0.04	0.10	LIII	-0.17	-0.09	LIII
BM Per	0.19	0.29	LIII	0.19	0.22	LIII	0.13	0.23	LIII	0.15	0.21	LIII	0.01	0.09	LIII
CI Per	-0.34	-0.31	LIII	-0.30	-0.24	LIII	-0.26	-0.18	LIII
DW Per	0.12	0.22	LIII	-0.17	-0.14	LIII	0.05	0.15	LIII	0.10	0.16	LIII	0.03	0.11	LIII
GP Per	-0.43	-0.33	LIII	-0.34	-0.31	LIII	-0.27	-0.17	LIII	-0.39	-0.33	LIII	-0.70	-0.62	LIII
HQ Per	-0.08	0.02	LIII	-0.22	-0.19	LIII	-0.21	-0.11	LIII	-0.23	-0.17	LIII	-0.30	-0.22	LIII
HZ Per	0.03	0.13	LIII	-0.10	-0.07	LIII	-0.13	-0.03	LIII	-0.17	-0.11	LIII	-0.16	-0.08	LIII
MM Per	0.07	0.17	LIII	-0.02	0.01	LIII	-0.06	0.04	LIII	-0.03	0.03	LIII	-0.06	0.02	LIII
OT Per	0.25	0.35	LIII	-0.08	-0.05	LIII	-0.29	-0.19	LIII	-0.05	0.01	LIII	-0.07	0.01	LIII
SV Per	0.17	0.27	LIII	0.06	0.09	LIII	-0.03	0.07	LIII	0.05	0.11	LIII	-0.09	-0.01	LIII
SX Per	0.10	0.20	LIII	0.08	0.11	LIII	-0.01	0.09	LIII	-0.01	0.05	LIII	-0.03	0.05	LIII
UX Per	0.22	0.32	LIII	-0.07	-0.04	LIII	0.03	0.13	LIII	0.05	0.11	LIII	0.04	0.12	LIII
UY Per	0.26	0.36	LIII	0.21	0.24	LIII	0.07	0.17	LIII	0.15	0.21	LIII	0.05	0.13	LIII
V440 Per	0.07	0.20	LII	0.02	0.10	LII	-0.39	-0.16	LII	-0.02	0.09	LII	-0.18	-0.07	LII
V891 Per	0.23	0.33	LIII	0.06	0.09	LIII	0.02	0.12	LIII	0.05	0.11	LIII	0.00	0.08	LIII
VX Per	0.35	0.45	LIII	0.25	0.28	LIII	0.06	0.16	LIII	0.13	0.19	LIII	0.06	0.14	LIII
VY Per	0.27	0.37	LIII	0.09	0.12	LIII	0.05	0.15	LIII	0.07	0.13	LIII	0.03	0.11	LIII
AD Pup	0.04	0.06	LEM	-0.09	-0.05	LEM	0.02	-0.02	LEM	-0.10	-0.05	LEM	-0.02	0.03	LEM
AP Pup	0.06	0.08	LEM	-0.11	-0.07	LEM	-0.05	-0.09	LEM	-0.09	-0.04	LEM	-0.14	-0.09	LEM
AQ Pup	0.36	0.36	TS	-0.02	0.02	LEM	0.06	0.06	TS	0.25	0.25	TS	0.05	0.05	TS
AT Pup	0.29	0.31	LEM	-0.20	-0.16	LEM	0.19	0.15	LEM	-0.04	0.01	LEM	-0.15	-0.10	LEM
BC Pup	0.20	0.20	TS	-0.07	-0.07	TS	-0.14	-0.14	TS	-0.13	-0.13	TS	-0.18	-0.18	TS
BM Pup	0.17	0.17	TS	-0.02	-0.02	TS	TS	0.04	0.04	TS	-0.01	-0.01	TS
BN Pup	0.22	0.22	TS	0.16	0.16	TS	0.23	0.23	TS	0.16	0.16	TS	0.09	0.09	TS
CE Pup	0.18	0.28	LIII	0.07	0.10	LIII	0.31	0.41	LIII	0.02	0.08	LIII	-0.08	-0.00	LIII
CK Pup	0.17	0.17	TS	-0.08	-0.08	TS	-0.02	-0.02	TS	0.02	0.02	TS	-0.08	-0.08	TS
HW Pup	-0.02	-0.02	TS	-0.12	-0.12	TS	-0.06	-0.06	TS	-0.05	-0.05	TS	-0.11	-0.11	TS
LS Pup	0.42	0.42	TS	0.10	0.10	TS	0.04	0.04	TS	0.09	0.09	TS
MY Pup	0.13	0.15	LEM	-0.18	-0.14	LEM	-0.18	-0.22	LEM	-0.06	-0.01	LEM	-0.14	-0.09	LEM
NT Pup	0.34	0.44	LIII	0.01	0.04	LIII	-0.15	-0.05	LIII	-0.05	0.01	LIII	-0.20	-0.12	LIII
RS Pup	0.73	0.75	LEM	0.19	0.23	LEM	0.21	0.17	LEM	0.31	0.36	LEM	-0.03	0.02	LEM
V335 Pup	0.17	0.27	LIII	0.03	0.06	LIII	-0.04	0.06	LIII	0.10	0.16	LIII	-0.04	0.04	LIII
VW Pup	0.11	0.11	TS	-0.04	-0.04	TS	-0.33	-0.33	TS	-0.03	-0.03	TS	-0.08	-0.08	TS
VX Pup	0.16	0.26	LIII	-0.16	-0.12	LEM	-0.11	-0.15	LEM	-0.12	-0.07	LEM	-0.10	-0.05	LEM
VZ Pup	0.06	0.08	LEM	0.30	0.30	TS	0.01	0.01	TS	0.25	0.25	TS	0.11	0.11	TS
WW Pup	-0.30	-0.30	TS	-0.38	-0.38	TS	-0.34	-0.34	TS	-0.36	-0.36	TS	-0.70	-0.70	TS
WX Pup	0.22	0.24	LEM	-0.02	0.02	LEM	-0.15	-0.05	LIII	-0.12	-0.07	LEM	-0.04	0.01	LEM
WY Pup	0.21	0.21	TS	-0.14	-0.14	TS	0.05	0.05	TS	-0.01	-0.01	TS	0.01	0.01	TS
WZ Pup	0.09	0.09	TS	-0.11	-0.11	TS	0.14	0.14	TS	0.07	0.07	TS	0.04	0.04	TS
X Pup	0.42	0.42	TS	0.35	0.35	TS	-0.01	-0.01	TS	-0.01	-0.01	TS	0.09	0.09	TS
KQ Sco	0.70	0.70	TS	0.48	0.48	TS	0.26	0.26	TS	0.18	0.18	TS
RV Sco	0.41	0.51	LIII	0.20	0.23	LIII	0.01	0.11	LIII	0.16	0.22	LIII	0.11	0.19	LIII
RY Sco	0.36	0.36	TS	0.17	0.17	TS	0.08	0.08	TS	0.15	0.15	TS	-0.05	-0.05	TS
V470 Sco	0.55	0.55	TS	0.26	0.26	TS	0.18	0.18	TS	0.23	0.23	TS	0.08	0.08	TS
V482 Sco	0.38	0.48	LIII	0.23	0.26	LIII	0.15	0.25	LIII	0.19	0.25	LIII	0.08	0.16	LIII
V500 Sco	0.19	0.19	TS	0.12	0.12	TS	-0.12	-0.12	TS	0.03	0.03	TS	-0.14	-0.14	TS
V636 Sco	0.31	0.41	LIII	0.29	0.32	LIII	0.09	0.19	LIII	0.11	0.17	LIII	-0.02	0.06	LIII
V950 Sco	0.27	0.37	LIII	0.11	0.14	LIII	0.06	0.16	LIII	0.15	0.21	LIII	-0.02	0.06	LIII
BX Sct	0.46	0.56	LIII	0.27	0.30	LIII	0.27	0.37	LIII	0.21	0.27	LIII	0.15	0.23	LIII
CK Sct	0.32	0.42	LIII	0.25	0.28	LIII	0.10	0.20	LIII	0.13	0.19	LIII	0.00	0.08	LIII
CM Sct	0.33	0.43	LIII	0.19	0.22	LIII	0.03	0.13	LIII	0.15	0.21	LIII	0.04	0.12	LIII
CN Sct	0.56	0.66	LIII	0.45	0.48	LIII	0.32	0.42	LIII	0.32	0.38	LIII	0.17	0.25	LIII
EV Sct	0.25	0.25	TS	0.56	0.56	TS	0.06	0.06	TS	0.26	0.26	TS	0.10	0.10	TS
EW Sct	0.07	0.20	LII	0.15	0.23	LII	-0.10	0.13	LII	0.08	0.19	LII	-0.01	0.10	LII
RU Sct	0.41	0.41	TS	0.23	0.23	TS	0.42	0.42	TS	0.32	0.32	TS	0.16	0.16	TS
SS Sct	0.15	0.25	LIII	0.18	0.21	LIII	0.24	0.34	LIII	0.14	0.20	LIII	0.06	0.14	LIII
TY Sct	0.45	0.55	LIII	0.40	0.43	LIII	0.29	0.39	LIII	0.26	0.32	LIII	0.07	0.15	LIII

continued on next page

Table 5. continued.

Name	[Na/H] _{lit}	[Na/H]	Ref.	[Al/H] _{lit}	[Al/H]	Ref.	[Mg/H] _{lit}	[Mg/H]	Ref.	[Si/H] _{lit}	[Si/H]	Ref.	[Ca/H] _{lit}	[Ca/H]	Ref.
UZ Sct	0.79	0.79	TS	0.60	0.60	TS	0.32	0.32	TS	0.45	0.45	TS	0.22	0.22	TS
V367 Sct	0.30	0.30	TS	0.33	0.33	TS	-0.01	-0.01	TS	0.16	0.16	TS	0.01	0.01	TS
X Sct	0.41	0.41	TS	0.34	0.34	TS	0.12	0.12	TS	0.32	0.32	TS	0.14	0.14	TS
Y Sct	0.38	0.48	LIII	0.28	0.31	LIII	0.08	0.18	LIII	0.16	0.22	LIII	0.03	0.11	LIII
Z Sct	0.71	0.71	TS	0.51	0.51	TS	0.14	0.14	TS	0.33	0.33	TS	0.13	0.13	TS
AA Ser	0.98	0.98	TS	0.50	0.50	TS	0.28	0.28	TS	0.47	0.47	TS	0.16	0.16	TS
BQ Ser	0.12	0.25	LII	0.14	0.22	LII	-0.14	0.09	LII	0.07	0.18	LII	-0.05	0.06	LII
CR Ser	0.61	0.61	TS	0.29	0.29	TS	0.32	0.32	TS	0.28	0.28	TS	0.11	0.11	TS
DV Ser	0.72	0.82	LIII	0.59	0.62	LIII	0.67	0.77	LIII	0.46	0.52	LIII	0.37	0.45	LIII
DG Sge	0.38	0.48	LIII	0.10	0.13	LIII	0.14	0.24	LIII	0.18	0.24	LIII	0.09	0.17	LIII
GX Sge	0.27	0.37	LIII	0.31	0.34	LIII	0.16	0.26	LIII	0.21	0.27	LIII	0.01	0.09	LIII
GY Sge	0.29	0.39	LIII	0.24	0.27	LIII	0.15	0.25	LIII	0.26	0.32	LIII	0.17	0.25	LIII
S Sge	0.20	0.33	LII	0.11	0.19	LII	-0.17	0.06	LII	0.10	0.21	LII	-0.03	0.08	LII
AP Sgr	0.47	0.60	LII	0.08	0.16	LII	0.25	0.48	LII	0.27	0.38	LII	0.24	0.35	LII
AV Sgr	0.87	0.87	TS	0.50	0.50	TS	0.73	0.69	LEM	0.47	0.47	TS	0.18	0.18	TS
AY Sgr	0.32	0.32	TS	0.19	0.19	TS	0.20	0.20	TS	0.23	0.23	TS	0.11	0.11	TS
BB Sgr	0.36	0.49	LII	0.15	0.23	LII	0.14	0.25	LII	0.12	0.23	LII
U Sgr	0.21	0.34	LII	0.21	0.29	LII	-0.17	0.06	LII	0.08	0.19	LII	-0.04	0.07	LII
V1954 Sgr	0.62	0.62	TS	0.27	0.27	TS	0.17	0.17	TS	0.47	0.47	TS	0.25	0.25	TS
V350 Sgr	0.23	0.36	LII	0.32	0.40	LII	0.19	0.42	LII	0.13	0.24	LII	0.08	0.19	LII
V773 Sgr	0.30	0.30	TS	0.05	0.05	TS	0.20	0.20	TS	0.30	0.30	TS	0.14	0.14	TS
VY Sgr	0.78	0.78	TS	0.66	0.66	TS	0.36	0.36	TS	0.28	0.28	TS	0.18	0.18	TS
W Sgr	0.18	0.31	LII	0.07	0.15	LII	-0.25	-0.02	LII	0.05	0.16	LII	-0.07	0.04	LII
WZ Sgr	0.59	0.59	TS	0.57	0.57	TS	0.02	0.02	TS	0.30	0.30	TS	0.17	0.17	TS
XX Sgr	0.29	0.29	TS	0.24	0.24	TS	-0.01	-0.01	TS	0.11	0.11	TS	0.00	0.00	TS
Y Sgr	0.27	0.40	LII	0.23	0.31	LII	-0.08	0.15	LII	0.09	0.20	LII	0.05	0.16	LII
YZ Sgr	0.25	0.38	LII	0.17	0.25	LII	-0.17	0.06	LII	0.11	0.22	LII	-0.02	0.09	LII
AE Tau	0.05	0.15	LIII	-0.06	-0.03	LIII	-0.15	-0.05	LIII	-0.11	-0.05	LIII	-0.14	-0.06	LIII
AV Tau	0.17	0.19	LEM	0.09	0.13	LEM	0.12	0.08	LEM	0.04	0.09	LEM	-0.03	0.02	LEM
EF Tau	-0.48	-0.35	LII	-0.46	-0.38	LII	-0.74	-0.51	LII	-0.65	-0.54	LII	-0.62	-0.51	LII
EU Tau	0.24	0.37	LII	-0.01	0.07	LII	-0.28	-0.05	LII	0.04	0.15	LII	-0.05	0.06	LII
ST Tau	0.29	0.39	LIII	0.11	0.15	LEM	0.08	0.04	LEM	0.08	0.13	LEM	0.06	0.11	LEM
SZ Tau	0.27	0.40	LII	0.10	0.18	LII	-0.18	0.05	LII	0.07	0.18	LII	-0.02	0.09	LII
LR TrA	0.15	0.25	LIII	0.36	0.39	LIII	0.47	0.57	LIII	0.28	0.34	LIII	0.22	0.30	LIII
R TrA	0.49	0.59	LIII	0.12	0.15	LIII	0.21	0.31	LIII	0.23	0.29	LIII	0.10	0.18	LIII
S TrA	0.41	0.51	LIII	0.16	0.19	LIII	0.28	0.38	LIII	0.14	0.20	LIII	-0.03	0.05	LIII
AE Vel	0.14	0.24	LIII	0.20	0.23	LIII	0.06	0.16	LIII	0.03	0.09	LIII	-0.20	-0.12	LIII
AH Vel	0.53	0.55	LEM	0.16	0.20	LEM	0.14	0.10	LEM	0.12	0.17	LEM	0.04	0.09	LEM
AX Vel	0.12	0.16	LEM	0.13	0.09	LEM	0.20	0.25	LEM	0.03	0.08	LEM
BG Vel	0.21	0.31	LIII	-0.11	-0.07	LEM	0.10	0.20	LIII	0.09	0.14	LEM	0.08	0.13	LEM
CS Vel	0.27	0.37	LIII	0.26	0.29	LIII	0.08	0.18	LIII	0.12	0.18	LIII	-0.08	-0.00	LIII
CX Vel	0.33	0.43	LIII	0.21	0.24	LIII	0.52	0.62	LIII	0.17	0.23	LIII	0.10	0.18	LIII
DK Vel	0.21	0.31	LIII	0.11	0.14	LIII	0.10	0.20	LIII	0.15	0.21	LIII	0.02	0.10	LIII
DR Vel	0.29	0.31	LEM	0.26	0.30	LEM	0.21	0.17	LEM	0.20	0.25	LEM	0.26	0.31	LEM
EX Vel	0.15	0.25	LIII	0.15	0.18	LIII	0.07	0.17	LIII	0.08	0.14	LIII	0.01	0.09	LIII
EZ Vel	0.17	0.17	TS	0.01	0.01	TS	-0.03	-0.03	TS	0.02	0.07	LEM	-0.08	-0.08	TS
FG Vel	0.17	0.27	LIII	0.15	0.18	LIII	0.01	0.11	LIII	0.02	0.08	LIII	-0.18	-0.10	LIII
FN Vel	0.14	0.24	LIII	0.15	0.18	LIII	0.23	0.33	LIII	0.14	0.20	LIII	0.09	0.17	LIII
RY Vel	0.44	0.46	LEM	0.40	0.44	LEM	0.01	0.11	LIII	0.18	0.23	LEM	0.13	0.18	LEM
RZ Vel	0.35	0.45	LIII	0.45	0.48	LIII	0.43	0.39	LEM	0.28	0.33	LEM	-0.23	-0.18	LEM
ST Vel	0.28	0.38	LIII	0.09	0.13	LEM	0.26	0.22	LEM	0.12	0.17	LEM	0.09	0.14	LEM
SV Vel	0.39	0.49	LIII	0.10	0.13	LIII	0.11	0.21	LIII	0.17	0.23	LIII	0.10	0.18	LIII
SW Vel	0.21	0.23	LEM	0.28	0.32	LEM	0.28	0.24	LEM	-0.03	0.02	LEM	0.05	0.10	LEM
SX Vel	0.32	0.34	LEM	-0.10	-0.06	LEM	-0.03	0.07	LIII	0.13	0.18	LEM	-0.01	0.04	LEM
T Vel	0.33	0.35	LEM	0.29	0.33	LEM	0.32	0.28	LEM	0.28	0.33	LEM	0.29	0.34	LEM
V Vel	-0.01	0.01	LEM	-0.06	-0.02	LEM	0.05	0.01	LEM	-0.12	-0.07	LEM	-0.11	-0.06	LEM
XX Vel	0.21	0.31	LIII	0.17	0.20	LIII	0.11	0.21	LIII	0.14	0.20	LIII	0.00	0.08	LIII
AS Vul	0.62	0.72	LIII	0.42	0.45	LIII	0.29	0.39	LIII	0.30	0.36	LIII	0.27	0.35	LIII
DG Vul	0.42	0.52	LIII	0.21	0.24	LIII	0.26	0.36	LIII	0.21	0.27	LIII	0.05	0.13	LIII
S Vul	0.22	0.32	LIII	0.27	0.30	LIII	0.06	0.16	LIII	0.11	0.17	LIII	0.03	0.11	LIII
SV Vul	0.05	0.18	LII	0.12	0.20	LII	-0.17	0.06	LII	0.04	0.15	LII	-0.04	0.07	LII
T Vul	0.15	0.28	LII	0.10	0.18	LII	-0.13	0.10	LII	0.04	0.15	LII	-0.01	0.10	LII
U Vul	0.28	0.38	LIII	0.17	0.20	LIII	0.09	0.19	LIII	0.16	0.22	LIII	0.01	0.09	LIII
X Vul	0.17	0.30	LII	0.14	0.22	LII	-0.20	0.03	LII	0.09	0.20	LII	-0.02	0.09	LII